Studies of hybrid MIMO

P.F. Sammartino and C.J. Baker

Award number FA8655-05-1-3051
Option 3**, phase IV, item** 3001
Submitted to EOARD

Department of Electronic and Electrical Engineering
University College London
August 2008

REPORT DOCUMENTATION PAGE

Form Approved OMB No. 0704-0188

1. REPORT DATE *(DD-MM-YYYY)*	2. REPORT TYPE	3. DATES COVERED *(From – To)*
03-09-2008	Final Report	3 June 2005 - 06-Oct-08

4. TITLE AND SUBTITLE

Studies of Hybrid MIMO

5a. CONTRACT NUMBER
FA8655-05-1-3051

5b. GRANT NUMBER

5c. PROGRAM ELEMENT NUMBER

6. AUTHOR(S)

Professor Christopher J Baker

5d. PROJECT NUMBER

5d. TASK NUMBER

5e. WORK UNIT NUMBER

7. PERFORMING ORGANIZATION NAME(S) AND ADDRESS(ES)

University College London
Torrington Place
London WC1E 7JE
United Kingdom

8. PERFORMING ORGANIZATION REPORT NUMBER

N/A

9. SPONSORING/MONITORING AGENCY NAME(S) AND ADDRESS(ES)

EOARD
Unit 4515 BOX 14
APO AE 09421

10. SPONSOR/MONITOR'S ACRONYM(S)

11. SPONSOR/MONITOR'S REPORT NUMBER(S)
Grant 05-3051

12. DISTRIBUTION/AVAILABILITY STATEMENT

13. SUPPLEMENTARY NOTES

14. ABSTRACT

This report results from a contract tasking University College London as follows: The grantee will investigate hybrid MIMO (Multiple Input Multiple Output)/beamforming approaches to improve radar target detection, tracking and classification.

15. SUBJECT TERMS

EOARD, target identification, radar, Mathematical Modeling

16. SECURITY CLASSIFICATION OF:			17. LIMITATION OF ABSTRACT	18, NUMBER OF PAGES	19a. NAME OF RESPONSIBLE PERSON
a. REPORT	b. ABSTRACT	c. THIS PAGE			GEORGE W YORK, Lt Col, USAF
UNCLAS	UNCLAS	UNCLAS	UL	179	**19b. TELEPHONE NUMBER** *(Include area code)* +44 (0)1895 616163

This effort has been sponsored by the Air Force Office of Scientific Research, Air Force Materiel Command, USAF, under grant number FA8655-05-1-3051.

It is certified that there were no subject inventions to declare during the performance of this grant.

The following papers derived from this study have been accepted or submitted for publication.

1. P.F. Sammartino, C.J. Baker, H.D. Griffiths – "A comparison of algorithms for MIMO and netted radar systems" – 2^{nd} International Waveform Diversity & Design Conference, Lihue, Hi, $22^{th}-27^{th}$ Jan 2006,

2. P.F. Sammartino, C.J. Baker, H.D. Griffiths – "Target Model Effects On MIMO Radar Performance" – 2006 IEEE ICASSP, International Conference on Acoustic, Speech and Signal Processing, Toulouse, Fr, $14^{th}-19^{th}$ May 2006,

3. P.F. Sammartino, C.J. Baker, H.D. Griffiths – "MIMO performance in clutter environment" – CIE Rad 2006, International Conference, Shanghai, Ch, $16^{th}-19^{th}$ Oct 2006,

4. P.F. Sammartino, C.J. Baker, H.D. Griffiths – "A comparison of algorithms for MIMO and netted radar systems" – IEEE radar 2007, Whaltham, Ma, $17^{th}-20^{th}$ Apr 2007,

5. H.D. Griffiths, C.J. Baker, P.F. Sammartino, M. Rangaswamy – "MIMO as a radar network" – submitted as a chapter contribution for "MIMO Radar", Wiley books,

6. P.F. Sammartino, C.J. Baker, H.D. Griffiths, M. Rangaswamy – "Processing in distributed radar networks, part 1: systems types and false alarm performance" – Submitted to IEEE transactions on Aerospace and Electronic Systems,

7. P.F. Sammartino, C.J. Baker, H.D. Griffiths, M. Rangaswamy – "Processing in distributed radar networks, part 2: systems types and detection" – Submitted to IEEE transactions on Aerospace and Electronic Systems,

8. P.F. Sammartino, C.J. Baker, H.D. Griffiths, M. Rangaswamy – "Effects of decentralized processing in networks of radars" – IET Radar 2007, International Conference on Radar Systems, Edinburgh, UK, 15^{th}–18^{th} Oct 2007,

9. P.F. Sammartino, C.J. Baker, M. Rangaswamy – "Coverage in radar networks" – 41^{st} Conference on Signals, Systems, and Computers, Asilomar, Pacific Grove, CA, 4^{th}-7^{th} Nov 2007,

10. P.F. Sammartino, C.J. Baker, M. Rangaswamy – "MIMO radar, theory and experiments" – CAMSAP 2007, St. Thomas, US Virgin Islands, 12^{th}-14^{th} Dec 2007.

11. P.F. Sammartino, C.J. Baker, M. Rangaswamy – "Moving target localization with multistatic radar systems" – Radarcon 2008, Rome, Italy, 26^{th} - 30^{th} May 2008.

Contents

Chapter 1

Introduction

The concept of using radiofrequency waves in order to detect metal objects was firstly developed at the beginning of the last century. The word RADAR (**RA**dio **D**etection **A**nd **R**anging) itself was coined many years later, in 1941, although since the 1930s there was a very high interest in investigating and improving the capabilities of these systems. The basic principle of a radar system is to receive a copy of the transmitted waveform after reflecting from a target. The transmitter and the receiver can be co-located (monostatic radars) or separated in space (bistatic radars). We describe the basic principles of these systems in Chapter 3.

Radar systems have been developed constantly over time and nowadays they are applied in a wide variety of ways. Some of them include air traffic control, target recognition and tracking, weather monitoring, imaging, global navigation, automatic systems guidance, road speed control, through-the-wall vision, etc.... Originally designed, developed and built with analog technology, in the past radar systems could generally perform one or two main tasks only. However, in recent years, they have been taking advantage of developments in digital technology. A combination of digital signal processing and array antennas has allowed radar systems to become much more versatile. As a consequence future generations of radar systems are being designed to perform multiple tasks. These are the so-called 'multi-role' radars or 'multi-function' radars (although there is not a strict definition yet).

1.1 Overview and motivation

1.1.1 The radar network concept

A radar network consists of transmitters and receivers distributed over a geographic area such that it is possible to view targets at different aspect angles. Transmitters and receivers can be co-located or not. A schematic example of such a network is shown in Figure 1.1. Signal processing techniques for radar networks has received considerable attention and this has spawned a wide variety of system structures and processing methods that can be employed.

In this case, the same data acquired by a radar network can be processed in a number of different ways, leading to a range of performance levels. In this thesis we describe and compare four different signal processing algorithms. These vary from processing of fully coherent signals to processing incoherent signals. The processing approaches can be 'centralized' (i.e. the detection decision is taken at a single processing unit) or 'decentralized' (decisions are taken at individual receivers in the radar network across all possible mono/bistatic pairs). The statistical properties of the signals resulting from the differing signal processing approaches lead to substantial differences in their performance in terms of FAR and even more so when subject to either accidental or deliberate interference (jamming). Such an analysis allows a detailed examination of the benefits and drawbacks associated with radar networks and processing schemes. This provides a simple but thorough interrogation enabling the potential of radar networks in terms of their false alarm performance to be assessed.

Results for monostatic systems are also reported to provide a well understood benchmark. The achievable detection performance is computed as a function of (*i*) processing method, (*ii*) RCS model of the target and (*iii*) the number of nodes comprising the radar network. Furthermore, the sensitivity of each system is calculated to show the extent of the range coverage that these differing systems could potentially achieve. In order to provide a fair comparison of the processing types, the total Effective Radiated Power (ERP) is maintained constant in transmission regardless of the number of nodes comprising the network. In other words, a monostatic radar with a fixed power in transmission P_t and a specific antenna gain

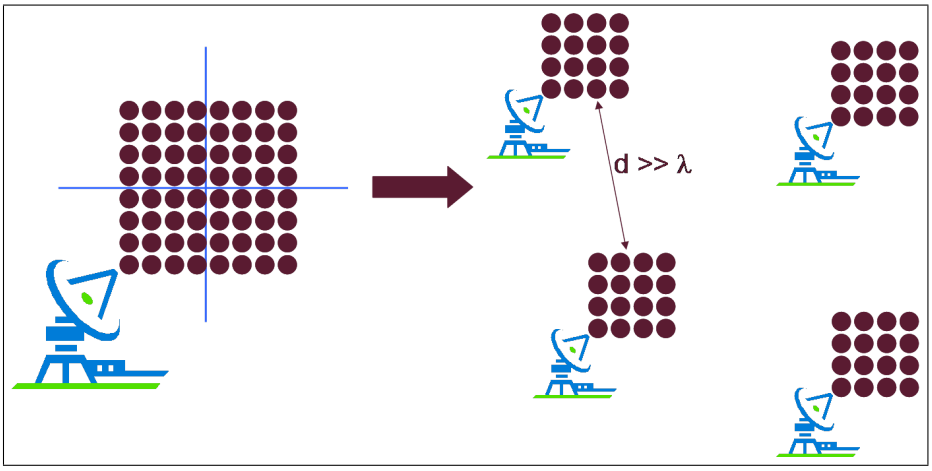

Figure 1.1: From the monostatic to the MIMO concept

G is compared to a radar network comprised by a number of devices (say L) all able to transmit and receive, using a fraction of the power in transmission $\left(\frac{P_t}{L}\right)$ and with antennas with a fraction of the gain $\left(\frac{G}{L}\right)$. Such decision has been taken in order to provide a fairer comparison between the radar network and the monostatic performance. Actually it would not be hard to demonstrate that, whenever each transmitter of the radar network is fed with as much power as the monostatic case and the tx/rx antenna have the same gain, the performance are expected to be higher, simply for the fact that an increased amount of energy is injected into the system.

Figures 1.2 and 1.3 show an example of the antenna patterns when the original antenna is split in $L = 4$ smaller antennas. As is known, not only the gain is lower, but also the pattern is wider. Therefore some drawbacks of applying this approachthis approach to the MIMO concept, in the way the comparison with traditional monostatic radar is made in this thesis, are (*i*) the reduced SNR expected in every receiver and (*ii*) the smaller angular resolution of each antenna. However, as seen in Chapters 5 and 10, the increased number of processable signals together with the achieved angular diversity can recover performance. In Chapter 4 the considered processing approaches for this concept of radar systems are reported in detail.

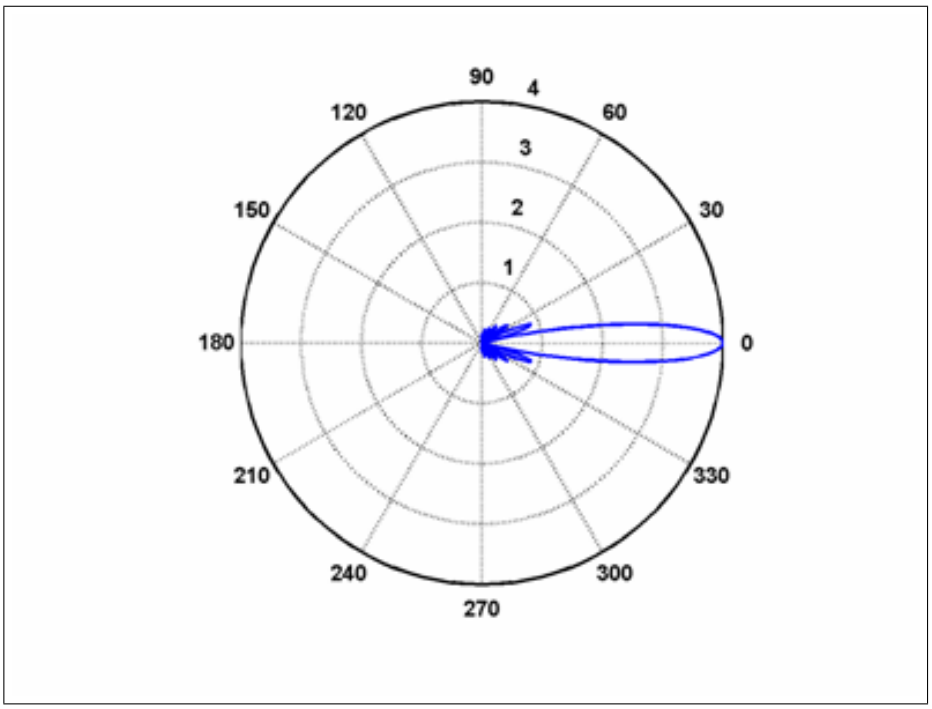

Figure 1.2: Monostatic beam

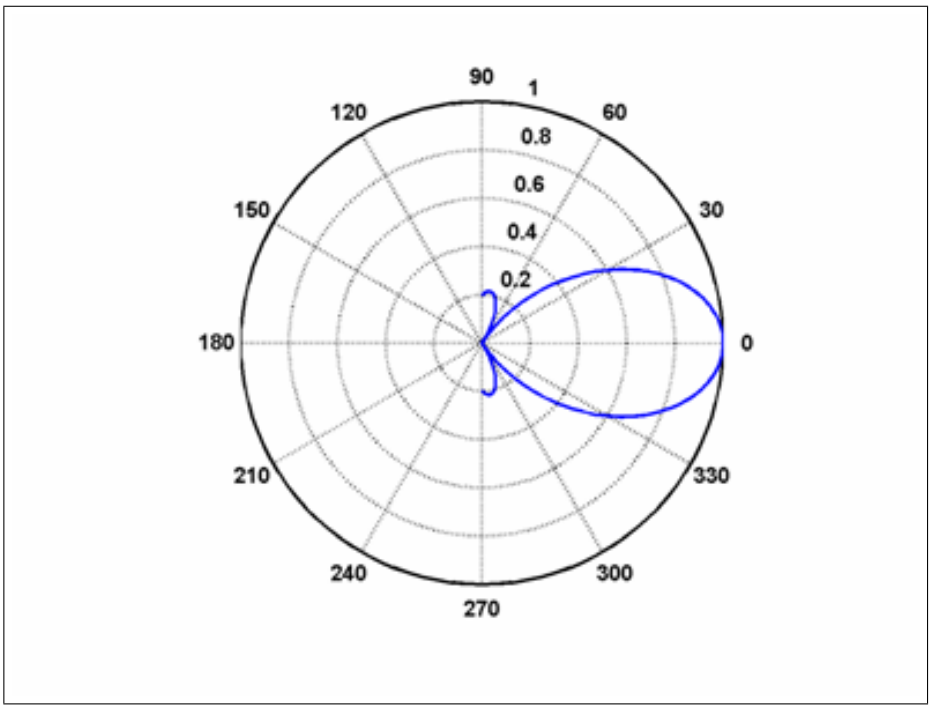

Figure 1.3: MIMO single antenna beam

1.1.2 The MIMO concept

MIMO (Multiple Input – Multiple Output) is a recent developed concept that has attracted much interest in application to communication systems. This is because it allows enchanced performance of a communication channel in terms of data transfer (capacity) without requiring additional bandwidth or power in transmission. This technique employs a number of antennas, say M, in transmission and others, say N, in reception.

Although a more complete discussion on the research on this topic is reported in Chapter 2, in the following Section we provide a brief overview of the principles of this system as applied within this thesis. This allows a more fundamental understanding of the MIMO concept as applied to radar to be developed. In particular, this concept is investigated and discussed whereas its application to radar networks lead to a new exploitation of the resources, allowing to increase the accuracy, jamming tolerance, parameter estimation, etc. . . of a radar system.

MIMO concept as a communication system

It has been extensively reported in literature that MIMO systems show improvements in channel capacity and subsequent performance of communication systems in several ways (Chapter 2). They transmit and receive a number of signals (e.g. x_1, x_2, x_3 Ĕ etc) on differing elements simultaneously. At the receiver a MIMO decoder operates on each of the antenna elements. MIMO antennas are spaced by multiple of wavelengths, usually between 1 and 10. This allows, in an indoor environment, independent samples of the interfering signals in reception. Each antenna element receives signals coming from any of the transmit elements, thus:

$$\begin{array}{rcl} r_1 & = & h_{11}x_1 + h_{12}x_2 + \ldots + h_{1M}x_M + n_1 \\ r_2 & = & h_{21}x_1 + h_{22}x_2 + \ldots + h_{2M}x_M + n_2 \\ \vdots & \vdots & \vdots \\ r_N & = & h_{N1}x_1 + h_{N2}x_2 + \ldots + h_{NM}x_M + n_N \end{array} \tag{1.1}$$

where h_{ij} are the channel weights and n_k the possible disturbances incoming in the receiver (noise, jammers, multipath, clutter). This can be written in a compact way as:

$$\mathbf{r} = \mathbf{H}\mathbf{x} + \mathbf{n}. \tag{1.2}$$

By treating the set of channels as a matrix the individual data streams x_i can be recovered. To do this the disturbance vector d and the channel matrix **H** must be estimated and respectively subtracted and inverted to recover the individual data streams from the vector **r**. This is equivalent to solving N simultaneous equations with M unknowns. The matrix can only be inverted or pseudo-inverted if there are sufficient paths between the transmitter and receiver.

MIMO is at the moment widely used in indoor wireless applications, since it allows dramatic increase of the capacity of the channel and reduces the limitations due to fading, multipath and other secondary effects. This technology is still being developed, with increasing potential, as MUltiuser MIMO (MU-MIMO), Network MIMO or Intelligent Antennas MIMO (IA-MIMO), with different applications. Details are reported in Section 2

MIMO: from communications to radar systems

MIMO basic principles are being applied to radar systems and a number of publications have recently begun to emerge. These suggest there are advantages to using this technique. As much as in wireless communications, the spacing of antennas is crucial in radar systems. Some authors, on the contrary, apply the MIMO technique to an array of antennas spacing the elements up to 10 wavelengths as in wireless communications. Other authors point out that the distance d between antenna elements in a MIMO system, for achieving angular diverse measurements of the Radar Cross Section (RCS) of a target and therefore independency of the received signals, should be as

$$d \geq \frac{\lambda R}{D}, \tag{1.3}$$

where λ is the wavelength, R is the target range and D the target's main dimension. As a consequence, assuming for instance a 20-meter wide target at 100 Km and a wavelength of 3 cm, the spacing d between the antenna elements should be 150 m.

In the migration from the MIMO communication concept to the MIMO radar concept, another point that requires to be stressed is that in radar systems it is not of interest to maximize the capacity of the channel. This may seem debatable, but it is extremely important because a number of concepts that characterize the MIMO communication system have to be understood in depth before applying them to radar systems. In fact, the maximization of the channel information is the core of the MIMO developed so far in communications. On the contrary, the radars' channel capacity is extremely low, but still this is not of interest. This is due, of course, to the ultimate purpose of a radar system which is detecting targets in an unknown or non-cooperative environment, rather than transmitting and/or receiving data from cooperative devices.

Other Authors (e.g. from [65] to [63]) have been investigating MIMO as a technique based on two arrays of antennas transmitting and receiving different codes from different (sub)elements. Here the distance between the elements is kept relatively small, i.e. in the order of the wavelength, and therefore angular diversity cannot be achieved. However this application, exploiting either orthogonal or partially correlated codes (e.g. from [55] to [64]), has been shown to overcome the standard array of antenna performance and to provide an extra degree of freedom, allowing formation of multiple beams at the same time which can be used for tracking or jammer rejection.

MIMO concept as a radar system

When evaluating the MIMO concept from a communication to a radar basis, equation (1.3) is crucial. This equation states clearly that it is not possible to achieve angular diversity and consequent differing measurements of the RCS of a target, when antennas are closely spaced. This is the real basis of MIMO radar as independent samples of a target can be combined to provide a better estimate of the underlying RCS. This is also valid for clutter and multipath, since the proximity of the antennas do not allow decorrelation of all the received signals. Therefore in radar systems, the antennas should be separated by distances not comparable with the wavelength. This generates a number of secondary effects,

which require at least a strong awareness, that have not been taken into account in the analysis of MIMO as a communication systems.

First of all the coherency between the antenna elements is totally lost. This is due to the increased distance that scrambles the received phases from element to element. Secondly, whenever more than one code (waveform) is used in transmission, these cannot be considered as 'orthogonal' anymore, even if they have been designed with this property. Actually, two codes, say $w_i(t)$ and $w_k(t)$ are called 'orthogonal' when the following property applies:

$$w_i^*(t) \cdot w_k(t) = 0, \tag{1.4}$$

where * is the conjugate operator.

In radar systems employing several waveforms, each received signal goes through a bank of matched filters performing all the possible cross-correlations between the received signal itself and the reference waveforms, as in equation (1.5)

$$R_{w_{i,k}}(\tau) = w_i(t) \otimes w_k(t) = \int_{-\infty}^{+\infty} w_i^*(t)\, w_k(t-\tau)\, dt, \tag{1.5}$$

where $\otimes$ is the cross-correlation function and τ is a delay. If the transmitting antennas are closely spaced, the delay in the time of arrival of all the waveforms, supposed transmitted at the same time, is negligible and equation (1.5) can be expressed as equation (1.4) which still holds. As a result, when a peak in the cross-correlation of a waveform with itself occurs, the cross-correlations with all the other used waveform is 0 and therefore there are no interferences (noise apart).

When the antennas are far away from one another, transmission and reception are not synchronized anymore because the paths between the transmitters, the target and the receivers have different lengths, usually much more than a resolution cell. In this case the corresponding different times of arrival of the echoes generate delays mismatching the orthogonality of the codes. Being unaware of this issue may lead to detection of multiple targets which in fact can be generated by the echoes from one target only. Of course it is possible to estimate the peak of the auto-correlation of a waveform and cancel it in the other received signals, but it requires additional efforts in signal processing.

1.2 Aim

This programme examines distributed radar concepts trying to understand true relative performance, system utility and to evaluate novel forms of MIMO. It provides a platform for the more detailed research to follow. The overall aim of the work described here is to compare the performance, under various practical operating conditions, of different ways of implementing a MIMO radar system and to relate them with the netted radar concept. We also briefly discuss a novel 'frequency MIMO' concept that allows the advantage of MIMO without having to have multiple distributed sensors.

1.3 Thesis layout

Chapter 2 shows the literature produced so far for MIMO systems in communications and radar systems. Additional publications on mono/bistatic radars are reported as well.

In Chapter 3 basic features of the mono/bistatic radar systems are reported. This provides a platform to have a better understanding of the multistatic scenarios described further in this thesis.

In Chapter 4 we discuss of the number of processing that it is possible to apply to a radar network. Their performance as a function of signal to noise ratio has been evaluated for various models of targets as well as after the introduction of secondary effects such as multipath and clutter are reported in Chapters 5 and 6. Chapter 8 reports the achievable coverage.

Data acquired with the UCL radar network are analyzed in Chapter 10 for both validating the theoretical results achieved in the previous Chapters and introducing a way for localization and tracking with multistatic systems.

Finally in Chapter 13 we provide the conclusions of the work produced so far and suggest further improvements and investigations for possible future developments.

Chapter 2

Literature review

In this section a summary of the literature is presented, covering radar networks, MIMO systems, together with a brief survey on general radar systems.

The literature review is divided in four parts. The first part is made of general publications in radar. The second discusses clutter in monostatic and bistatic systems. The third is a significant survey of the papers published on the netted radar concept. Finally the last one focuses specifically on MIMO as a radar system concept.

The theory underlying radar systems is reported in a number of publications. Because radar is a quite mature technology, a variety of books is currently on the market and no attempt is made here to review all the literature published on radar. However, among these, [1, 2, 3] are a significant survey of monostatic radar systems. As well, [4, 5] are a benchmark for the principles of bistatic systems. Chapter 3 reports an explanation of the most relevant concepts developed, as applied in this thesis, in order to improve the understanding of the results presented in the rest of this work. The principles of the information theory and the statistical signal processing are respectively covered fairly and comprehensively in [6, 7, 8].

Publications [9] to [19] represent are significant with respect to clutter as utilized inn this thesis. Whereas clutter is present in most of the radar applications, many studies have been carried out over the last 60 years. As a consequence, robust theories and a number of models have been proposed to describe this phenomenon, although not all problems have been solved. Section 3.5 reports a

brief survey of the principal models applied nowadays. Little is still known about the detailed pulse-to-pulse behaviour of bistatic clutter. Even less is known about the actual relationships between simultaneous measurements of monostatic and bistatic clutter from the same area. This is a very important issue for optimizing the processing of received echoes in multistatic systems pointing at the same time to a specific location. [20, 21, 22, 23, 26] are on the contrary a basic survey on the most common detection approaches, which are discussed in 3.6. However, a detailed analysis of simulated mono-bistatic clutter is outside the scope of this thesis.

Thirdly, in recent times the concept of linking two or more radars together found new applications and therefore a further stage of developments is ongoing. Whilst in the past radar networks were comprised of many receivers but one transmitter only, recent works on waveform diversity allow multiple sources of transmission at the same time.

With 'multistatic systems' it is usually referred to a broad range of radar systems, such as

i networks of monostatic radars (often termed 'netted radars' and already used in diverse applications),

ii systems comprised of multiple transmitters and receivers widely separated in space and

iii sometimes single transmitter and multiple receivers.

The first and the third cases have already been investigated, at least partially. However, the capabilities of autonomous integrated systems of multiple transmitters and receivers are still to be fully discovered. In [27] the author defines a Multisite Radar System as "a radar system including several spatially separated transmitting, receiving and (or) transmitting-receiving facilities where information of each target from all sensors are fused and jointly processed". When the system is comprised of more than one transmitter, the requirement of using multiple waveforms can lead to an overall optimization of the resources, but can on the other hand provides additional problems in the system design: actually, to make this work, in each receiver it must be possible to distinguish the different

signals, avoiding cross-detection of targets. In other words, the difference in time of arrival must be adequately mitigated in the matched filtering to avoid that the echo from the the waveform '*a*' is recognized as a target after the filter matched on the waveform '*b*'. This leads to the conclusion that with multiple and widely separated radar devices very low cross-correlation codes must be used. [28] and [29] focus about this issue, suggesting quasi-orthogonal codes so to allow multiple simultaneous transmission. Alternatively, transmitters may employ pseudo-random codes, such as noise codes as in [30], mitigating this effect. However, it has to be pointed out that whilst also processing techniques may allow to cancel cross-interferences, losses may arise from consistent differences in the measured RCS, reducing the low cross-correlation characteristic of the codes. An additional technique for separating signals after matched filtering is the usage of 'frequency diversity', when each transmitter works on a different carrier frequency. Although in this case waveform diversity is not important anymore, whereas the separation is allowed by the multiple carriers, the higher costs in terms of frequency occupation do not always make this solution easily feasible.

A good introduction to netted radars, including applications for tracking, is in [31, 32, 33] where basic concepts are introduced. However, they investigated principally the case of one transmitter and multiple bistatic receivers. More detailed studies on the Recently [34, 35, 36, 37, 38] investigated further the topic of multistatic radar, providing an insight in particular for the scheduling, the hardware and the sensitivity and the ambiguity function.

Finally, multistatic collection and analysis of data is a concept that has been recently re-developed in MIMO systems. Although it is recognized that a huge quantity of papers and publications has been produced in the literature about MIMO for communication systems, where the improvements in performance achievable in terms of capacity of the communication channel are shown to be very significant, publications about MIMO as applied to radar systems have become relevant only in the last couple of years, as interest in this topic has developed only recently.For brevity and relevance to this research, we only examine the literature relevant to the MIMO and distributed radar concept.

Publications from [39] to [48] are about MIMO communication systems. These are of limited interest if applied directly to the topic discussed in this thesis.

However, they provide a starting point to evaluate the migration from MIMO communication to MIMO radar systems. In particular, [39] describe in detail the full background on MIMO wireless. The other publications focus on specific problems, such as multipath, spectral efficiency and interference cancellation. However, whereas the MIMO concept has been developed for communication systems, most of these publications develop and investigate theoretical aspects which are not exactly related to a radar approach to the topic and have to be reconsidered if they are to be applied to radars.

Most relevant for the purposes of this thesis are the first papers on MIMO radar systems, e.g. from [49] to [54], in which the authors stressed the point that a MIMO radar system operating in the 'spatial diversity' mode manages to take advantage of effects, such as glint, that in conventional radar systems introduce a loss in achievable performance. This part will be reviewed in detail as it is the most relevant for this proposed work.

So far it generally stands out that a distributed MIMO radar system makes use of orthogonal signals on transmit and have M transmitting and N receiving antennas in order to be able to distinguish between the signals with a bank of matched filters. Furthermore, the RCS responses of a common target are assumed to be independent and to have uncorrelated amplitudes and phases.

In [49], that is the starting point of the concept of MIMO radar systems, the authors develop a general approach to the problem together with a model for the received signal under the assumption of additional white Gaussian noise. Here the most relevant concept is that radars have to be far away from one another in order to exploit spatial diversity. This is clearly stated when the authors demonstrates that the spacing d_t between the antennas should be

$$d_t \geq \frac{\lambda R}{D} \tag{2.1}$$

where R is the distance of the target, λ the wavelength, D the dimension of the target. Here authors highlight in few paragraphs that with MIMO systems it is possible to distinguish more than one object within one resolution cell. This is an idea that should have been developed as the benefits that it might yield to the concept of MIMO applied to radar systems are considerable. Unfortunately the

background of this paper is in the communications systems: this is clear when the Cramer-Rao bound for the performance is here developed under the hypothesis of a multistatic Swerling II-distributed RCS.

Publications [50] and [51], from the same authors, investigate further the MIMO application to radar systems. As [51] is a more complete work on spatially distributed MIMO radar systems, where the authors express the MIMO radar system they developed in full, also expanding concepts present in the previous works, it is worth to give a full and deep critique on it.

Here it is assumed that there are M transmitters and N receivers and that the waveforms are distinguishable after matched filtering. The authors often refer to 'orthogonal' waveforms, as in the communications system. In a radar system background it is more accurate to speak about 'low-cross-correlation' waveforms, as every incoming signal is passed into one or more matched filters in parallel that perform a correlation with one or more waveforms. If the target is present, all the transmitted waveforms are received: the incoming signal is processed through a filter bank and M signals are available at its output. Then, considering this process for N receiving antennas a total of MN signals can be processed by entire system. In these papers all the outputs are packed into a vector $\mathbf{x}$, where the q^{th} element can be expressed as below:

$$x_q = r_k * s_h \tag{2.2}$$

and r_k is the signal received by the k^{th} antenna, s_h is the hk^{th} transmitted waveform, $k = 1..N$, $h = 1..M$ and $q = (k-1)M + h$. Under these assumptions $\mathbf{x}$ is as follows:

$$\mathbf{x} = \begin{cases} \mathbf{n}, & H_0, \\ \sqrt{\frac{E}{M}}\boldsymbol{\alpha} + \mathbf{n}, & H_1, \end{cases} \tag{2.3}$$

where E is the total supplied power, $H_{1/0}$ is the hypothesis of target respectively present/not-present, $\mathbf{n}$ is Gaussian white complex noise, supposed to be $\sim CN\left\{0, \sigma_n^2 I_{MN}\right\}$, and $\boldsymbol{\alpha}$ a value taking into account all the parameters of the radar equation, included the phase-shift due to the path length and the transmitted energy of the signal. In these papers, for the sake of simplicity, $\boldsymbol{\alpha}$ has been

assumed as $\sim CN\left\{0, \sigma_n^2 I_{MN}\right\}$, i.e. normalization has been applied to the signal and noise powers.

Furthermore here the authors present a Likelihood Ratio Test (LRT) developed for this system and the analysis of its resulting performance. It is convenient here to report in more details some achievements as they provide a background and a starting point for the results presented in this work. As is well known, the optimal detector in this sense is given by

$$\log \frac{p(\mathbf{r}|H_1)}{p(\mathbf{r}|H_0)} \underset{H_0}{\overset{H_1}{\gtrless}} \lambda, \tag{2.4}$$

where $p(\mathbf{r}|H_1/0)$ is the PDF under the hypotheses of target respectively present/not-present, and λ is the threshold set on the probability of false alarm. Under the assumptions on n it is demonstrated that this structure for the detector is equivalent to the following:

$$\|\mathbf{x}\|^2 \underset{H_0}{\overset{H_1}{\gtrless}} \lambda, \tag{2.5}$$

From equation (2.3) it has been inferred that, under the assumption for $\mathbf{n}$ and $\boldsymbol{\alpha}$, $\mathbf{x}$ is the realization of a Gaussian random variable even when the target is present. By this it has been possible to write in closed form the performance of spatial MIMO. From a mere statistical point of view the sum of the squared value of L Gaussian random variables generates a chi-square random variable with L degrees of freedom. In the specific case, the PDF of $\xi = \|\mathbf{x}\|^2$, where each element of $\mathbf{x}$ is a complex Gaussian random variable, will be a chi-squared PDF with $2MN$ degrees of freedom. This can be expressed as follows:

$$p(\xi) = p(\|\mathbf{x}\|^2) = \begin{cases} \frac{\sigma_n^2}{2}\chi^2_{2MN}(\xi), & H_0, \\ \left(\frac{E}{2M} + \frac{\sigma_n^2}{2}\right)\chi^2_{2MN}(\xi), & H_1, \end{cases} \tag{2.6}$$

where the variances has been divided of a factor 2 in order to consider both real and imaginary parts of the complex Gaussian variables. Then the probability of

false alarm can be written as:

$$P_{FA}(\lambda) = \Pr\left\{\frac{\sigma_n^2}{2}\chi^2_{2MN}(\xi) \geq \lambda\right\} = \Pr\left\{\chi^2_{2MN}(\xi) \geq \frac{2\lambda}{\sigma_n^2}\right\}, \tag{2.7}$$

so, inverting this formula, the threshold guaranteeing a certain false alarm rate is given by:

$$\lambda = \frac{\sigma_n^2}{2} F^{-1}_{\chi^2_{2MN}}(1 - P_{FA}), \tag{2.8}$$

where $F^{-1}_{\chi^2_{2MN}}(z)$ denotes the inverse cumulative distribution of the chi-squared PDF computed in z.

As $\mathbf{x}$ has a chi-squared distribution when the target is present (equation (2.6)), it is possible to achieve a closed form also for the probability of detection:

$$\begin{aligned} P_d(\lambda) &= \Pr\left\{\left(\frac{E}{2M} + \frac{\sigma_n^2}{2}\right)\chi^2_{2MN}(\xi) > \lambda\right\} = \\ &= \Pr\left\{\chi^2_{2MN}(\xi) > \frac{2\lambda}{\frac{E}{M} + \sigma_n^2}\right\} = \\ &= 1 - F_{\chi^2_{2MN}}\left(\frac{\sigma_n^2}{\frac{E}{M} + \sigma_n^2} F^{-1}_{\chi^2_{2MN}}(1 - P_{FA})\right). \end{aligned} \tag{2.9}$$

This is the utmost preliminary result in [51].

Moreover in these publications comparisons between the MIMO system and an array of antennas and a MISO (Multiple Input, Single Output) system are reported. Although the shown results represent a first sight into MIMO potentialities, these publications are still written for a communication approach to the problem, as, for example, plots of p_d (probability of detection) vs. p_{fa} (probability of false alarm) are reported.

At a first stage a Gaussian model of the variables under observation is a reasonable choice, as a closed form can be very useful to compute and then to compare the system performance. Unfortunately most targets do not have a noise-like scattering behaviour and the PDF associated with their RCS measurements can be complicated. As soon as secondary or additional non-Gaussian effects

such as those of high resolution clutter are considered, it can be extremely hard, if not impossible, to achieve a closed form expression for the performance.

In [53, 54] the same idea of MIMO as discussed in this thesis is developed. In these recent publications, the authors distinguish a MIMO system with widely separated antennas from a multistatic system through "the joint processing of signals for transmission and reception". At the same time they provide a quite precise description of what their system, they refine the law for determining the minimum distance between the elements to allow angular diversity, they also discuss the ambiguity function of such a system and finally they provide a comparison of the detectors.

Papers [55, 56] stress the point on the necessity of having a number of waveforms with particular low cross correlation properties in order to make MIMO work. Although authors here do not investigate the effects of having a number of many antennas in transmission and reception, they develop particular polyphase codes, with a certain grade of tolerance to Doppler. As they point out, without low-cross-correlation codes, MIMO radar systems are not feasible unless it is possible to distinguish during the processing the several waveforms in transmission for merging and exploiting in a further processing all the multistatic and increased information gathered.

It has to be acknowledged that other authors, as from [57] to [66], used the MIMO as an array of antennas ([67] is a good book for understanding the basic principles of these electronic systems) for beamforming using multiple orthogonal signals. These are vaguely or not at all related to the work proposed in these pages, so just a brief summary is given. Within these publications, a significant survey of MIMO radar systems with both co-located and separated antennas is provided in [57] by contributions from different authors. Worth of interest are also (i) the formalization in [58] of the model of the channel matrixes as function of time and of their effect on the final pdf of the received signal and (ii) the overall analysis of the MIMO communication channel in [59].

In [60] authors develop an expression for the performance in case of a general coloured noise. This paper includes also a first study about performance in clutter, although it is still done in a communication way, expressing the Chernoff upper and lower bound limits for the probability of detection. A description of the

mutual information exchangeable is provided as well. A limit of this paper is that it considers fully known and constant the channel matrix, while, especially in the radar field, it is well known that it may change in time. Thus in real systems it is necessary to trade this knowledge with an estimation of the real channel matrix that has to be appropriately updated in time. This publications provides a deeper overview of the capacities of the MIMO system and nonetheless a better formulation of the system model.

As the MIMO radar is a relatively new concept in the scientific literature, most of the papers published at the beginning of this work did not take into account many fundamental aspects, such as the CFAR capabilities of the overall system, the performance achievable in most of the standard operative configurations, the response to different target models and the loss of performance due to mismatches in estimating most of the parameters involved in the several usages of a radar system.

Finally, it is worth of mention the publication [66]. Here the authors provide a precise, concise and quite exhaustive description of MIMO as with co-located antennas, addressing many of the issues described in previous publications through the search of eigenvalues and eigenvectors of a particular system. In particular, terming $\mathbf{s}$ the multi-waveform transmitted signals, the best configuration for such a system in terms of maximization of SNR and optimization of the resources in transmission and reception is given by the solution of the following constrained system

$$\begin{aligned} &\max_{\mathbf{s}} \left\{ \mathbf{s}' E\left\{ H' H \right\} \mathbf{s} \right\} \\ &s.t. \begin{cases} E\left\{ H' H \right\} \mathbf{s} = \lambda_{\max} \mathbf{s} & \text{(transmitter)} \\ H_w = R^{-1} H_T & \text{(receiver)}, \\ H = H_T H_w \end{cases} \end{aligned} \tag{2.10}$$

where $'$ is the Hermitian operator,H_T is the multi-waveform channel matrix and R is the multiwaveform nuisance correlation matrix, which can include clutter, multipath and jammerers, $E\{x\}$ is the expected value of x and finally $\lambda_{\max}$ is the maximum of the eigenvalues of $E\{H'H\}$. Although this result comes directly from an extension of the single-waveform problem, the analysis provided by the authors suggests to use multiple orthogonal waveforms in a first moment where

the environment is still unknown and therefore to switch to more conventional methods or reduce the number of transmitted waveforms to achieve the best results reducing the overall complexity of the system. However, whereas this topic is of marginal interest for this thesis, publications on MIMO radar systems with co-located antennas will not be discussed further.

Chapter 3

Fundamentals of monostatic and bistatic radars

In this Chapter the basic principles of monostatic and bistatic radars are described. This provides a well understood context in which multistatic systems can be subsequently introduced and examined.

The underlying concept of radar systems is to transmit an EM signal and receive the echo from objects that it intercepts in a, generally, unknown environment. The radar system then processes the signals appropriately to acquire as much information as possible. In most common applications, radar systems are applied to detect, locate and track targets. Alternatively another wide range of usage is in the field of imaging from aircraft or spacecraft systems. Radar systems can transmit continuous waves (CW), i.e. without solution of transmission, or pulses, i.e. transmitting for a relatively short time and receiving for the remaining time before another pulse is transmitted. In the rest of this work CW radars are not considered. In pulsed systems, it is evident that the shorter the pulse width, the higher the accuracy of the localization. However, a number of constraints limiting the lower duration of a single pulse are to be taken into account: the most common are (*i*) the frequency occupation of the signal, that can be considered at first as inversely proportional to its time duration (Section 3.2) and (*ii*) the peak and average power that the electronic physical devices are capable of handle.

In this Chapter a survey of the most common issues of monostatic and bistatic

systems and the trade-offs generally applied to compromise between the different requirements is reported. In particular, Section 3.1 introduces the matched filtering concept as in radar systems, in Section 3.2 the resolution as function of the bandwidth is described, in Section 3.3 the Doppler shift due to the velocity of a target is reported, Section 3.4 shows how the RCS of a target may change in multistatic systems, Section 3.5 presents the knowledge in modelling clutter and finally 3.6 gives an overview of the possible detection approaches that is possible to implement in a radar system.

3.1 The matched filtering

After the transmission of a waveform $s(t)$, with length T_s, the receiving antenna gathers all the returning echoes. As in all electronic device, thermal noise is always present in reception. Therefore, a simple model of the incoming signal $r(t)$ can be written as follows:

$$r(t) = H_{0/1}\alpha s(t - T) + n(t), \tag{3.1}$$

where $H_{0/1}$ is either 0 or 1 according to the absence or presence of a target generating an echo, α is an attenuating factor as in Section 3.4, $n(t)$ is the thermal noise and $s(t - T)$ is the echo of the target received T time after the transmission, with

$$T = \frac{2R}{c}, \tag{3.2}$$

where R is the target distance and c the speed of light.

It is widely recognized that 'matched' filtering of the received signal is the best approach to maximize the signal-to-noise ratio (SNR), under the hypothesis of white noise n, and therefore make the signal standing out against the noise. In this process the received signal $r(t)$ is processed through a filter whose impulse response $h(t)$ is equal to

$$h(t) = s^*(-t), \tag{3.3}$$

where * is the conjugate operator and the domain $-t$ indicates that its shape is specular to the original one. Adding a causality constraint, equation (3.3) can be written as

$$h(t) = s^*(T_s - t), \tag{3.4}$$

where T_s is the length of $s(t)$. The matched filtering process is valid for both monostatic and bistatic systems. The matched filter is used as it maximize the SNR of the received signal, as reported in [1].

3.2 Resolution

In pulsed radar the delay between the transmission and the reception of the backscattered waveform is directly dependent on the range of the target. For a not-compressed pulse of duration τ, i.e. for a signal that is different from 0 only in the interval of time between 0 and τ, the resolution Δr achievable for discriminating two targets relatively close can be expressed as in [1]:

$$\Delta r = \frac{c\tau}{2cos(\beta/2)}, \tag{3.5}$$

where c is the speed of light, β is the bistatic angle between the transmitter, the target and the receiver and the bandwidth of the signal B can be expressed as

$$B = \frac{1}{\tau}, \tag{3.6}$$

that leads to the conclusion that the resolution is given by

$$\Delta r = \frac{c}{2Bcos(\beta/2)}. \tag{3.7}$$

In the monostatic case $\beta = 0$ and therefore the following well-known expression is achieved:

$$\Delta r = \frac{c}{2B}. \tag{3.8}$$

Whereas in fact the resolution power of any waveform depends on its frequency bandwidth, rather than its time duration, which cannot be as wide as desired for a number of technical and organizational reasons (e.g. available frequencies for transmission, maximum bandwidth of the amplifiers and the antennas comprising the system, other communication devices using contiguous frequencies, fractional band ratio, etc...), in a short time the idea that it is more convenient to transmit compressed pulses, i.e. with a specific shape in time rather than rectangular ones, was developed. As a consequence it is common knowledge that compressed shorter signals have the same resolution as uncompressed longer.

3.3 Doppler frequency

After receiving a number of echoes from a target, it is possible to process them coherently to gather information about its Doppler frequency, and consequently its radial velocity. In general terms, the Doppler shift can be expressed as

$$f_D = \frac{1}{\lambda}\frac{\partial(R_{tx} + R_{rx})}{\partial t}. \tag{3.9}$$

Therefore, in a bistatic configuration a 0 Doppler frequency is associated to targets moving on the iso-range curves which are well known to be ellipses. Rearranging equation (3.9), the following can be expressed as

$$f_D = \frac{2V}{\lambda} cos\,(\delta)\, cos\left(\frac{\beta}{2}\right), \tag{3.10}$$

where δ is the angle between the velocity vector of the target and bisector of β, as in Figure 3.1. If $\beta = 0$,

$$f_D = \frac{2V}{\lambda} cos\,(\delta)\,, \tag{3.11}$$

that is the well known monostatic case.

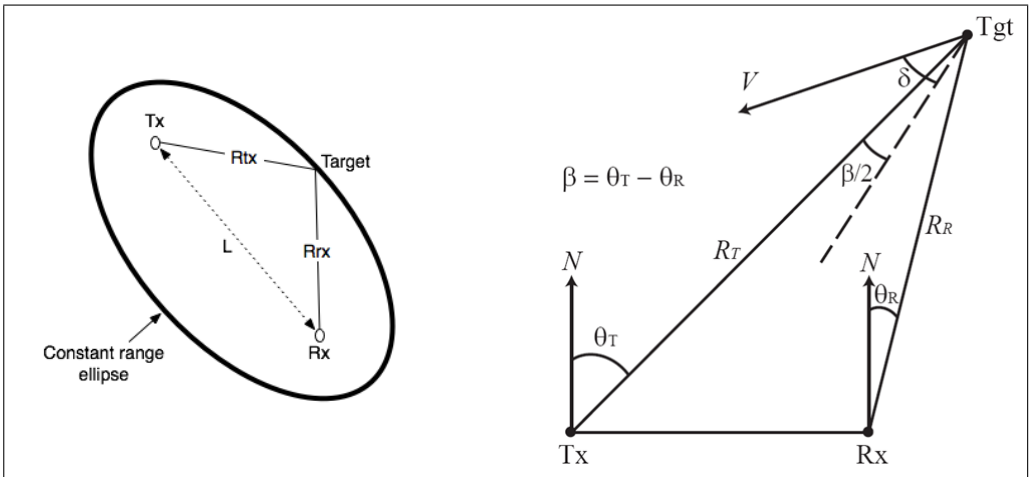

(a) Bistatic iso-range curve (b) Bistatic geometry for Doppler

Figure 3.1: Bistatic geometry

3.4 Radar Cross Section

There are diverse reasons behind the different RCS response of a target as a function of a number of the parameters of the radar. In a monostatic system differences in aspect angles produce a variety of backscattering levels. Whilst for particular reflectors, such as a dihedral or a flat plate (Figures 3.2 and 3.3 respectively) the backscattering variation as a function of the aspect angle has a sort of regularity, common targets, such as airplanes, helicopters, tanks, etc... are well known to change quite rapidly, e.g. within few consecutive scans, according to the range, size and geometry. Even few milliradians can have a severe impact on the measurable amplitude of the signal [1]. Figure 3.4 provides a simplified example of this concept.

In concept, bistatic RCS has the same behaviour as the monostatic. In particular, it has to be pointed out that simultaneous monostatic and bistatic measurements usually provides significantly different levels in the echo of the signal.

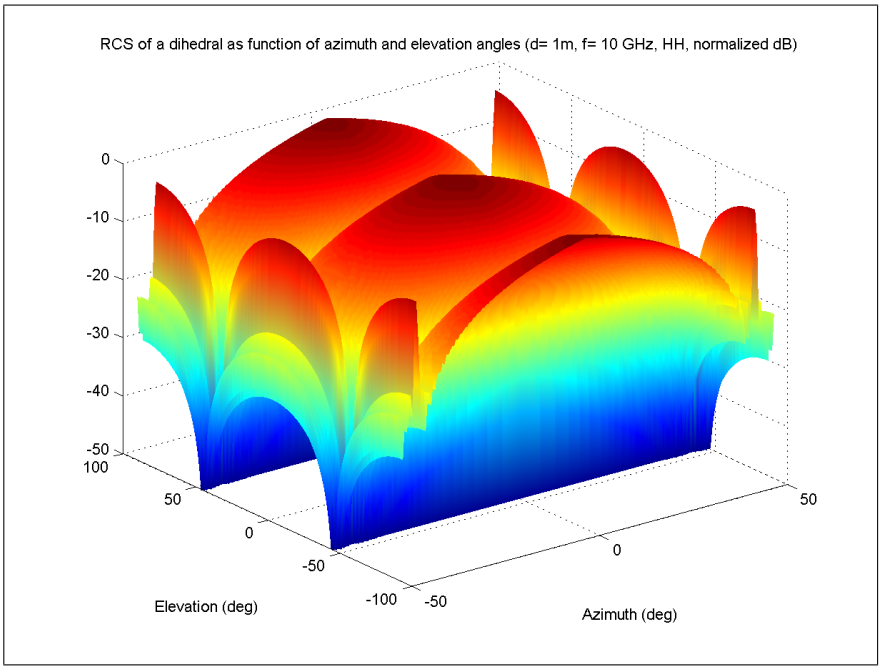

Figure 3.2: Monostatic RCS of a dihedral

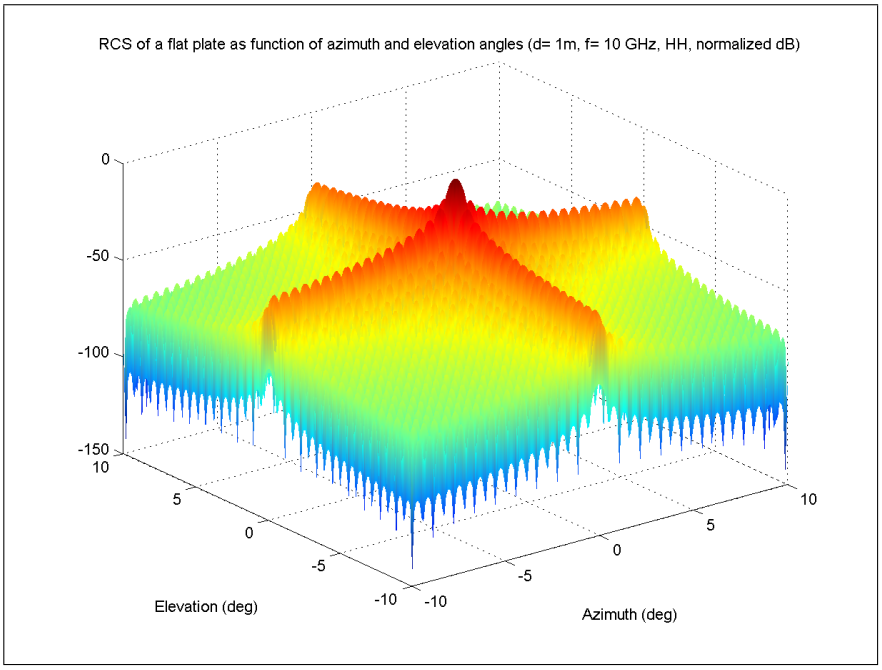

Figure 3.3: Monostatic RCS of a flat square plate

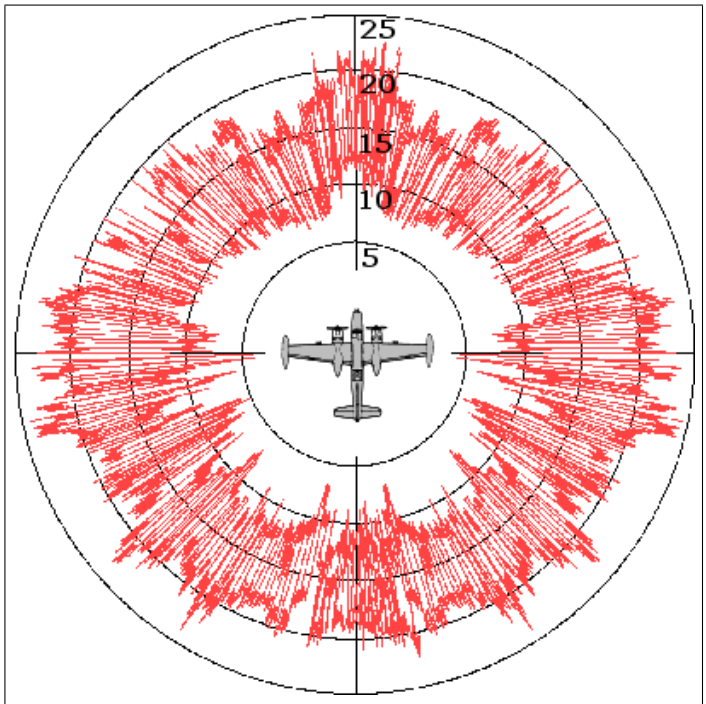

Figure 3.4: Monostatic RCS

3.5 Clutter

Clutter has been deeply investigated in the past, whereas it is present in most of the radar applications. Being reflected from the environment in which the targets are, clutter cannot usually be rejected with pattern design. Actually the clutter is usually represented as the sum of the elemental scatterers. As a consequence of the movement of each single component, a Doppler shift is generated. The spectrogram of the clutter can be quite spread across the frequencies, because of the single scatterers' movement. In some applications, such as weather forecasting, the main Doppler shift can be used to retrieve the speed of the wind. However, in most of the cases, the Doppler component due to the clutter can mask the velocity of real targets. Recently, sophisticated ways for removing clutter, creating specific nulls in the pattern of the antenna at specific times, e.g. STAP, have been developed. In the next sections, general model of clutter are presented,

together with some approximation of the way in which Doppler and wind speed are linked.

In more general terms, it has to be pointed out that, although the knowledge about monostatic and bistatic clutter is quite exhaustive, little is known about the correlation properties of monostatic and bistatic clutter samples acquired from the same area and at the same time. For this purpose, Section 11 shows a first insight to this topic.

3.5.1 Clutter models

There are 4 main models for describing clutter analytically. These models are widely adopted not only because they are a practical tool for describing statistically the clutter, but also because they fit the reality quite well. These are: (*i*) Gaussian, generally used for ground clutter, (*ii*) K and (*iii*) Log-normal, usually describing sea clutter, and finally (*iv*) Weibull, which can model both in different conditions.

It is widely accepted that echoes from the clutter can be written as the product of two independent random variables. Commonly it is written:

$$\mathbf{c} = \sqrt{\tau}\mathbf{x}, \tag{3.12}$$

where $\mathbf{x}$ is an m-dimensional complex Gaussian circular vector, termed 'speckle'. Statistically, $\mathbf{x}$ can be described as a 0-mean value vector with unit variance and correlation matrix $\mathbf{M}_x$, where clearly

$$\mathbf{M}_x = E\left\{\mathbf{x}\mathbf{x}^H\right\}. \tag{3.13}$$

Many authors use the compact writing

$$\mathbf{x} \sim CN\{0, \mathbf{M}_x\}. \tag{3.14}$$

τ is the 'texture' and represents the power associated to the speckle. It is worth pointing out that τ is a non-negative variable. The product model as in equation (3.12) has been shown to describe accurately the scattering mechanism. It has also to be pointed out clearly that, whilst the speckle $\mathbf{x}$ decorrelates in a short

time, usually comparable to multiples of the Pulse Repetition Interval (PRI), the texture τ decorrelates in a longer time, in the order of seconds, so within the time on target, τ can be considered constant.

Therefore, the four models described at the beginning of this Section differ from one another on the statistic of the texture. These are as in Table 3.1, where the mean value and the variance are as in the Table 3.2.

Distribution	Expression
Gaussian	$p(\tau) = \frac{\tau}{\sigma_\tau} \exp\left\{-\frac{\tau^2}{2\sigma_\tau}\right\}$
K	$p(\tau) = \frac{1}{\Gamma(\nu)} \left(\frac{\nu}{\mu}\right)^{\nu} \tau^{\nu-1} \exp\left\{-\frac{\nu}{\mu}\tau\right\}$
Weibull	$p(\tau) = \frac{k}{q} \left(\frac{\tau}{q}\right)^{k-1} \exp\left\{-(\tau/q)^k\right\}$
Log-Normal	$p(\tau) = \frac{1}{\sqrt{2\pi}\tau\sigma_{\log}} \exp\left\{-\frac{[\log(\tau) - T]^2}{2\sigma_{\log}^2}\right\}$

Table 3.1: Common probability densidty functions for the texture

Distribution	Mean	Variance
Gaussian	0	σ_τ
K	μ	$\frac{\mu^2}{\nu}$
Weibull	$q\Gamma\left(1 + \frac{1}{k}\right) = \mu$	$q^2\Gamma\left(1 + \frac{2}{k}\right) - \mu^2$
Log-Normal	$\exp\left\{\mu + \sigma_{\log}^2/2\right\} = \mu$	$\exp\left\{\sigma_{\log}^2 - 1\right\}\mu^2$

Table 3.2: Texture statistics

3.5.2 Spectral distribution

As reported at the beginning of this Section, clutter is generally comprised of the coherent sum of the echoes from a number of elemental scatterers. These includes leaves, drops of rain, snow flakes and waves. For the sake of simplicity, assume that the radar platform is not moving: whenever these single components move

within the same range cell, they add a Doppler shift on the clutter echoes. Whereas the speed of the single elements can vary significantly, it is usually possible to describe statistically the spectrum of the clutter as a random variable with a mean value, which is dependent on the average speed of the elements, and a variance, which has been shown [3] to be a function of the type of clutter, its average speed and some radar parameters as the wavelength, the angular velocity of the antenna and its aperture. It is clear that fixed clutter, such as buildings or rocks, do not have a Doppler shift and therefore in this case the spectrum is concentrated at the frequency $f = 0$.

As a result, the spectrogram of the clutter is spread over a number of frequencies. In addiction it is possible that two or more kinds of clutter (e.g. ground and rain clutter) are present within the same range cell. In this case the spectrogram can be made up of two or more components, as in a bimodal distribution.

Typical models for describing the spectrum $S_c(f)$ of the clutter are (*i*) the Dirac function (fixed clutter), (*ii*) Gaussian, (*iii*) two-sided exponential, (*iv*) power law, (*v*) autoregressive, (*vi*) Lorentzian (i.e., autoregressive of order 1) and finally and (*vii*) Voigtian (convolution of the Gaussian and Lorentzian), as reported in Table 3.3, where A is a general constant that takes into account the power of the clutter spectrum (in some formulas, for convenience, it groups other constants which are usually reported as separated), f_0 its the centroid of the spectrum, β is a constant linked to the decay of the clutter spectrum, λ is the wavelength, α is generally 2 or 3 in sea clutter modelling, p usually varies between 2 and 5, ϵ_n is white noise and finally f_V is a scale frequency for the Voigtian function.

Dirac	$S_c(f) = A\delta(f)$
Gaussian	$S_c(f) = \frac{A}{\sigma_f} \exp\left\{-\frac{(f-f_0)^2}{2\sigma_f^2}\right\}$
2-sided exponential	$S_c(f) = \frac{\beta\lambda}{4} \exp\left\{-\frac{\beta\lambda}{2}\lvert f\rvert\right\}$
Power law	$S_c(f) = A/f^{\alpha}$
Autoregressive	$c[n] = \epsilon_n - \sum_{i=1}^{p} a_j c[n-j]$
Lorentzian	$S_c(f) = \frac{A}{(f-f_0)^2 + A}$
Voigtian	$S_c(f) = \frac{A}{\pi} \int_{-\infty}^{+\infty} \frac{e^{-x^2}}{\left(\frac{f-f_0}{f_V} - x\right)^2 + A^2} dx$

Table 3.3: Typical models for the clutter spectrum

Figure 3.5 shows an asymmetrical spectrum, which is in general typical of sea clutter, of real clutter data (HH and VV components) and the corresponding fittings with sums of a Gaussian and a Voigtian functions.

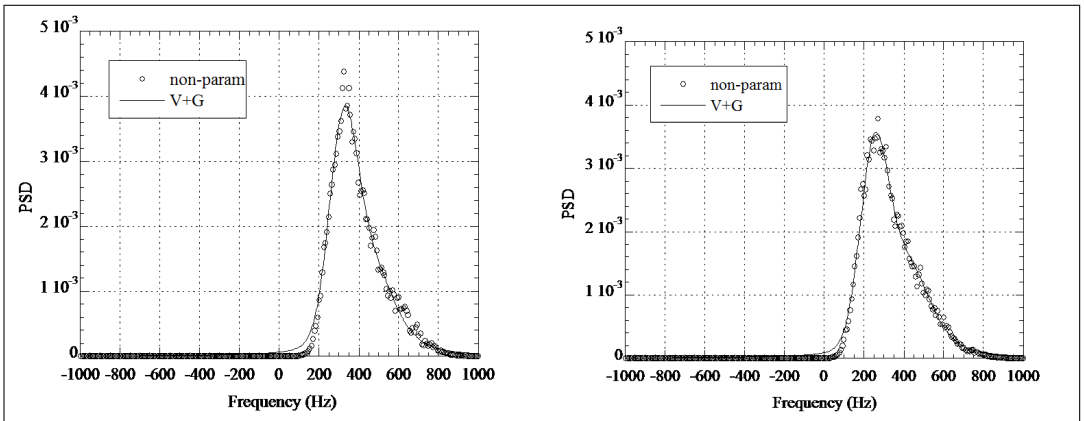

(a) HH spectrum and fitting

(b) VV spectrum and fitting

Images courtesy of Prof. Maria Sabrina Greco, Università di Pisa

Figure 3.5: Clutter spectra and fittings

3.6 Detection approach

In reception two assumptions are usually considered in processing the signals: target present or target not present. This is commonly described as follows:

$$r(t) = \begin{cases} n(t), & H_0, \\ s(t - t_0) + n(t), & H_1, \end{cases} \tag{3.15}$$

where H_0 and H_1 indicate the hypotheses of target not present and present, respectively, and n groups all the possible nuisance that can affect the radar. Under this assumption, the radar approach to signal processing consists in keeping the probability that a target is declared when it is not present as low as possible, i.e. within predetermined limits, allowing at the same time a reasonably high probability of detecting the target when present.

Assuming, for instance, to declare detection when the power of the received signal after matched filtering $\tilde{r}$, where

$$\tilde{r} = r * h = (s + n) * h = \tilde{s} + \tilde{n}, \tag{3.16}$$

is greater than a given threshold θ, the decision rule is as follows:

$$\begin{cases} |\tilde{r}|^2 \geq \theta & \Rightarrow \quad D_1 \\ |\tilde{r}|^2 < \theta & \Rightarrow \quad D_0. \end{cases} \tag{3.17}$$

Therefore in a decision process, four events are possible, clearly function of the output of the detector D_i and the actual presence of the target H_i, $i = 1, 2$. These are as in Table 3.4.

	H_0	H_1
D_0	Correct	Wrong
D_1	Wrong	Correct

Table 3.4: Decisions in the decision process

Correct decisions are obviously desirable. However, being the noise and the target echoes random variables, rather than certain signals, wrong decisions can happen

and therefore the decision rule has to be designed to avoid them as much as possible. From a statistical point of view, then, Table 3.4 can be written as Table 3.5 where the probabilities P of correct or wrong detection are expressed clearly.

	H_0	H_1
D_0	$P(\|\tilde{r}\|^2 < \theta \| H_0) = P(\|\tilde{n}\|^2 < \theta)$	$P(\|\tilde{r}\|^2 < \theta \| H_1) = P(\|\tilde{s} + \tilde{n}\|^2 < \theta)$
D_1	$P(\|\tilde{r}\|^2 < \theta \| H_0) = P(\|\tilde{n}\|^2 \geq \theta)$	$P(\|\tilde{r}\|^2 < \theta \| H_1) = P(\|\tilde{s} + \tilde{n}\|^2 \geq \theta)$

Table 3.5: Statistics in the decision process

Usually it is referred to these probabilities as:

- Probability of false alarm: $P_{fa} = P(|\tilde{n}|^2 \geq \theta)$ – This is the probability of declaring detection when no target is present;
- Probability of detection: $P_D = P(|\tilde{s} + \tilde{n}|^2 \geq \theta)$ – This is the probability of a correct detection of a target;
- Probability of missed detection: $P_{MD} = P(|\tilde{s} + \tilde{n}|^2 < \theta)$ – This is the probability of missing the detection of a target.

The probability of not detecting a target when it is not present has always had negligible interest and therefore it is still not In turns, these probabilities can be expressed as follows:

$$\begin{aligned} P_{fa} &= \int_{\theta}^{+\infty} p(y = |\tilde{n}|^2)\, dy, \\ P_D &= \int_{\theta}^{+\infty} p(y = |\tilde{s} + \tilde{n}|^2)\, dy, \\ P_{MD} &= \int_{0}^{\theta} p(y = |\tilde{s} + \tilde{n}|^2)\, dy \quad = \quad 1 - P_D. \end{aligned} \tag{3.18}$$

It is worth highlighting clearly, in force of equation (3.18), the following two set of limits:

$$\begin{cases} \lim\limits_{\theta \to 0} P_{fa} &= 1, \\ \lim\limits_{\theta \to 0} P_D &= 1, \end{cases} \tag{3.19}$$

and

$$\begin{cases} \lim\limits_{\theta\to+\infty} P_{fa} &= 0, \\ \lim\limits_{\theta\to+\infty} P_D &= 0. \end{cases} \tag{3.20}$$

These limits are fundamental in radar systems, since they clearly demonstrate that it is not possible on average to achieve full detection of a target keeping the number of false alarms moderate. Alternatively, it is not possible to avoid completely false alarms, keeping the capacity of detection.

As a consequence, in radar system it is common to use the Neyman Pearson approach, which consists in (*i*) fixing a threshold θ so to constrain the P_{fa} within a predetermined value and at the same time (*ii*) minimizing the P_{MD}, i.e. maximizing the P_D. Whereas

$$|\tilde{s} + \tilde{n}|^2 \leq (|\tilde{s}| + |\tilde{n}|)^2 = |\tilde{n}|^2 \left(\sqrt{SNR} + 1\right)^2 \tag{3.21}$$

and

$$|s + n|^2 \geq (|\tilde{s}| - |\tilde{n}|)^2 = |\tilde{n}|^2 \left(\sqrt{SNR} - 1\right)^2, \tag{3.22}$$

maximizing the SNR increases the P_D. For this purposes, a matched filter as described in 3.1 is usually employed. A detector with a limited P_{fa} is usually termed as guaranteeing the CFAR (Constant False Alarm Rate) condition. From a mathematical point of view, it can be shown that the Neyman Pearson approach is a problem of constrained optimization using a Lagrange multiplier, say ξ. The rule can be expressed as

$$\max_{\theta} \left\{ P\left(|\tilde{r}|^2 \geq \theta | H_1\right) - \xi \left[P\left(|\tilde{r}|^2 \geq \theta | H_0\right) - P_{fa} \right] \right\}. \tag{3.23}$$

The most used CFAR techniques are the LRT (Likely Ratio Test), its more general version GLRT (Generalized LRT) and the CA-CFAR (Cell Average CFAR). The first two rules decide according to

$$\frac{p\left(\tilde{r}|H_1\right)}{p\left(\tilde{r}|H_0\right)} \underset{H_0}{\overset{H_1}{\gtrless}} \theta_{LRT} \tag{3.24}$$

in the LRT case or to

$$\frac{\max\limits_{P}\{p(\tilde{r}|H_1)\}}{\max\limits_{P}\{p(\tilde{r}|H_0)\}} \underset{H_0}{\overset{H_1}{\gtrless}} \theta_{GLRT} \tag{3.25}$$

in the GLRT case, where each pdf is maximized on the parameters P on which depends. The CA-CFAR will be described and used in Chapter 6.

Other decision rules, such as the MEP (Minimum Error Probability) and the Bayes minimum risk, are widely described in literature of decision theory, but are rarely applied in radar systems. In particular, the MEP minimizes the following total error probability of error P_e:

$$P_e = P(H_0)\,P(D_1|H_0) + P(H_1)\,P(D_0|H_1)\,, \tag{3.26}$$

i.e. the sum of P_{fa} and P_{MD}, weighted with the probability of the events H_0 and H_1, respectively. Whereas

$$P(D_0|H_1) = P_{MD} = 1 - P_D = 1 - P(D_1|H_1)\,, \tag{3.27}$$

equation (3.26) can be rewritten as

$$\begin{aligned} P_e &= P(H_0)\,P(D_1|H_0) + P(H_1)\,(1 - P(D_1|H_1)) = \\ &= P(H_1) + \{P(H_0)\,P(D_1|H_0) + P(H_1)\,P(D_1|H_1)\} = \\ &= P(H_1) + \left\{P(H_0)\,P_{fa} + P(H_1)\,P_D\right\}. \end{aligned} \tag{3.28}$$

By minimizing the part into curly brackets, this criterion is therefore equivalent to the Neyman-Pearson's when $P(H_0)$ and $P(H_1)$ are known and equal to $\frac{1}{2}$. However, since this is not always the case in radar system and the two latter probabilities are unknown, this detector, although particularly efficient, is not commonly used.

Similarly The Bayer minimum risk is uncommon. This detector tries to minimize the following cost function C:

$$C = \sum_{i=0}^{1} \sum_{j=0}^{1} C_{i,j} P\left(H_j\right) P\left(D_i | H_j\right). \tag{3.29}$$

Whereas the costs of correct decisions cannot be different from 0, i.e. $C_{0,0} = C_{1,1} = 0$, the cost function can be reduced to

$$\begin{aligned} C &= C_{1,0} P\left(H_0\right) P\left(D_1 | H_0\right) + C_{0,1} P\left(H_1\right) P\left(D_0 | H_1\right) = \\ &= C_{1,0} P\left(H_0\right) P_{fa} + C_{0,1} P\left(H_1\right) P_{MD}, \end{aligned} \tag{3.30}$$

which is a generalized version of the MEP detector.

Finally, it has to be pointed out that in more general terms the decision rule can be more complicated. A generalized expression can be

$$\begin{aligned} f\left(\tilde{\mathbf{r}}\right) \geq \theta\left(\tilde{\mathbf{r}}\right) &\Rightarrow D_1 \\ f\left(\tilde{\mathbf{r}}\right) < \theta\left(\tilde{\mathbf{r}}\right) &\Rightarrow D_0, \end{aligned} \tag{3.31}$$

where $\mathbf{r}$ a vector or a matrix comprised of either a number of received signals at different pulses, ranges or elementary antennas (the latter within the same array) and $f(\mathbf{x})$ and $\theta(\mathbf{x})$ are arbitrary (but appropriate) functions of $\mathbf{x}$.

Chapter 4

Systems

In recent times the idea that a radar network can offer improved and more versatile performance has been progressively developed (from [49] to [27]). A radar network usually consists of a number of transmitter and receivers that can be co-located or not. Although a robust synchronization has to be performed and an increased quantity of data has to be jointly processed, the achievable benefits can be worth of these efforts. These are, for example:

(i) an improved detection capability due to multistatic scintillation of the target, that enhance the possibilities of getting one or more sharp echoes from the target,

(ii) a joint estimation of most the target position and DOA, that increase the resolution power of the single nodes and, consequently,

(iii) the capability of resolving multiple target within the resolution cell on one single node,

(iv) increase the information in the same bandwidth occupation using low-cross-correlation codes,

(v) an increased ECCM capabilities.

In this section simple models for describing the signals are reported together with the first results achieved. MIMO systems operate incoherently. The netted

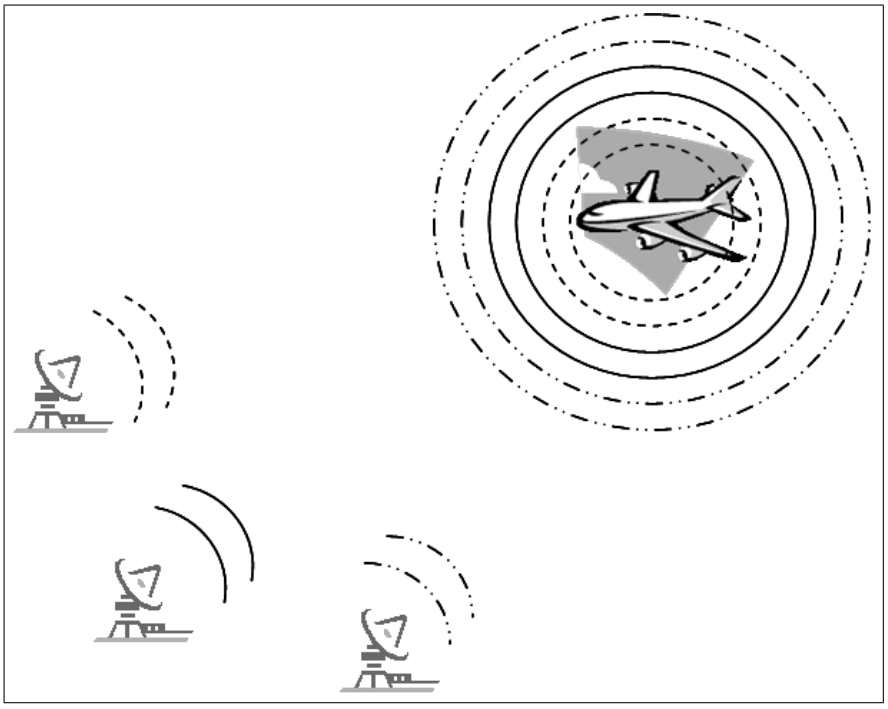

Figure 4.1: MIMO spatial diversity and netted radar configuration

radar systems operate totally coherently. To fairly compare the four systems the same amount of total energy in transmission has been assigned to the antennas.

4.1 Spatial MIMO system

The MIMO spatial diversity model that will be described have the conventional form of MIMO that has appeared in the literature ([49], [50], [51]) and hence provides a useful start point for these studies. This form of MIMO radar system exploits measurements of independent samples of target scattering as the basis for improving the probability of detection.

Each antenna points at the target from a different aspect angle, so that the measurement of RCS into a certain receiver can differ from the other measurements of several dB or more, i.e. independent spatial samples of the scattering from the target are obtained. This implies that the model assumed for the target RCS is noise-like. This is a questionable assumption but provides a useful jump off point from previously published research ([49], [50], [51]). The experimental set up is

shown schematically in Figure 4.1 and the mathematical description is formulated as:

$$r_k(t) = \sum_{m=1}^{MN} \alpha_{k,m}(t)\, s_m\left(t - \frac{R_{m,k}}{c}\right) + n_k(t), \tag{4.1}$$

supposing $s_m(t)$ the m^{th} transmitted signal, $n_k(t)$ white Gaussian noise, $R_{m,k}$ the distance covered by the signal, and

$$\alpha_{k,m}(\sigma) = \sqrt{\frac{P_t}{M}} \sqrt{\frac{G_{tx} G_{rx} \lambda^2 \sigma}{(4\pi)^3 R_{m-ta}^2 R_{ta-k}^2}} \exp\left\{-j\frac{2\pi R_{m,k}}{\lambda}\right\} \tag{4.2}$$

a coefficient including the amplitude and the phase of the received signal, where G_{tx} and G_{rx} are respectively the gains of the transmitting and receiving antennas, σ the RCS of the target, P_t the transmitted power, R_{m-ta} and R_{ta-k} the distance transmitter-target and target-transmitter respectively. From equation (4.1) it is clear that the autocorrelation of the received signal will be made of four terms, these are:

1. sum of the auto-correlations $R_{s,m}(\tau)$ of the transmitted waveforms, where *s,m* stands for the m^{th} signal, i.e. $\sum_{m=1}^{M} \|\alpha_{k,m}(\sigma)\|^2 R_{s,m}(\tau)$,
2. the sum of the cross-correlation between two of the transmitted waveforms, i.e. $\sum_{m=1}^{M} \sum_{\substack{n=1 \\ n \neq m}}^{M} \alpha_{k,m} \alpha_{k,n}^{*} R_{m,n}(\tau + \tau_{m,n,k})$, where $\tau_{m,n,k}$ takes into account the difference in the paths,
3. the sum of the cross-correlation between the transmitted waveforms and the noise, i.e. $\sum_{m=1}^{M} \alpha_{k,m}(\sigma)\, s_m\left(t - \frac{R_{m,k}}{c}\right) \otimes n_k(t)$, and finally
4. the auto-correlation of the noise, i.e. $\sigma_n^2 \delta(\tau)$, where $\delta(\tau)$ is 1 for $\tau = 0$, 0 otherwise.

So, all together, it is possible to write the auto-correlation of the received signal as

$$
\begin{aligned}
R_k(\tau) = r_k(t) \otimes r_k(t) = \\
= \sum_{m=1}^{M} \|\alpha_{k,m}(\sigma)\|^2 R_{s,m}(\tau) + \sum_{m=1}^{M} \sum_{\substack{n=1 \\ n \neq m}}^{M} \alpha_{k,m} \alpha_{k,n}^{*} R_{m,n}(\tau + \tau_{m,n,k}) + \\
+ \sum_{m=1}^{M} \alpha_{k,m}(\sigma) s_m \left(t - \frac{R_{m,k}}{c} \right) \otimes n_k(t) + \sigma_n^2 \delta(\tau)
\end{aligned}
\tag{4.3}
$$

where with $\otimes$ we symbolize the correlation operator, function of the time delay τ . As the received signal will be processed in each receiver through a bank of filters that are matched to the different waveforms, it has more sense to express the result of the cross-correlation of the received signal with one, say the m^{th}, of the transmitted waveforms. This is:

$$
\begin{aligned}
r_k(t) \otimes s_m(t) = \\
\alpha_{k,m} R_m(t) + \alpha_{k,m} R_{m,n}(t + \tau_{m,n,k}) + n_k(t) \otimes s_m \left(t - \frac{R_{m,k}}{c} \right)
\end{aligned}
\tag{4.4}
$$

The two latter elements in equation (4.4) represent the incoming noise into the processing scheme. Apart from the one directly dependant from the noise/jamming present in reception, this equation highlights how the use of low-cross-correlation codes is vital for the discussed system in order not to affect the discrimination of the transmitted waveforms and therefore to lose all the benefits of multistatic data collection.

4.2 Frequency MIMO system

Here we introduce a novel form of MIMO radar that attempts to exploit frequency rather than spatial diversity. The principle relies on the simultaneous transmission of multiple independent frequencies from each element of an array antenna as shown schematically in Figure 3.2. This has the advantage of being able to use the MIMO technique in a compact single radar site form.

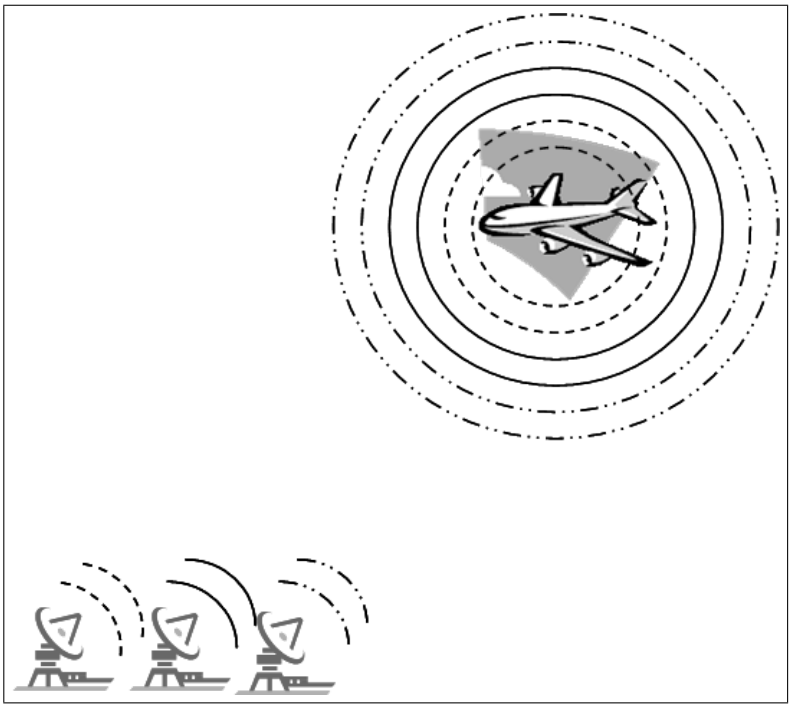

Figure 4.2: Frequency MIMO diversity and configuration

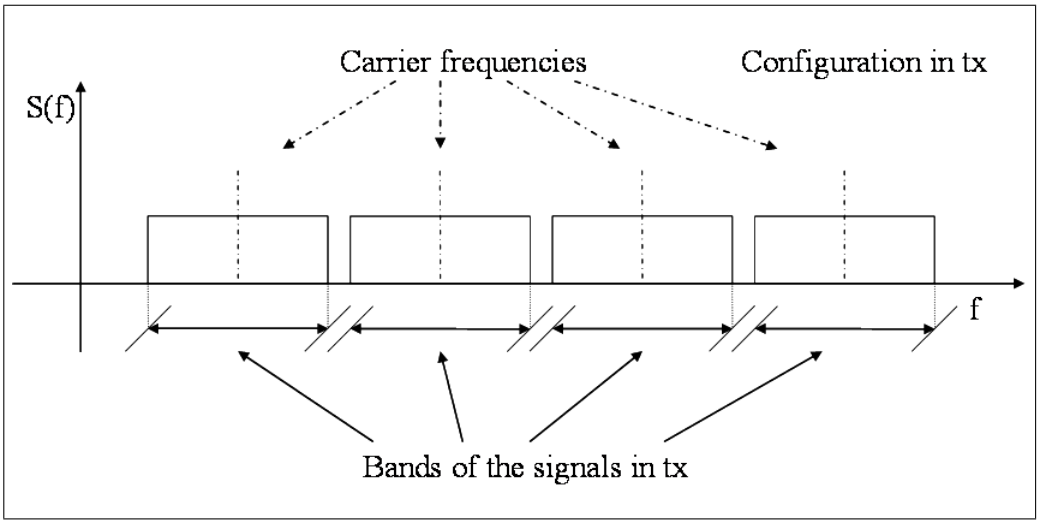

Figure 4.3: frequency MIMO diversity model

The bands and the carrier frequencies of the M transmitted signals have to be chosen such that they do not overlap and are not adjacent, in order to (i) get independent measurements of the RCS of the target after an appropriate matched filtering and to (ii) avoid the Doppler-shifted spectra of the received signals to overlap. Clearly, this will be dependent on the complete target scattering function (i.e. over all angles, frequencies and polarizations). Mathematically we have:

$$r_k(t) = \sum_{m=1}^{M} \alpha_k(\sigma, f_m)\, s_m\left(t - \frac{R_{m,k}}{c}\right) + n_k(t), \tag{4.5}$$

supposing f_m to be the carrier frequency of the m^{th} signal,

$$\alpha_{k,m}(\sigma, f_m) = \sqrt{\frac{P_t}{M}} \sqrt{\frac{G_{tx} G_{rx} \lambda_m^2 \sigma(f_m)}{(4\pi)^3 R_{m-ta}^2 R_{ta-k}^2}} \exp\left\{-j\frac{2\pi R_{m,k}}{\lambda_m}\right\} \tag{4.6}$$

a coefficient including the amplitude and the phase of the received signal, (σ, f_m) the RCS of the target at f_m and all the other symbols meaning as in equation (4.1). After M adequate band-pass filtering, in order to separate the different signals, and matched filtering, the autocorrelation of the $h^t h$ received signal the will be:

$$r_k(t) = F^{-1}\{R_k(f)\} = F^{-1}\left\{\alpha(\sigma, f_h, f) \otimes S_k(F) + \hat{N}_k(f)\right\}, \tag{4.7}$$

where f_h is the carrier frequency of the h^{th} signal transmitted and is the Inverse Fourier Transform. The power of $\hat{N}_k(f)$ has been limited by the band-pass filtering.

4.3 Netted radar systems

The third and fourth models that have been developed have the same physical layout as the spatial diversity MIMO but instead use conventional coherent processing.

In this systems the received signals will be processed through a bank of matched filters as in Section 4.1; after this the coherent summation will be performed. As the model of the received signal is the same of equation (4.1), the results of processing after the filtering are the same of equation (4.4) with all the relative

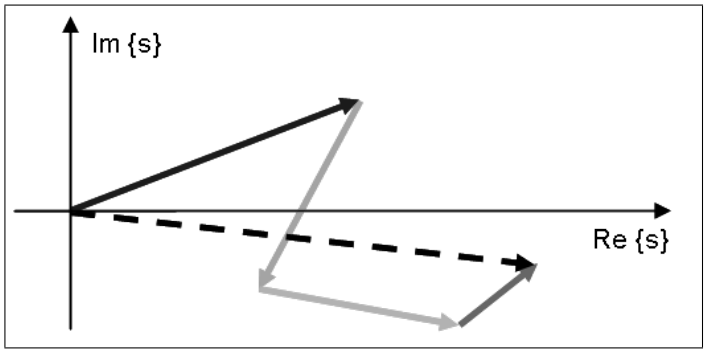

Figure 4.4: The coherent netted radar integration

considerations. Two different kinds of netted radar will be presented: the first one is what we termed “coherent netted radar”, while the second one is the “re-phased coherent netted radar”.

4.3.1 The coherent netted radar

This system gets the same samples of the spatial MIMO radar system, but it sums them coherently. We examine this not as a MIMO concept but to provide a means of comparison. The phases of the incoming signals are in this case highly correlated, as they depend from the target’s position and the geometry of the system. Yet it is well known that the phase wraps every half wavelength, so, given that the position of the target cannot be measured with this accuracy, the signals apparently have uncorrelated phases uniformly distributed between $-\pi$ and π . In Figure 4.4 it is shown what happens if 4 signals are coherently summed without processing the phases. In this case the phases results to be uniformly distributed and the overall coherent sum is a signal whose amplitude is much smaller than the sum of the amplitudes of the single elements. In the extreme case, when the amplitude is constant and the sum of the phases is 2π, it is possible to cancel the signal at all. As shown in the next sections, in such conditions this processing will provide us with the lower bound limit for the performance, as its SNR after integration will be statistically the same as in a single pulse case.

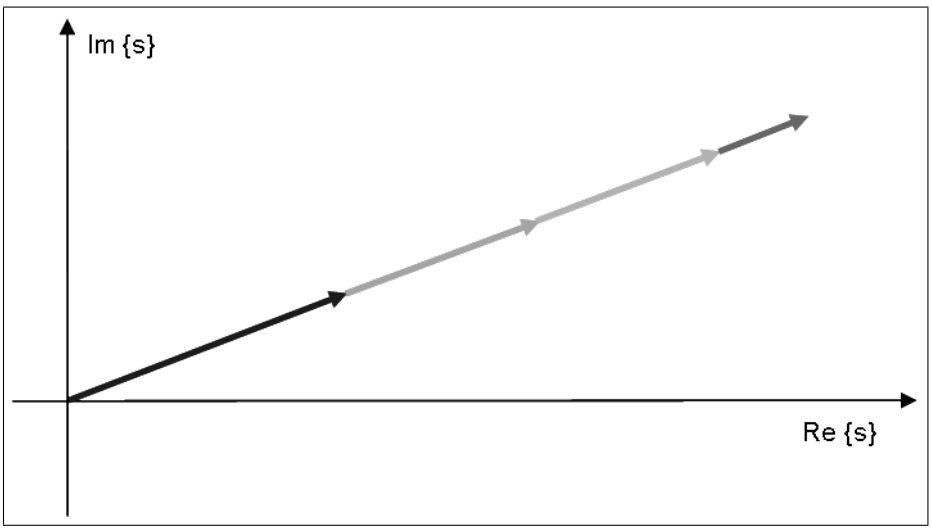

Figure 4.5: The re-phased coherent netted radar integration

4.3.2 The re-phased coherent netted radar

This system gets the same samples of the previous one, but it performs a re-phasing of the vectors according to the exact position of the target in order to maximize the signal-to-noise ratio (Figure 4.5) and subsequently the achieved performance. In this case the phases of the signals in Figure 4.4 have been opportunely re-aligned, so the amplitude of their sum is the biggest possible. Although this system is hardly feasible, unless impossible as it exploits a-priori information about the position of the target, that on the contrary should be estimated by the radar system itself, it provides the upper bound limit for the performance as it maximizes the signal to noise ratio. We considered it in order to see what the losses of the MIMO processing are.

Chapter 5

Performance

In this section the performances of the four radar system concepts are reported. In order to get a fair comparison, we provide the systems the same power in transmission. This means that systems with a lower number of nodes have an increased available power. Furthermore, in comparing the frequency MIMO to the other systems, the same number of transmitters has been considered. Thus, in approaching the frequency MIMO performance, the same configuration of the spatial MIMO has been taken into account, relocating all the nodes in the same position and trading the spatial diversity with the frequency diversity.

5.1 False Alarm Rate

Here we report the probability of false alarm against threshold in the case where only white Gaussian noise with zero mean value and normalized variance is input to the receivers.

When only white noise incomes into the receivers, spatial MIMO performs the incoherent summation of a number of samples and compare them with the threshold. The same process is made by the frequency MIMO. Here the only difference is that the noise affecting the spatial MIMO system has an equivalent bandwidth centred on the only carrier frequency, while the one affecting the frequency MIMO system is centred on the many carrier frequency used. When the equivalent noise bandwidth and the spectrum of the noise (here supposed white)

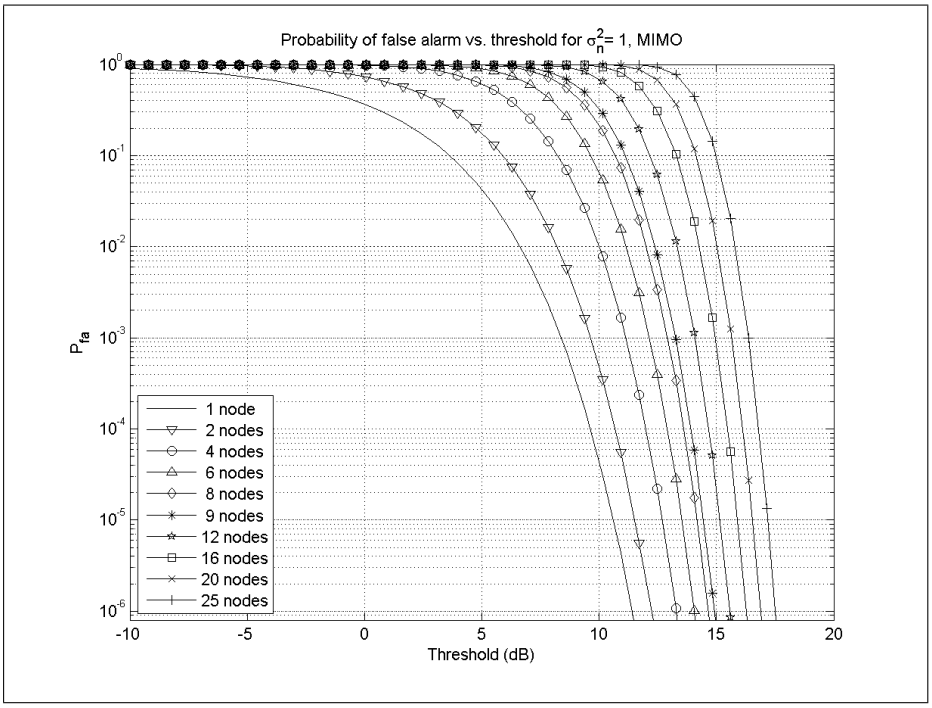

Figure 5.1: The MIMO diversity pfa performances

are the same for both spatial and frequency MIMO cases and the same number of signals are processed, the overall incoming noise power is statistically the same and consequently spatial and frequency MIMO perform equally.

Similarly, the processing of simple and re-phased coherent netted radar is the same; when no target is present, the coherent netted radar cannot align the phases of the signals coming from the target, so the two systems achieve the same results. As consequence of these, we report only two figures with the results for false alarm rate.

Figures 5.1 and 5.2 show the threshold required to achieve a chosen false alarm rate for a variety of numbers of overall processed signals. Fixing the false alarm rate to a certain value, say 10^{-6}, it is here shown that both MIMO systems have a performance advantage over coherent networks as a smaller threshold is required to achieve the same rate. The advantage achieved by the MIMO system is due to the incoherent processing of the signals effectively reducing the variability in the total received signal hence enabling a lower threshold to be set, i.e. the total noise power contributing to the detection decision is lower in the MIMO systems

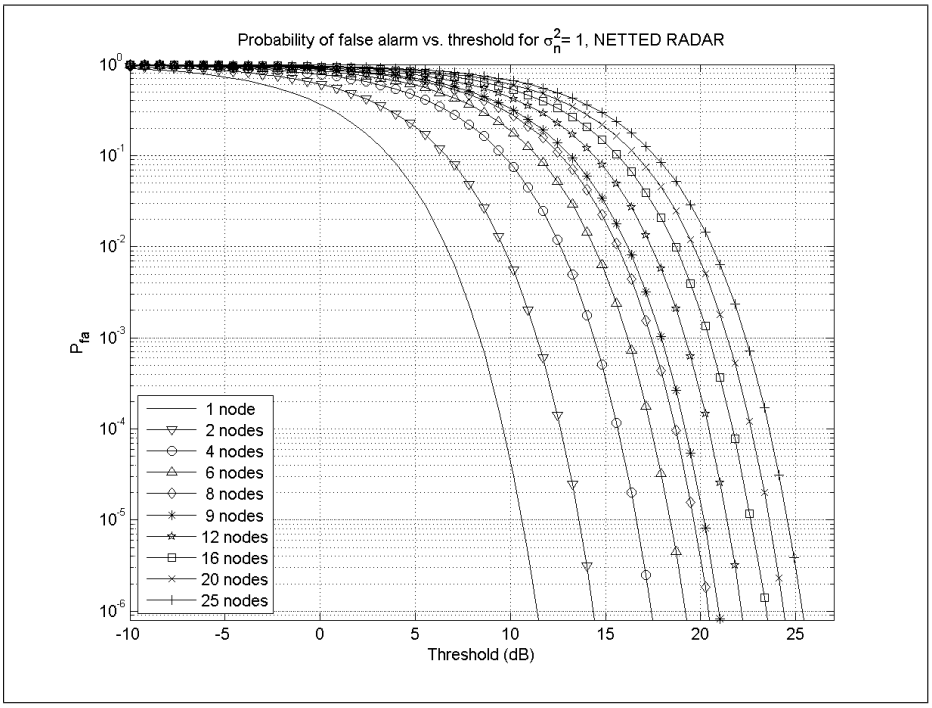

Figure 5.2: The NR diversity pfa performances

than in the netted ones: the coherent netted case requires a threshold of some 3 to 8 dB more to achieve an equivalent level of performance. The reduced threshold set with incoherent processing gives, as seen in the next section, an increased sensitivity to MIMO systems when used for detection.

5.2 Swerling I targets

Here we consider a Swerling I, i.e. noise-like distributed, target model when two to five radars are assumed to transmit and receive ($M = N = 2 \ldots 5$) respectively. We report also the performance of netted radar where the phase of all the incoming signals has been re-aligned, according to the exact position of the tracked target, so that they cohere constructively. Frequency MIMO is not explicitly reported in this section as the results are identical to those of the spatial MIMO case, given that the RCS of the target has a noise-like response in space as well as in frequency. The transmitted power is a constant in all the cases.

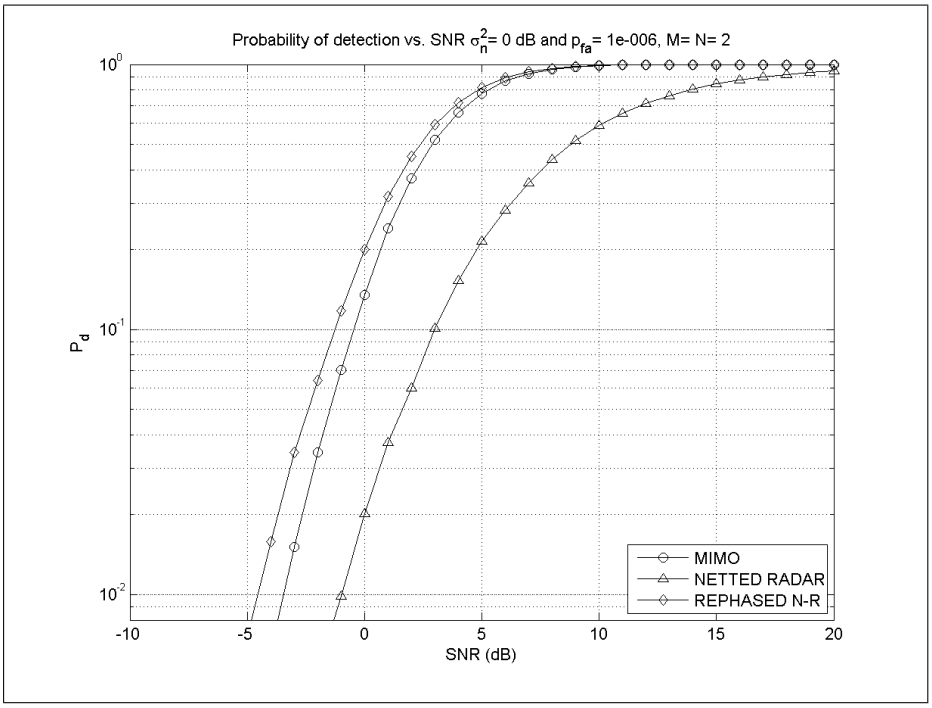

Figure 5.3: Swerling I pd performances, 4 processed signals

Figures from 5.3 to 5.6 show the probability of detection as a function of signal to noise ratio for a false alarm probability of 10^{-6}. The MIMO systems have performance in between those of the netted radars. In these Figures the losses for incoherent processing, compared to the re-phased netted radar, can be estimated from 0.5 to 3 dB, when respectively from 4 to 25 signals are taken into account for $P_d = 80\%$. Even if the re-phased netted radar performs best, as it maximizes the signal-to-noise ratio, the MIMOs achieve good results without requiring additional information about the effective position of the target. The good performance of the MIMO systems is due to the acquisition of independent samples effectively reducing the noise variance and to the lower threshold that has been possible to set as shown in the previous section.

Implementation of a MIMO system is much simpler than the coherent re-phased netted radar due to the very tight tolerance required for the re-phasing. Indeed this may prove impossible for distributed targets, i.e. the synchronization and data communication requirements are much less severe than for the fully coherent network.

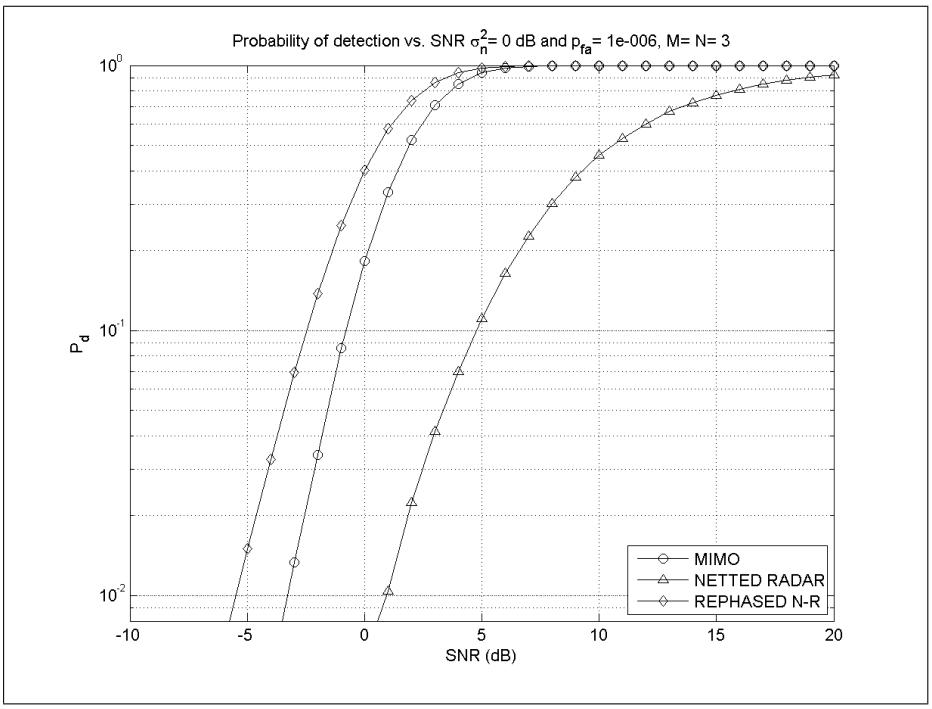

Figure 5.4: Swerling I pd performances, 9 processed signals

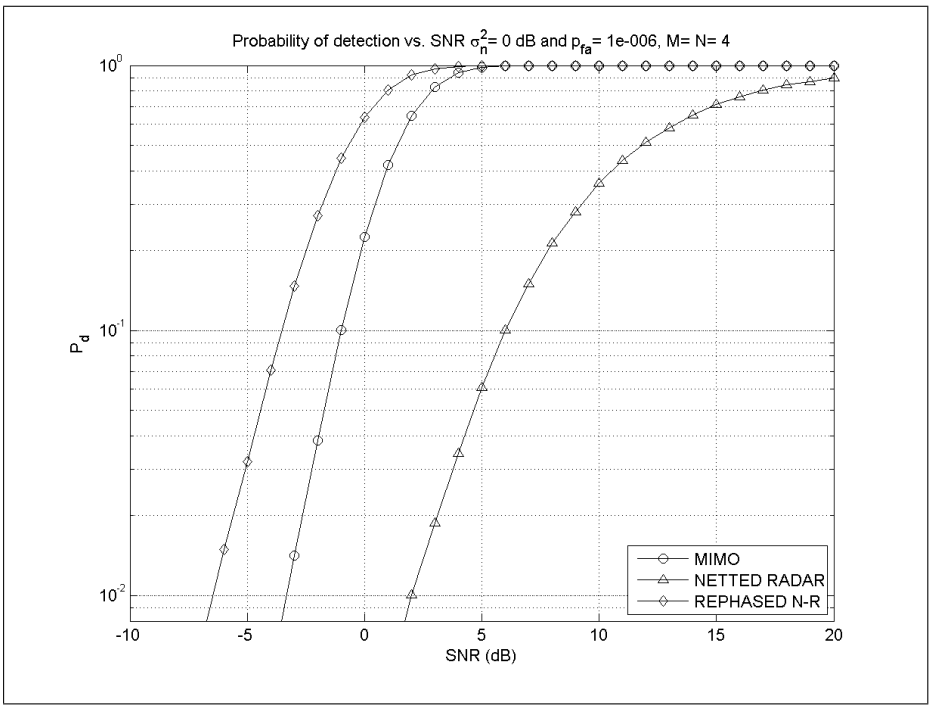

Figure 5.5: Swerling I pd performances, 16 processed signals

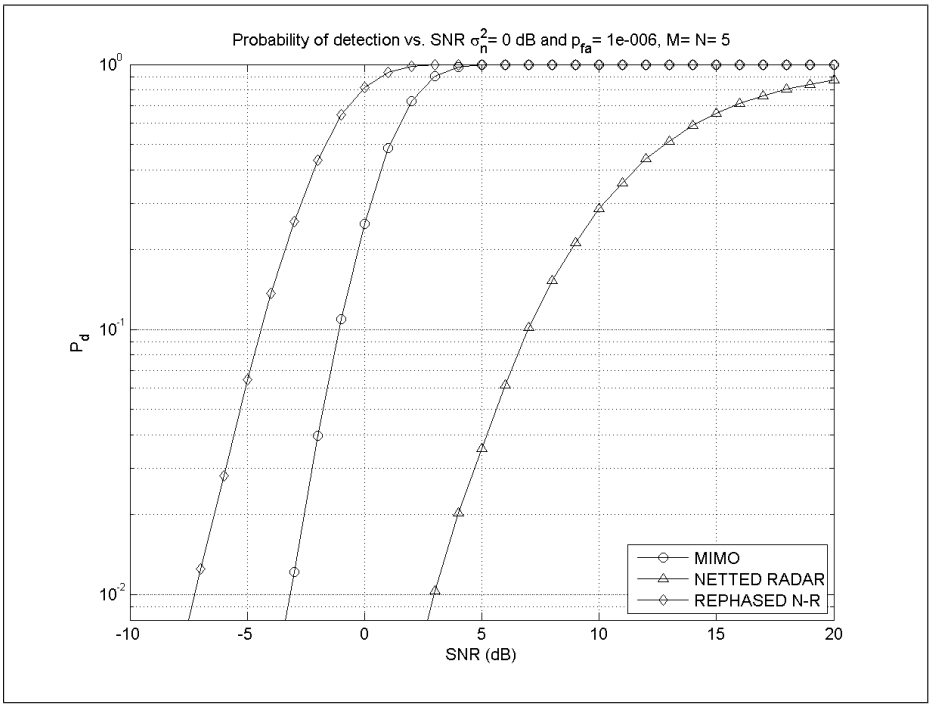

Figure 5.6: Swerling I pd performances, 25 processed signals

5.3 Swerling III targets

A Swerling III model corresponds to a target consisting of one dominant scatterer plus a number of smaller ones. The resulting PDF can be expressed as in equation (5.1) and it is representative of a chi square distribution with 4 degrees of freedom or, equivalently, with 2 complex degrees of freedom:

$$p(\sigma) = \frac{4\sigma}{\bar{\sigma}^2}\exp\left\{-\frac{2\sigma}{\bar{\sigma}}\right\}, \tag{5.1}$$

where $\bar{\sigma}^2$ is the variance of the RCS of the target.

The following Figures show the results for spatial MIMO, netter radar and rephased netted radar against a Swerling III target. Frequency MIMO is not reported as the RCS model is independent of the carrier frequency. Here it can be observed that the more spatial samples taken the better the resulting detection performance. Again the MIMO results fall between the two netted cases. The difference in performance with respect to the netted cases is greater with a Swerling III than

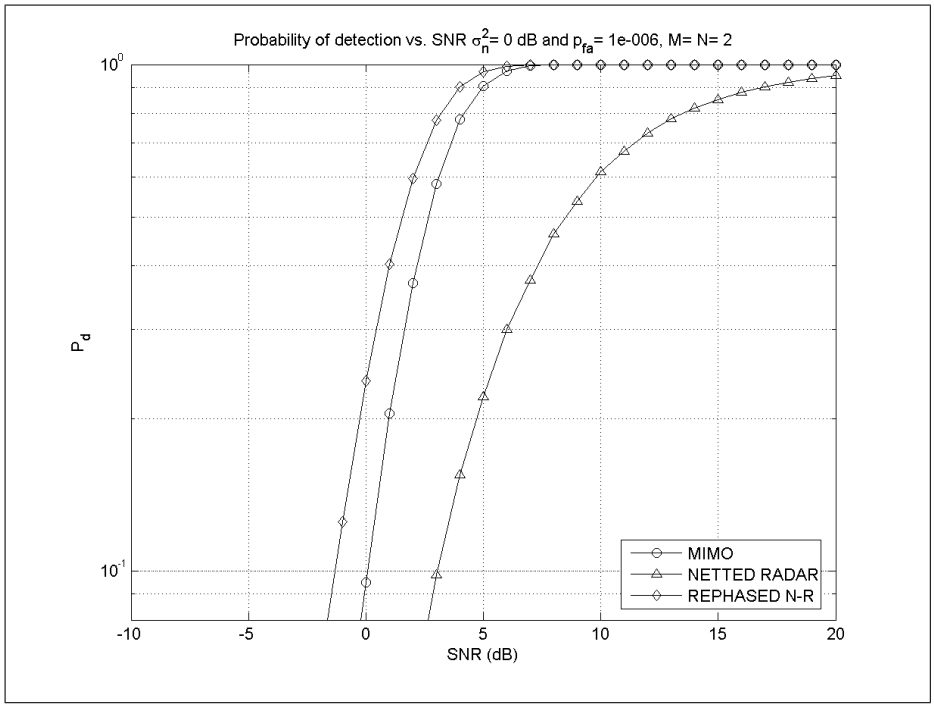

Figure 5.7: The NR diversity pfa performances

a Swerling I target. This is due the re-phased coherent net being able to take advantage of the partial target coherency.

For the spatial MIMO the lower the number of processed signals the lower the achieved performance. This reinforces the conviction that it is possible to improve the capacity of detection of a radar system by looking to the target from an increasing number of different angles.

However, this assumes that independent samples can always be taken. This may not be the cases when considering real targets and is partly examined by considering the sphere target (section 5.4). Also note that for the non re-phased netted case the performance decreases as the number of nodes increases. This may seem contrary to expectation but is explained by the increasing randomizing of the received signal phases with increasing number of independent looks.

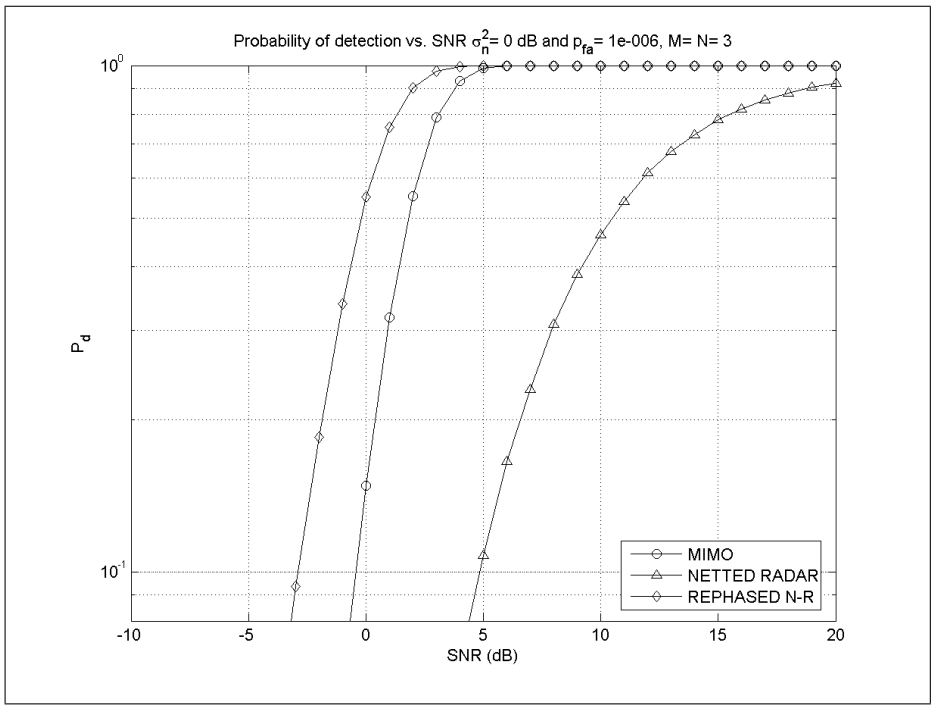

Figure 5.8: Swerling III pd performances, 9 processed signals

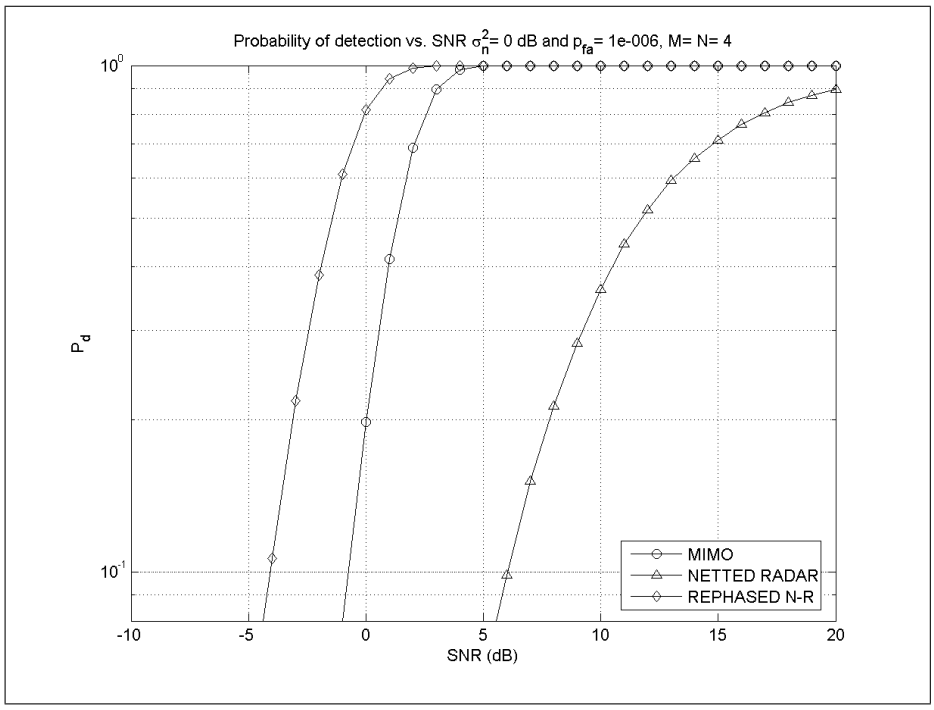

Figure 5.9: Swerling III pd performances, 16 processed signals

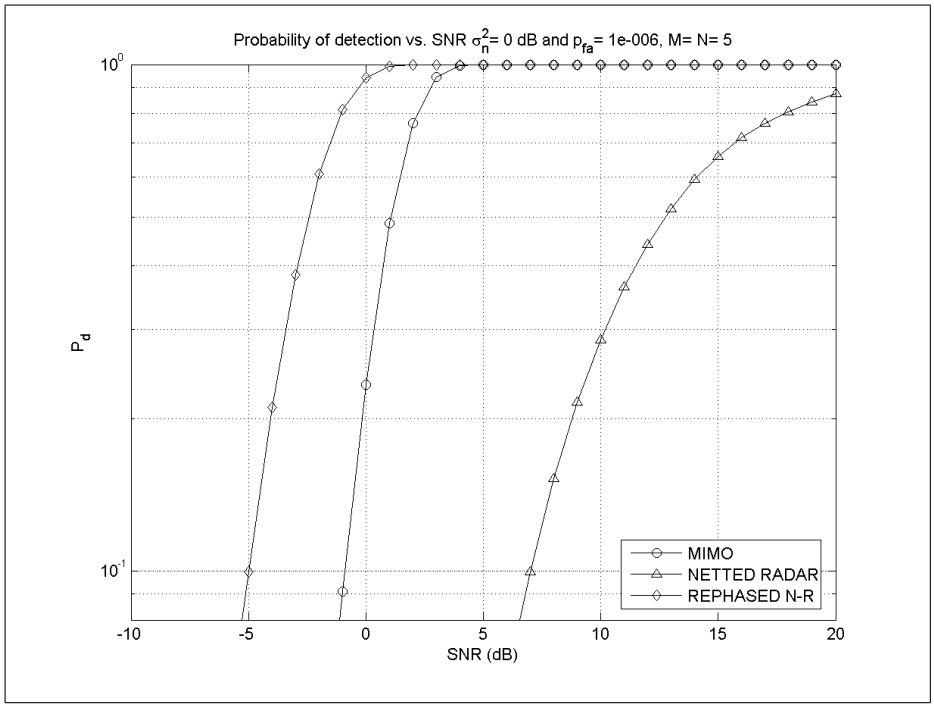

Figure 5.10: Swerling III pd performances, 25 processed signals

5.4 Spherical targets

A further comparison of the performances has been considered for the case of a spherical target as it exhibits a simple frequency dependence with radius. This case is explicative of highly correlated RCS, so it provides a first view of the MIMO performance when the target is not noise-like. Several values of the radius of the sphere r have been considered, in order to get the related performances of the systems. A frequency $f_0 = 3$ GHz has been chosen as the carrier frequency of the spatial MIMO and the netted radar, while, as in this case a frequency model for the RCS of the target was available, the carrier frequencies of the frequency MIMO vary in the range of $1 - 5$ GHz, with bandwidths that do not overlap each other. The RCS of a sphere as a function of the ratio $\frac{2\pi r}{\lambda}$ is plotted in Figure 5.11 to illustrate frequency dependence.

The results are shown in Figures from 5.12 to 5.17. The received SNR, shown in the x-axis, is computed at the wavelength $\lambda_0 = \frac{c}{f_0}$ (10 cm). When a frequency MIMO radar system has been considered, the reported performance is affected by

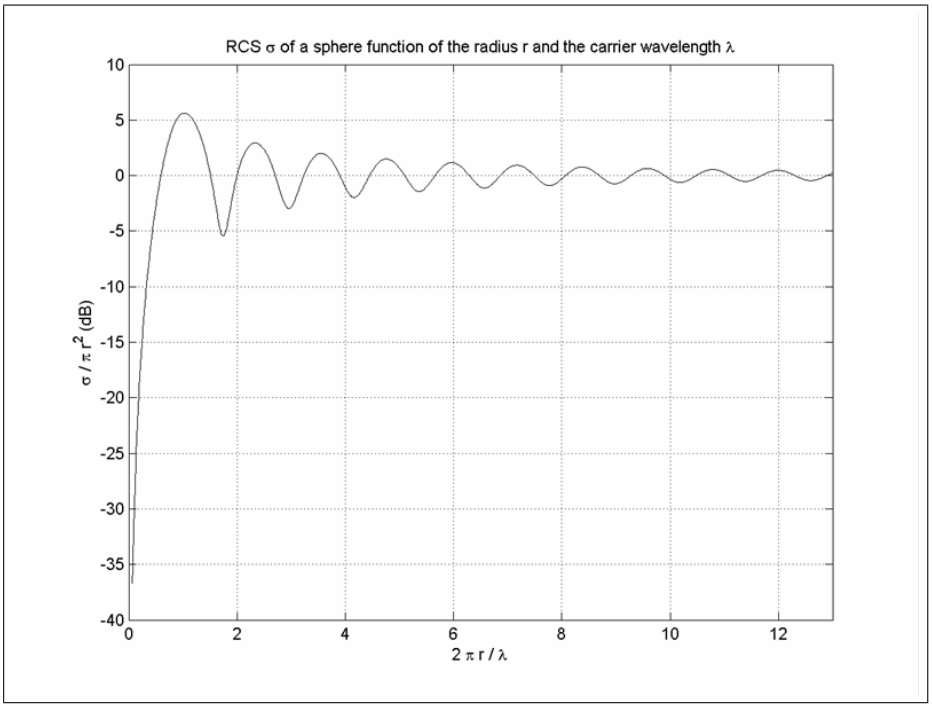

Figure 5.11: RCS of a sphere

the different responses of the RCS of a sphere to different wavelengths that modify the effective SNR value, according to the following:

$$SNR\,|_{\lambda} = SNR\,|_{\lambda_0} \frac{\sigma(r,\lambda)}{\sigma(r,\lambda_0)}, \tag{5.2}$$

where it is assumed $G_T(\lambda)G_R(\lambda)\lambda^2 = G_T(\lambda_0)G_R(\lambda_0)\lambda_0^2$ (in the expression of the SNR). This is done to provide a comparison between the systems where the values of the SNR change according to the differences of the measured RCS only and not the differences of gains of the transmitting/receiving antennas to different wavelengths.

The results provide evidence that, when frequency MIMO is applied, its performance can vary widely compared to spatial MIMO one. This is of course related to the ratios between the dimensions of the scatterers of the target and the carrier wavelengths and is discussed in Section 7.3. These fluctuations indicate that the two kinds of MIMO studied are based on different foundations. However, they also highlight the idea that the MIMO concept can be further extended by a

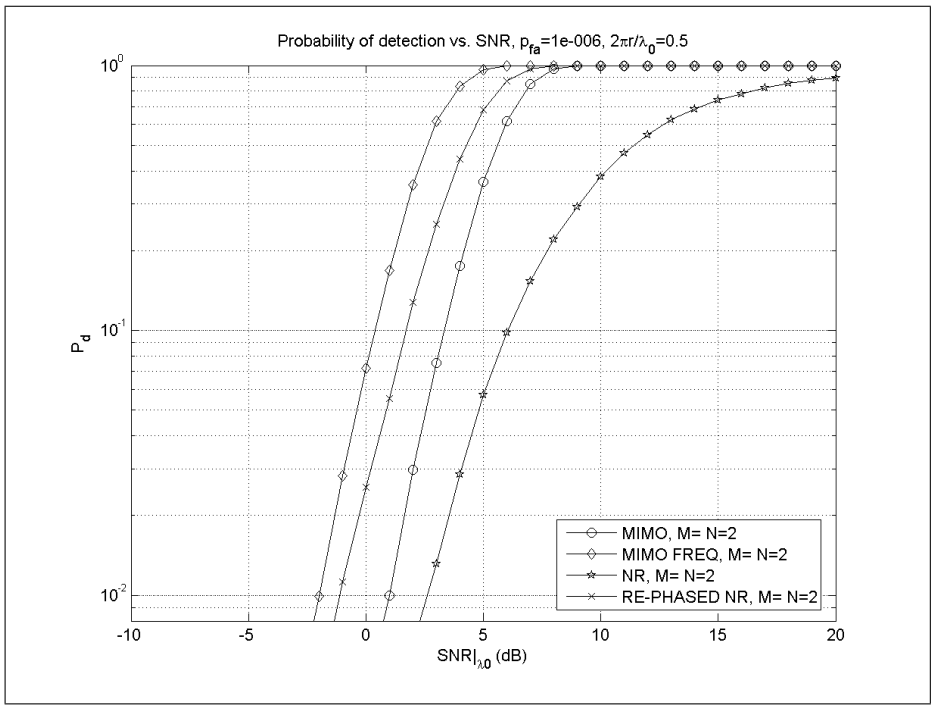

Figure 5.12: Compared performances for spherical target

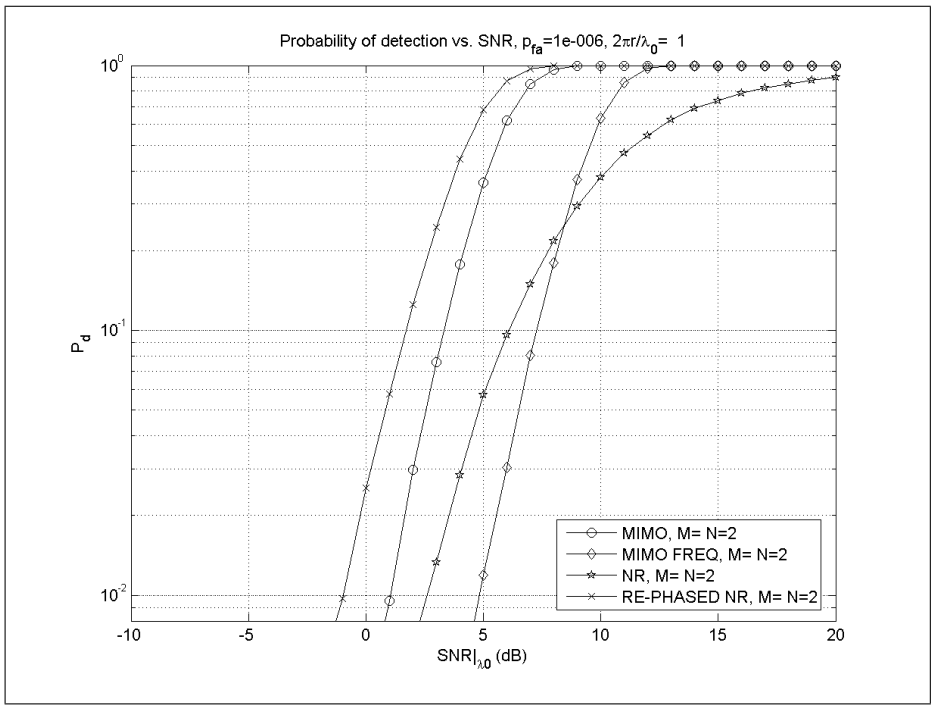

Figure 5.13: Compared performances for spherical target

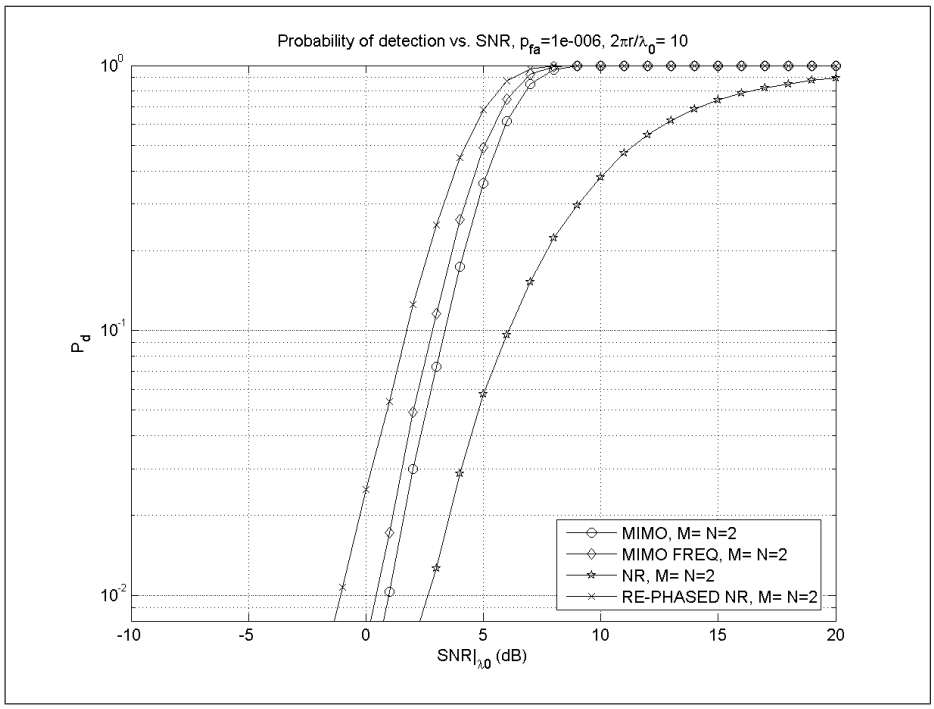

Figure 5.14: Compared performances for spherical target

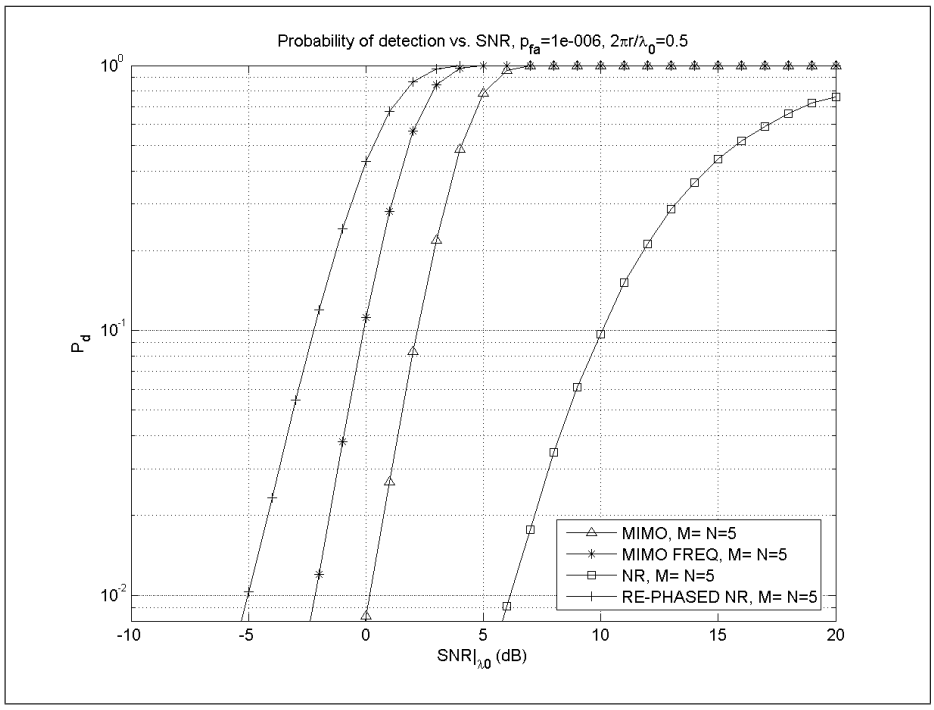

Figure 5.15: Compared performances for spherical target

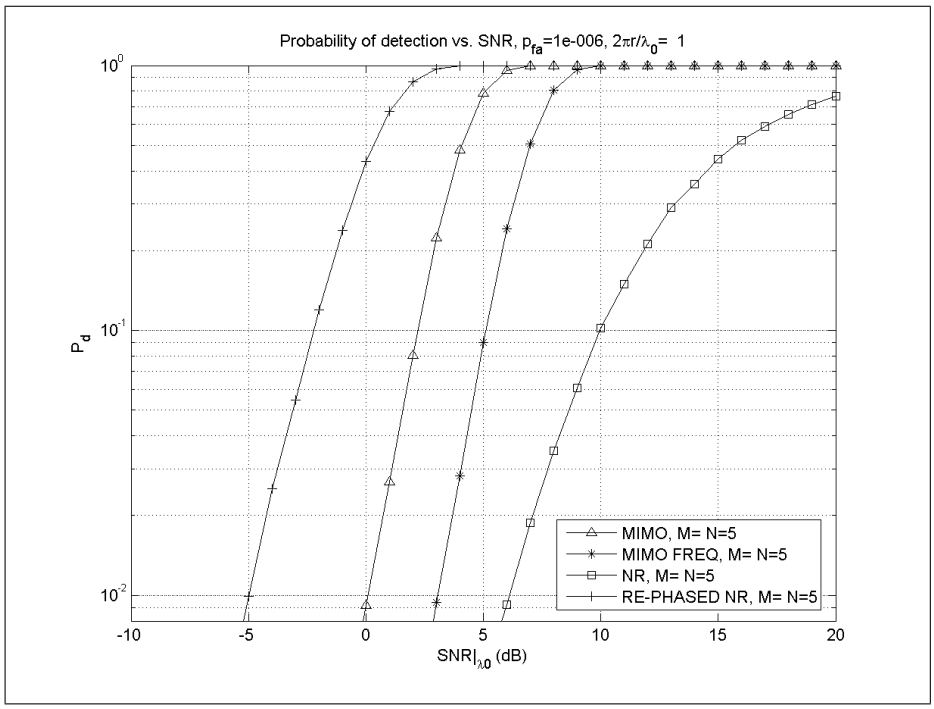

Figure 5.16: Compared performances for spherical target

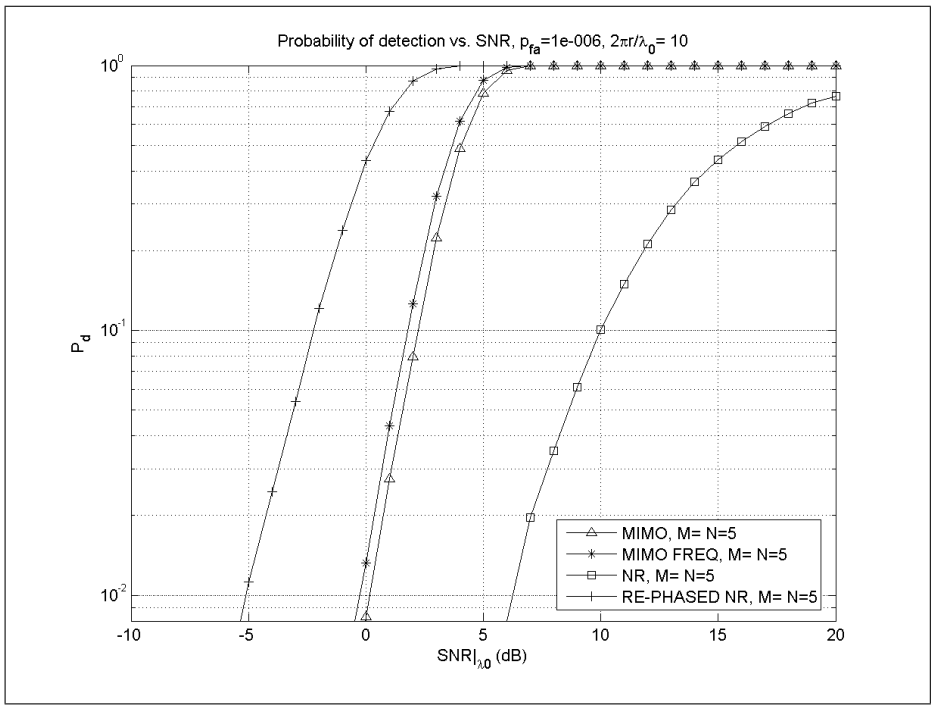

Figure 5.17: Compared performances for spherical target

joint implementation of frequency and spatial systems.

Chapter 6

Multipath and clutter

So far we have only considered different target models under noise limited conditions. It is more realistic to also include the effects of the environment such as clutter, propagation and multipath. Here we examine the introduction of the effects of multipath and clutter on the performance of the various distributed radar concepts.

6.1 Multipath

Here we introduce both white Gaussian noise and multipath into the received signal model. We assume again a Swerling-I-modelled target and we distinguish different kinds of multipath as shown in Figures 6.1 and 6.2.

As shown, each incoming signal can be affected by three different replicas. In addition, we take account of the fact that both monostatic and bistatic multipath effects can occur. We examine the possibilities of rough-surface scattering $\frac{\sigma_h}{\lambda}$ and smooth-surface scattering $\sigma_h = 0$, where σ_h is the standard deviation of the heights of the scattering surfaces. This last one may appear only theoretical, but it represents a sort of upper bound limit for the performance under the hypothesis of multipath, as it maximize the overall randomization of the incoming signals.

Under these assumptions, then, the signal incoming to the receiver will be made of the following five components for each transmitter/receiver pair:

i. direct signal: $s_0 = \alpha e^{j\phi_0} s$,

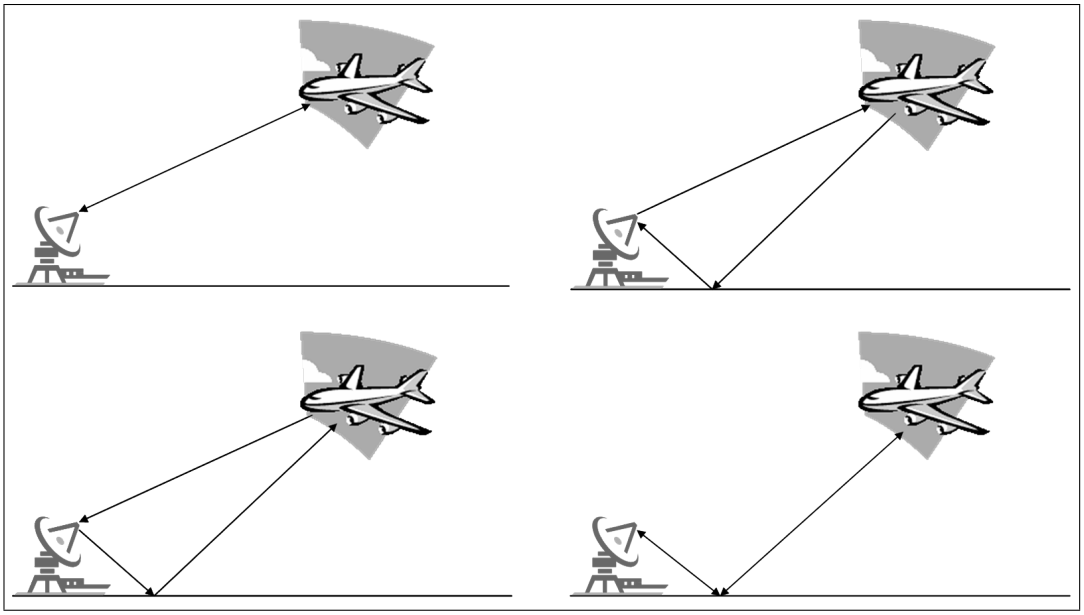

Figure 6.1: Monostatic direct signal and multipath

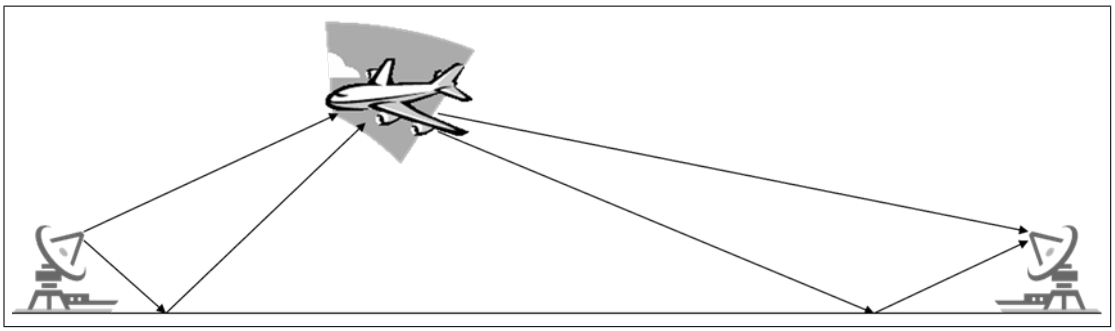

Figure 6.2: Bistatic direct signal and multipath

ii. transmitter⇝surface⇝target⇝receiver multipath signal: $s_1 = m\beta e^{j\phi_1} s$,

iii. transmitter⇝target⇝surface⇝receiver multipath signal: $s_2 = m\gamma e^{j\phi_2} s$,

iv. transmitter⇝surface⇝target⇝surface⇝receiver multipath signal: $s_3 = m^2\delta e^{j\phi_3} s$,

v. white Gaussian noise: $\mathbf{n}$,

where α, β, γ, and δ take into account the mono/bistatic measurements of the RCS, m is the reflection coefficient and ϕ_k, $k = 0..3$, is the phase of each signal due to the path length. Thus the signal r incoming to the matched filter can be written as:

$$\begin{aligned} r &= \left(\alpha e^{j\phi_0} + m\beta e^{j\phi_1} + m\gamma e^{j\phi_2} + m^2\delta e^{j\phi_3}\right) s + n = \\ &= s e^{j\phi_0}\left(\alpha + m\beta e^{j-\Delta\phi_1} + m\gamma e^{-j\Delta\phi_2} + m^2\delta e^{-j\Delta\phi_3}\right) + n = \\ &= s e^{j\phi_0}\left(\alpha + m\beta e^{j-\Delta\phi_1} + m\gamma e^{-j\Delta\phi_2} + m^2\delta e^{-j(\Delta\phi_1+\Delta\phi_2)}\right) + n, \end{aligned} \tag{6.1}$$

where $\Delta\phi_k = \phi_0 - \phi_k$.

Equation (6.1) can be easily inferred by geometrical and physical considerations. Furthermore we assumed that all the delays due to multipath are such that range cell migration is avoided, i.e. we have relatively narrowband signals. We also assume full illumination of the surface. Figures from 6.3 to 6.6 show the curves of detection for Swerling I target model including the effects of multipath and white Gaussian noise. Figures 6.3 and 6.4 show rough-surface performance with an incoherent-to-coherent-ratio (termed MPSR, multipath-to-signal-ratio, in the Figures) of −5 dB. For smaller values of this parameter the detection curves asymptotically approach the ones not affected by multipath effect. The performance is actually improved with the presence of rough surface multipath scattering. This is due to the greater randomisation of the received signal and hence has a greater likelihood of acquiring the desired independent samples. This is entirely consistent with the experience found in the application of MIMO to communications systems [47]. In Figures 6.5 to 6.6 it is possible to see the effects on the detection curves when the waveforms reflect on a smooth surface. In this case we have an incoherent-to-coherent-ratio (MPSR) of 0 dB. In both cases the multipath statistically produces an improvement of the capacity of detection.

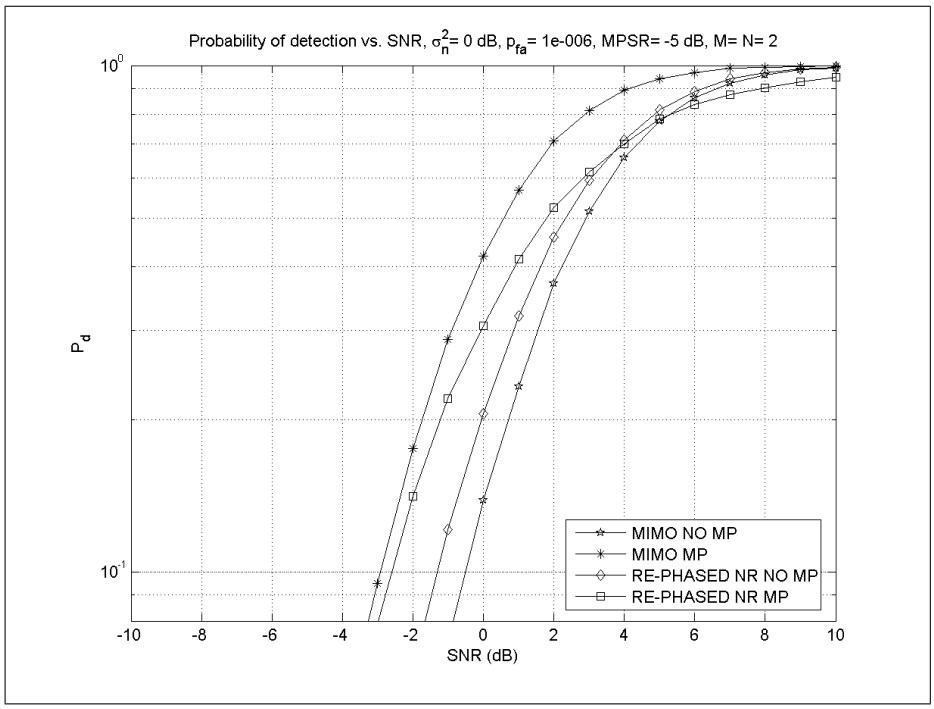

Figure 6.3: Compared performances for multipath effect

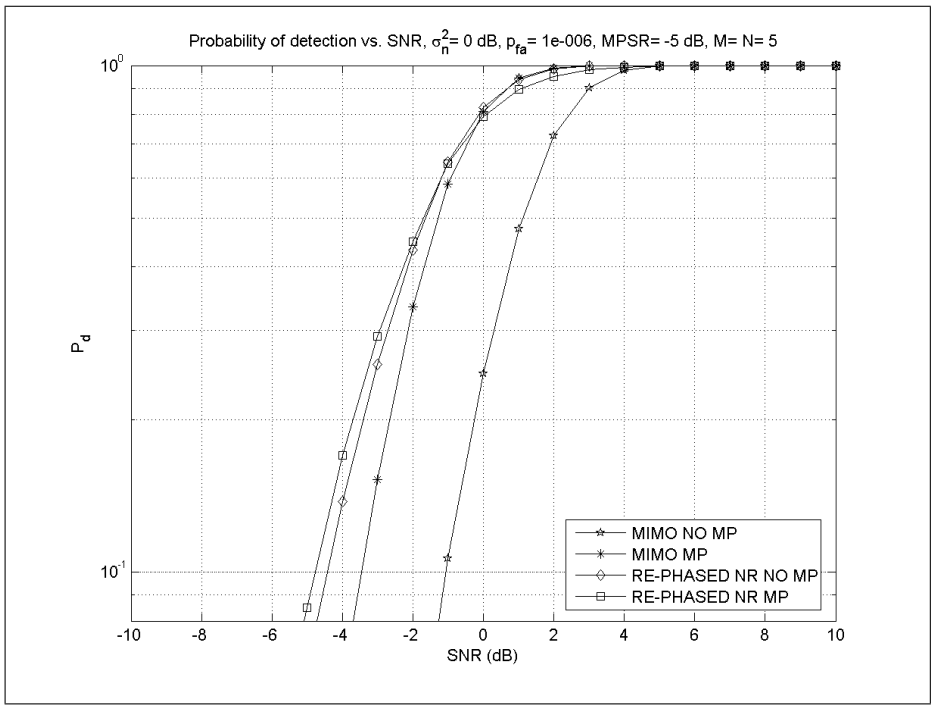

Figure 6.4: Compared performances for multipath effect

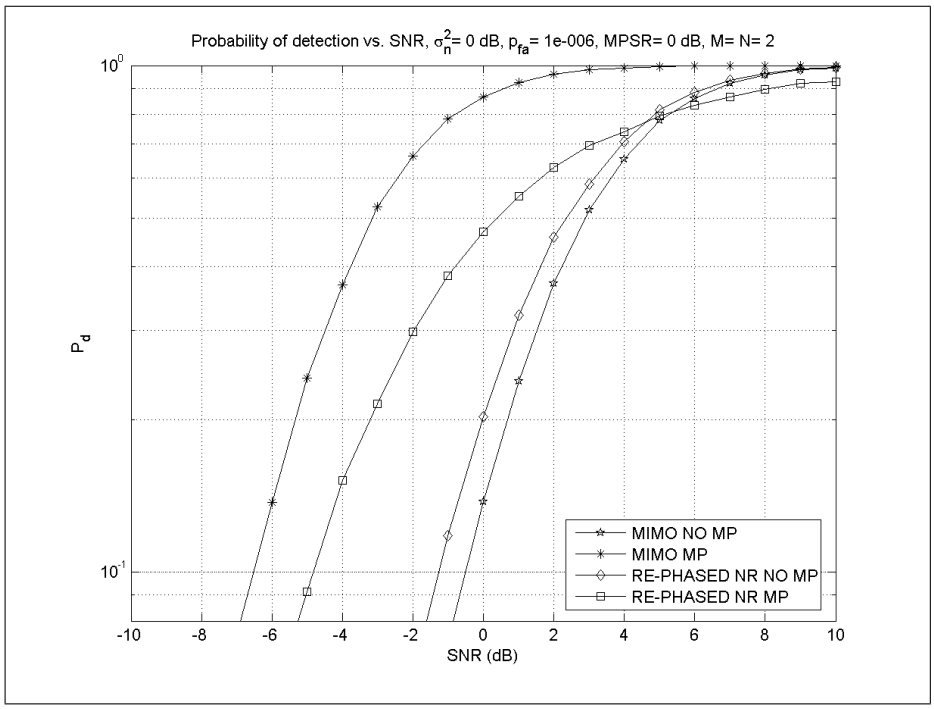

Figure 6.5: Compared performances for multipath effect

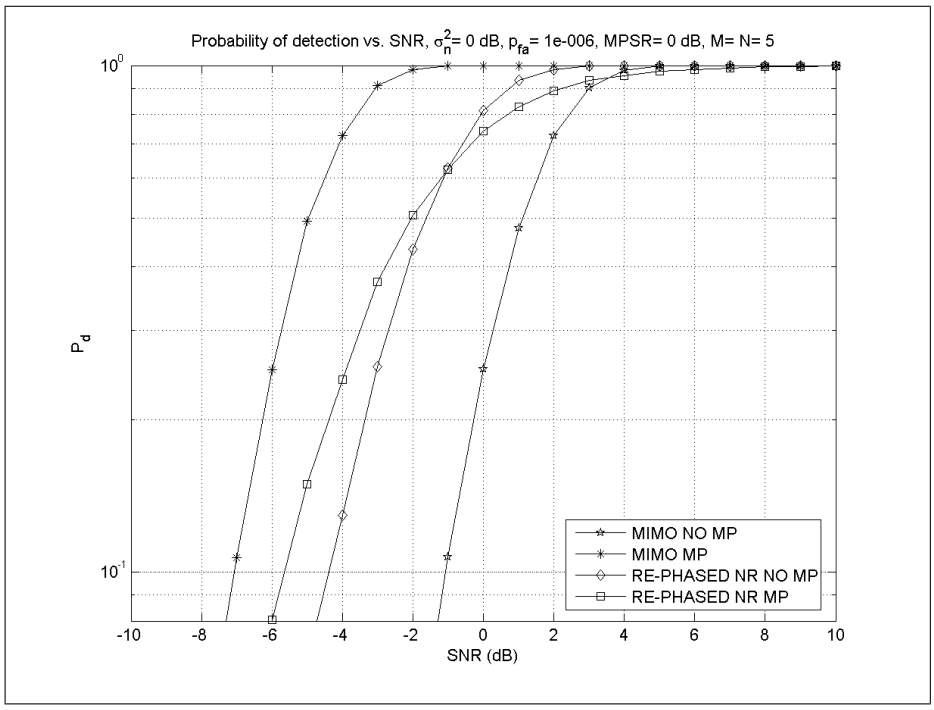

Figure 6.6: Compared performances for multipath effect

6.2 Clutter

In this section we examine the effects of K-distributed clutter on the performance of a spatial MIMO radar system and a netted radar re-aligning the phases of the incoming signals, so providing, as before, the theoretical upper bound limit for the performance of systems working on only one carrier frequency. The processing of the received echoes has to take into account the extra information provided and the environment that the radars are in. Thus here we propose two different ways for signal processing. Moreover, as the pdf of the total disturb has obviously changed, we report their performance in term of false alarm rate and probability of detection.

6.2.1 Signal models and statistical approach

In this section we describe the characteristics of the incoming signals. First of all we model the k^{th} received signal as:

$$r_k = \sum_{=1}^{M} (H_{0/1}\alpha_{m,k}s_m + c_{m,k}) + n_k \tag{6.2}$$

where:

- $H_{0/1}$ is 0 or 1 respectively in the absence or presence of target,
- $\alpha_{m,k}$ is an amplitude coefficient taking into account the parameters of the mono/bistatic radar equation, phase shift included,
- s_m is the m^{th} transmitted signal,
- $c_{m,k}$ is the clutter,
- n_k is the thermal noise,
- $m = 1..M$ is the number of transmitters and
- $n = 1..N$ is the number of receivers.

For the sake of simplicity the RCS of the target has been assumed Swerling II distributed for both the monostatic and the bistatic case. The clutter has been modelled as a K-distribution (from [10] to [14]). This means that the amplitude has a Gaussian distribution with a Γ-distributed variance. For echoes incoming from adjacent range cells, a correlation between the powers received has to been taken into account. Thus we introduced the following model for the amplitude of the clutter c:

$$c = \sqrt{\tau}x, \tag{6.3}$$

where x is the complex vector of the received echoes from different range cells and its pdf is given by

$$p(x|\tau) = \frac{1}{(2\pi\tau)^L \sqrt{|\mathbf{M}_x|}} \exp\left\{\frac{1}{2\tau} x^H \mathbf{M}_x^{-1} x\right\}, \tag{6.4}$$

where $\mathbf{M}_x$ is the covariance matrix of x given τ, i.e. $\mathbf{M}_x = E\left\{xx^H|\tau\right\}$, and the texture τ follows a Γ-distribution of shape parameter ν and expected value μ:

$$p(\tau) = \frac{1}{\Gamma(\nu)} \left(\frac{\nu}{\mu}\right)^{\nu} \tau^{\nu-1} \exp\left\{-\frac{\nu}{\mu}\tau\right\}, \quad \tau > 0. \tag{6.5}$$

The general element $m_x(h,k)$ of $\mathbf{M}_x$ has been taken equal to

$$m_x(h,k) = \rho_x^{|h-k|}, \tag{6.6}$$

where ρ_x is the correlation coefficient between two adjacent elements of the vector x. As usual the thermal noise has been modelled as a white complex Gaussian RV with zero mean value and variance σ_n^2.

So, considering clutter and noise to be mutually independent, it is possible to express the resulting pdf of the L-long vector of the disturbance as a complex Gaussian with zero mean value and covariance matrix equal to $\tau\mathbf{M}_x + \sigma_n^2\mathbf{I}_L$, where τ is distributed as in equation (6.5) and $\mathbf{I}_L$ is the LxL identity matrix.

In this analysis we also took into account a certain number (Q) of echoes received during the time on target. When integration in time is performed, the

clutter plus noise statistics change significantly. If in time the clutter echoes have textures τ_i, $i = 1..Q$, after the integration process the vector of the total disturbance can still be expressed as a complex Gaussian with zero mean value and covariance matrix given by

$$\sum_{i=1}^{Q}\left(\tau_i \mathbf{M}_x + \sigma_n^2 \mathbf{I}_L\right) = Q\sigma_n^2 \mathbf{I}_L + \mathbf{M}_x \sum_{i=1}^{Q} \tau_i. \tag{6.7}$$

The pdf of the RV $\tilde{\tau} = \sum_{i=1}^{Q} \tau_i$, that is the texture of the vector with the integrated contribution of clutter, can be expressed as Γ RV with shape parameter ν and mean value $Q\mu$ if the textures are uncorrelated with each other in the time domain. In this case it is clear that the higher Q, the better the approximation $\sum_{i=1}^{Q} \tilde{\tau}_i \approx Q\mu$, so the overall pdf of the disturb approaches asymptotically a Gaussian with mean value 0 and covariance matrix equal to $Q\left(\mu \mathbf{M}_x + \sigma_n^2 \mathbf{I}_L\right) = Q\sigma_n^2 (CNR\mathbf{M}_x + \mathbf{I}_L)$. Unfortunately this approximation can be difficult to evaluate the threshold for the false alarm rate in a closed form; in practice in real systems the number Q of integrated samples is directly dependent on time on target, so in most cases it is too small to approximate the overall pdf, thus to compute accurately thresholds for low and very low false alarm rate.

In addition, if the textures are correlated in time a more complex expression for the pdf of the disturbance vector can be found. If we assume, for example, a first order Markov structure for the texture component on Q elements, then we can write (as in [11]):

$$p(\bar{\tau}) = p(\tau_1) \prod_{i=1}^{Q-1} p(\tau_{i+1}|\tau_i), \tag{6.8}$$

where

$$\begin{aligned} p(\tau_{i+1}|\tau_i) = & \frac{\nu}{\mu} \frac{1}{\rho^{\nu-1}(1-\rho^2)} \left(\frac{\tau_{i+1}}{\tau_i}\right)^{\frac{\nu-1}{2}} \\ & \exp\left\{-\frac{\nu}{\mu}\frac{\tau_{i+1}+\rho^2\tau_i}{1-\rho^2}\right\} I_{\nu-1}\left[\frac{\nu}{\mu}\frac{2\rho\sqrt{\tau_i}\tau_{i+1}}{1-\rho^2}\right], \end{aligned} \tag{6.9}$$

and I_z is the modified Bessel function of first kind and order z. The covariance

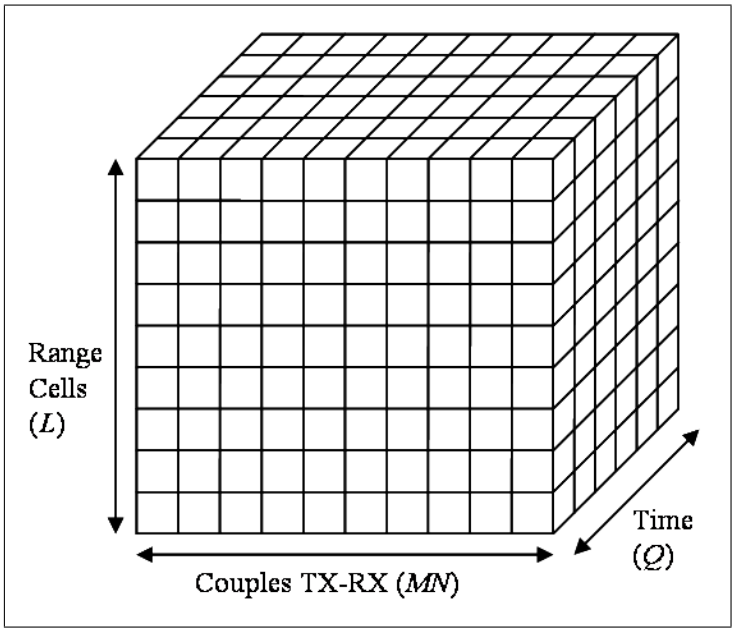

Figure 6.7: Multistatic data organization

matrix $\mathbf{M}_T$ in time has been assumed of the same kind as $\mathbf{M}_x$ with a different correlation coefficient.

6.2.2 Multistatic information and correlation

In multistatic systems it has to be considered that each transmitter-receiver couple provides a set of data of the form previously described. Thus the total data incoming into the system and suitable for processing should be organized in a three-dimensional matrix as shown in Figure 6.7. Clutter echoes from the same area generated by one of the M transmitted waveforms can have correlated values of the textures as observed in practice (from [10] to [14]).

Whilst correlation in time and range has been largely investigated, there is lack of knowledge about a possible correlation of the data in a multistatic configuration. Anyway it is reasonable to assume that echoes scattered by the same clutter can be partially correlated, especially under the hypothesis of narrowband due the relatively high number of elementary scatterers. Thus a third correlation matrix $\mathbf{M}_{t-r}$ can be introduced. At this stage we assume here that two clutter samples from the corresponding range cell $c_{m,k}(p)$ and $c_{n,h}(p)$, $n, m = 1..M$, $k, h = 1..N$,

$p = 1..L$, have a correlation coefficient 1 if $n = m$ and $k = h$, ρ_{t-r} if $n = m$ but $k \neq h$ and otherwise 0. The choice of 0 in the latter case can be explained due to the slightly (for far targets) different orientation of the range cells: when transmitters far away each other illuminate different-shaped range cells, although in the same area, the coherent sums of all the backscattered contributions of the clutter are not expected to be correlated with each other.

We might also hypothesize that multistatic clutter is not correlated either. However we should examine and compare all cases as currently insufficient knowledge exists about target and clutter scattering under bi and multi static conditions. Further studies will consider loss of performance when the whitening is performed with sub-optimal approaches, such as estimation of the correlation matrixes in range and time, and adaptive threshold setting in order to complete the clutter scenarios.

Clutter and its correlation properties in multistatic systems have still to be measured and analyzed via experimental results.

6.2.3 Signal processing and performance

Once data are collected, there is more than one way of processing them in order to get detection. In this section we will examine three ways that are respectively (i) a fixed threshold algorithm on the raw data, (ii) a fixed threshold algorithm whitening the incoming data, assuming that the exact correlation matrixes are known and (iii) finally an adaptive threshold algorithm on the raw data. These are reported in the following sub-sections, together with the corresponding results.

Generally we supposed that the RCS of a target, in a distributed system, pointing to a same area from different aspect angles, receives contributions that may have the same pdf, but may be uncorrelated with one another. Particularly in the following subsections we report the results for a multistatic Swerling II target.

Fixed threshold on raw data

A first method is to process data as it arrives at the receiver. This might not be the best case, but it avoids estimating the correlation matrixes: after initial processing, the data is available to the detectors; the two corresponding thresholds

(one for MIMO systems, the other for netted radars) ensuring false alarm rate have been recomputed due to the non-gaussian distribution of the total disturbance. These results have been reported in Figures from 6.8 to 6.11. In the first two figures, results for MIMO systems in terms of false alarm rate and probability of detection (for $P_{fa} = 10^{-4}$) are reported. In the other two Figures we reported the corresponding results for netted radar systems. Covariance matrixes have been considered as described in sections 6.2.1 and 6.2.2 with coefficients equal to 0.9 (range), 0.7 (time) and 0.3 (nodes). Results of false alarm rate against threshold for CNR equal to 0 and 30 dB and for 4, 9, 16 and 25 processed signals are shown.

As in the simple case, where only thermal noise had been considered, MIMO radar system allows a lower threshold to be set (from 5 to 10 dB lower for $P_{fa} = 10^{-4}$) in any configuration, if compared to the NR system. This means that a lower noise power is overall introduced in the detector. Data whitening produces the best performance as processing of raw data requires a threshold of 5 to 10 dB higher. So it is possible to perform a comparison between the probabilities of detection of the examined systems. Although the coherent integration of re-phased signals still achieves the best performances, these are extremely close (in the order of very few dB) to the MIMO's, totally in line with the results of the other sections, so that the reduced complexity of MIMO algorithm is surely an asset in the overall comparison with netted radar systems.

Fixed threshold on whitened data

First of all, given the covariance matrix in time, $\tau\mathbf{M}_T + \sigma_n^2\mathbf{I}_L$, we whitened the data in this domain, i.e. we attempt to remove the correlation, supposing to have a fully known correlation matrix. In so doing it is also possible to achieve, after integration, a simpler expression of the pdf of clutter plus noise, as can be inferred from 6.7.

As the detectors of both MIMO and NR system work on the row of the matrix in Figure 6.7, it is convenient to whiten data in this dimension as well. In fact, especially for netted radar systems, it is better to avoid clutter correlation as the coherent sum processed into the detector may enhance the disturb power, thus increasing false alarms.

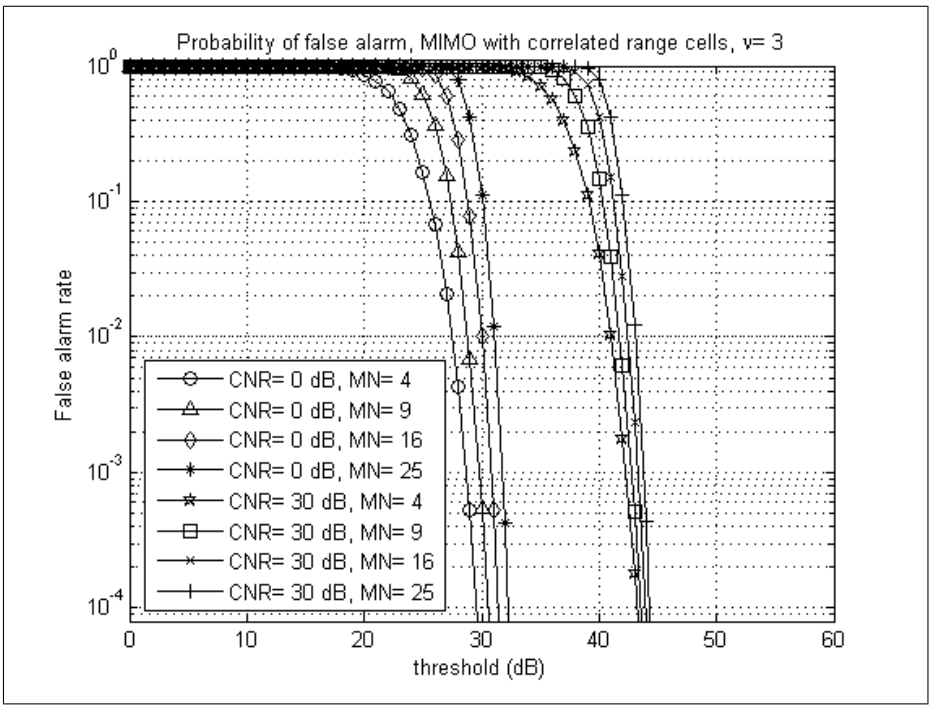

Figure 6.8: False Alarm Rate against threshold

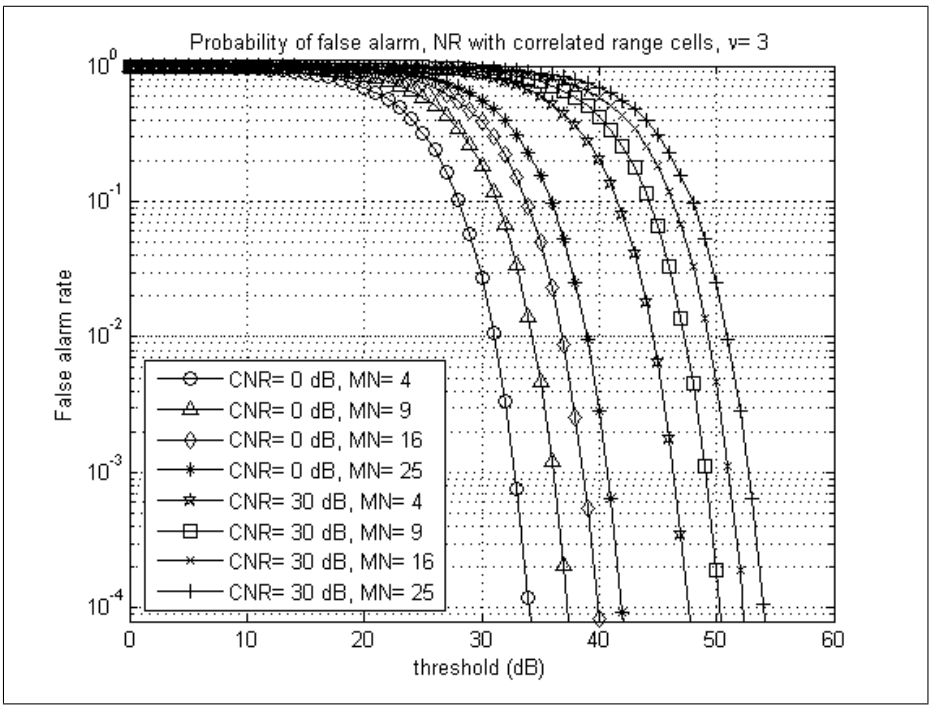

Figure 6.9: False Alarm Rate against threshold

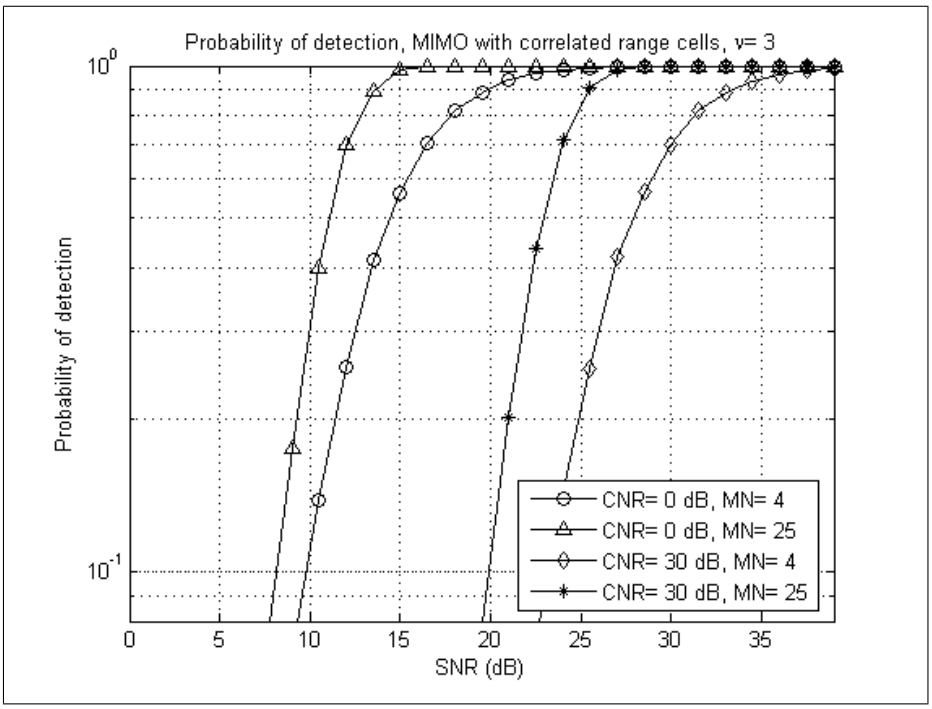

Figure 6.10: Probability of detection

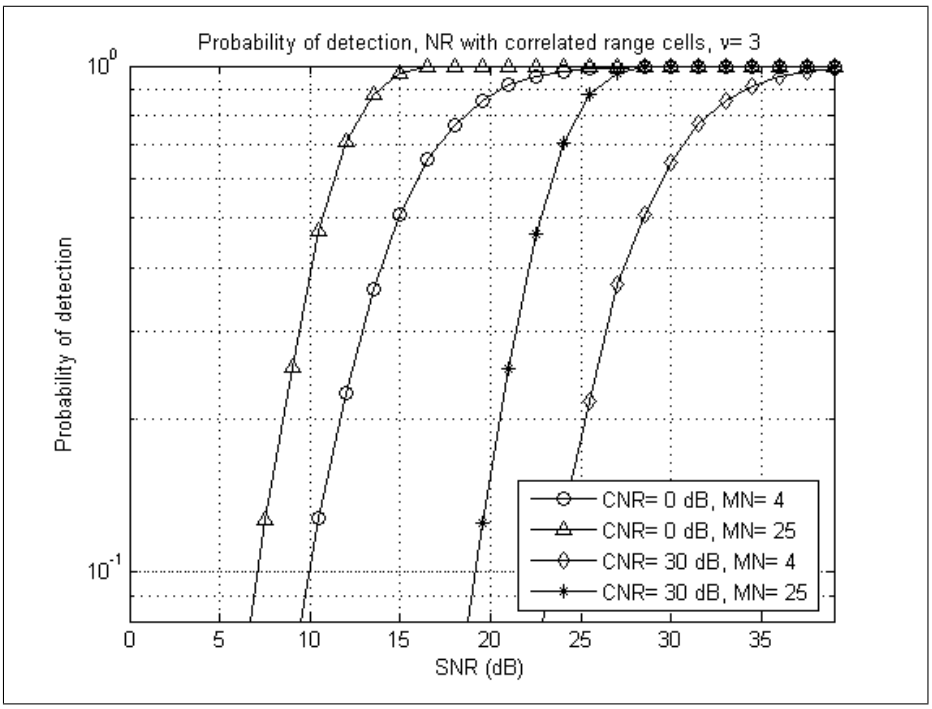

Figure 6.11: Probability of detection

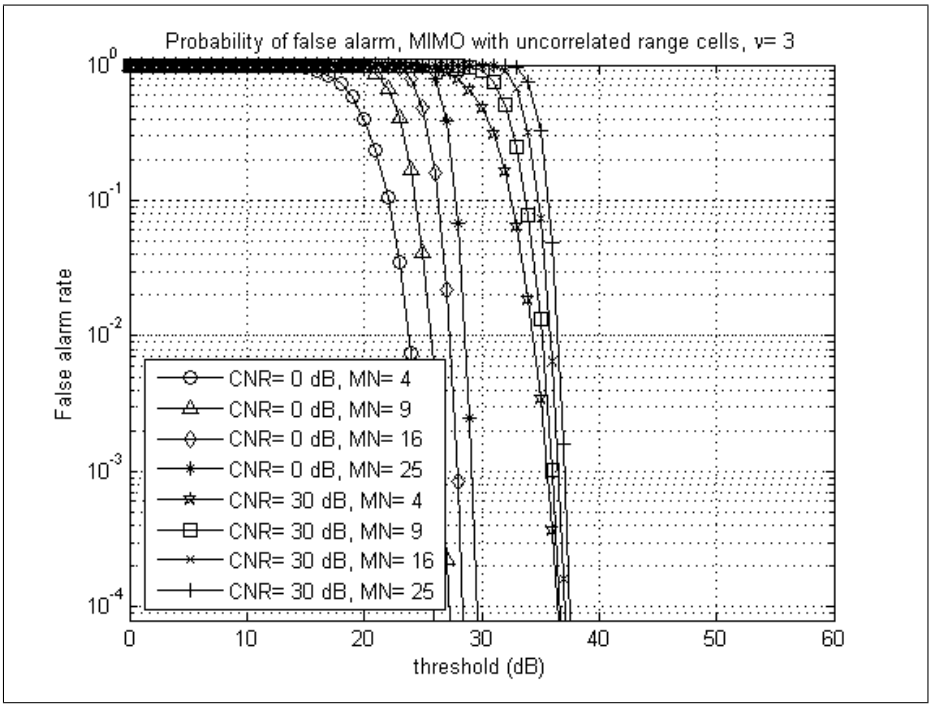

Figure 6.12: False Alarm Rate against threshold

A second method of processing is to remove the correlation in the 3 (or just 2, if range is not taken into account) dimensions. It is clear that, as detectors will work on the row of the matrix, a certain correlation on the columns of the 3D matrix in Figure 6.7 does not affect the decision process. After this operation it will be possible to write down a decision rule (threshold for CFAR condition) using the properties of the pdf of the disturbance (noise and clutter). It is worth highlighting that this solution cannot be performed without estimating the clutter texture on a limited number of cells, thus it is reasonable that practical errors in estimates produce mismatches in the data.

The improved performance (roughly from 5 to 10 dB compared to the previous set) of whitened systems highlights the importance of this kind of processing, so future studies can provide a deeper sight into the achievable results when correlation matrixes are estimated with sub-optimum algorithms and not a-priori known. In this scenario, the use of multistatic systems may lead to a higher accuracy in estimation, mutual exchanging the information between nodes.

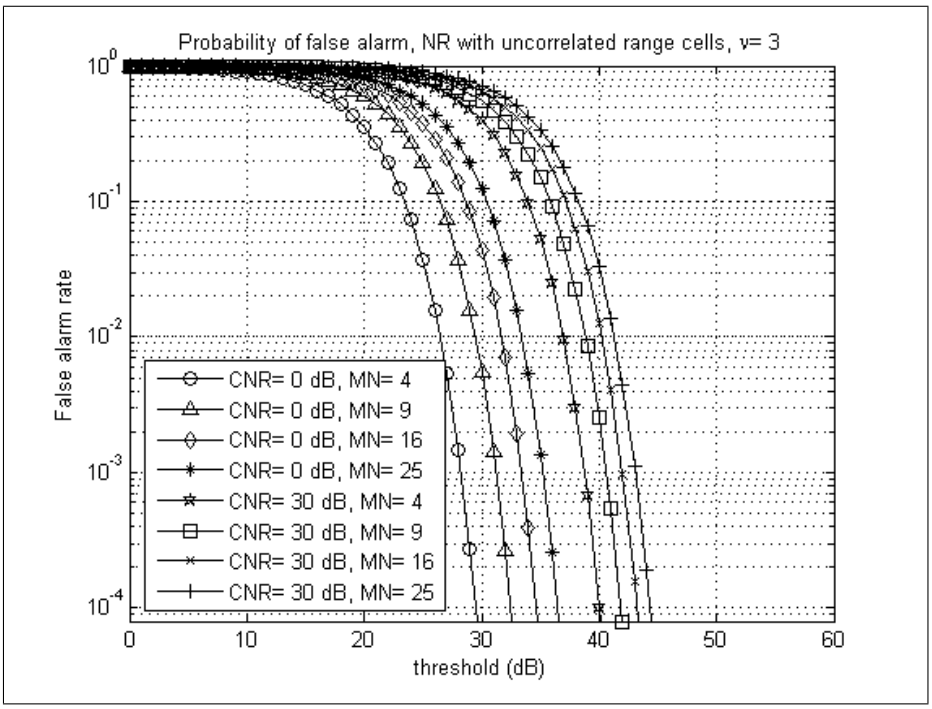

Figure 6.13: False Alarm Rate against threshold

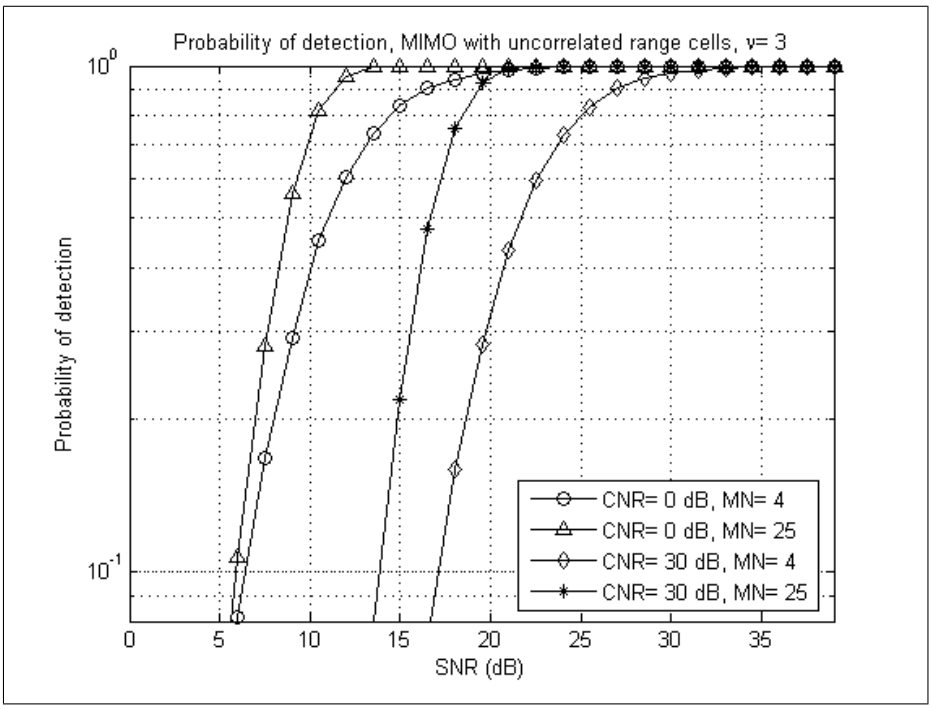

Figure 6.14: Probability of detection

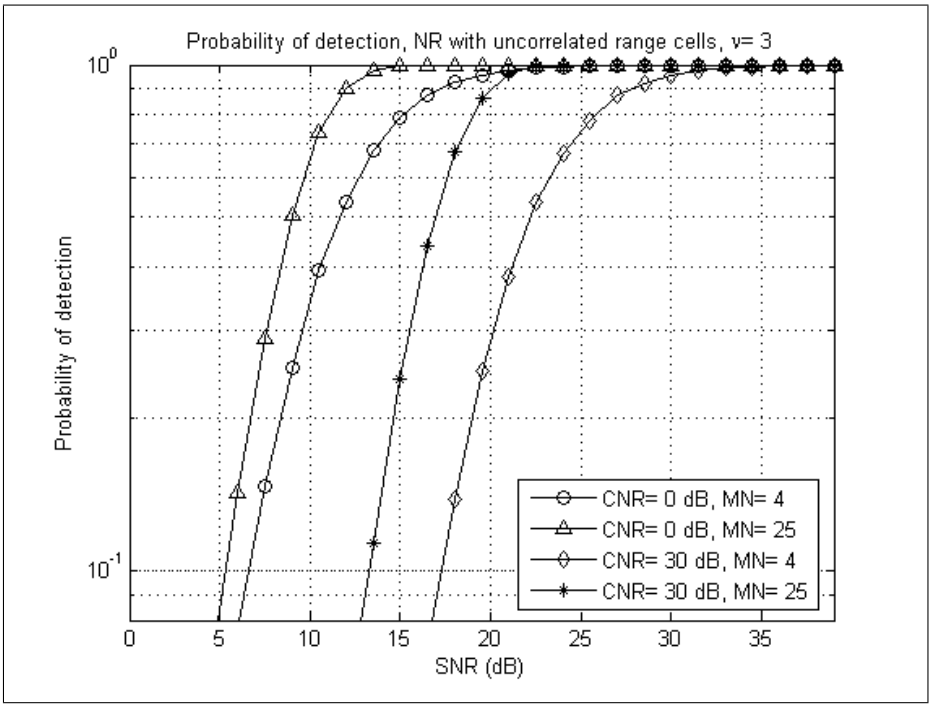

Figure 6.15: Probability of detection

Adaptive threshold (CA CFAR)on raw data

In this section we describe an adaptive CFAR algorithm for detection in a MIMO radar and RPNR systems operating in the same clutter conditions previously considered. We provide a statistical description of the signal processing and therefore we report the results in false alarm rate and detection. Moreover the incoherent algorithm taken into account is compared with a coherent way of processing the same data in order to provide a deeper understanding.

Here we apply to the radar network an adaptive Cell Averaging Constant False Alarm Rate (CA CFAR) incoherent algorithm in order to provide an increased tolerance to high power peaks that might occur when clutter is present. The CA CFAR is a well known algorithm ([15] and [24]). We examine two possible implementations of the CA CFAR algorithm; in both we estimate the clutter power using L range cells adjacent to the Cell Under Test (CUT). The only difference is in the choice of the cells used for this kind of estimation: in the first case the two adjacent cells to the CUT are taken into account, in the second they are disre-

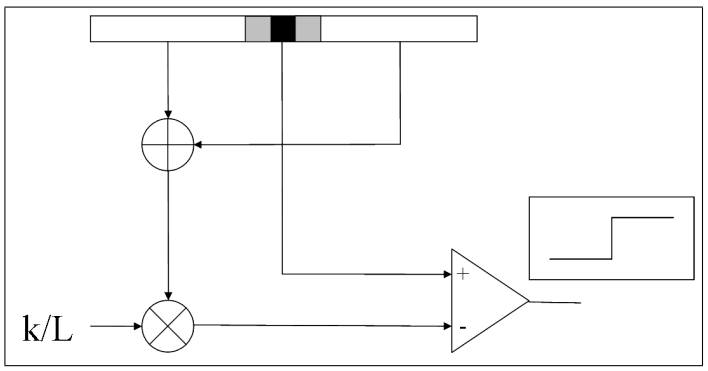

Figure 6.16: CA CFAR scheme for a monostatic radar

garded. In the latter case the presence of these two 'guard cells' can be justified since a target may occupy more than one resolution cell, so its backscattering power can take part in the adaptive threshold estimation, decreasing the overall probability of detection. However in the rest of the paper we assume that the target is within one resolution cell only. Figure 6.16 shows a symbolic scheme of a CA CFAR detector. The grey cells represent the 'guard cells' that in the second version of the algorithm will not been taken into account in estimating the detection threshold. The black cell is the CUT.

In the monostatic case the CA CFAR algorithm compares the power of the CUT with the sum of the power of L adjacent cells, opportunely averaged. So, terming x_m^2 the content of the CUT, the averaged power $|y_m|^2$ of the L adjacent cells can be expressed as (in the case of guarding cells the indexes should be opportunely shifted):

$$|y_m|^2 = \sum_{h=m-L/2}^{m-1} |x_h|^2 + \sum_{h=m+1}^{m+L/2} |x_h|^2. \tag{6.10}$$

The decision rule is therefore:

$$|x_m|^2 - \frac{k}{L}|y_m|^2 \underset{H_0}{\overset{H_1}{\gtrless}} 0, \tag{6.11}$$

where $\frac{k}{L}$ is an averaging parameter guaranteeing a certain FAR.

In the multistatic case we should assume that the centre of the CUT under observation is the same. Consequently, in accordance with the geometry of the system and the distance of the CUT, the received secondary data contains measurements of the surrounding area under various angles. In this case we have, from all the nodes, a vector X made of all the measurements from the CUT and a vector Y with the measurements coming from all the secondary data. The overall decision rule in the MIMO case can be therefore written as follows:

$$\sum_{q=1}^{MN} |x_m(q)|^2 - \frac{k}{L} \sum_{q=1}^{MN} |y_m(q)|^2 \underset{H_0}{\overset{H_1}{\gtrless}} 0, \tag{6.12}$$

When a RPNR system is considered, in the event of the presence of a target in the CUT, we operate coherently, assuming a full knowledge of the geometry and the target's position, in order to achieve the maximum SNR. As consequence of this, a coherent summation, aligning the phases of the echoes from the target, is performed and a CA CFAR decision is applied. Mathematically we can write that in this case the decision rule is:

$$\left| \sum_{q=1}^{MN} \hat{x}_m(q) \right|^2 - \frac{k}{L} \left| \sum_{q=1}^{MN} \hat{y}_m(q) \right|^2 \underset{H_0}{\overset{H_1}{\gtrless}} 0, \tag{6.13}$$

where $\hat{x}_m(q)$ and $\hat{y}_m(q)$ are respectively $x_m(q)$ and $y_m(q)$ after aligning the phases of the target only, when present.

Figures from 6.17 to 6.20 show the performance in FAR for different values of CNR, when the multiplicative factor k varies (L is set to 16 as in the previous sections). All these results have been generated for clutter with shape parameter $\nu = 3$. Changes in the value of this parameter lead to slightly different results whose overall behavior is similar to the one shown and therefore they are not reported.

In the MIMO case, Figures 6.17 and 6.18, the higher the number of nodes, the smaller the ratio $\frac{k}{L}$ guaranteeing the performance in terms of FAR. Moreover, a comparison of these figures highlights the loss of performance due to discarding the guard cells in the CA CFAR algorithm. This is evident particularly in the

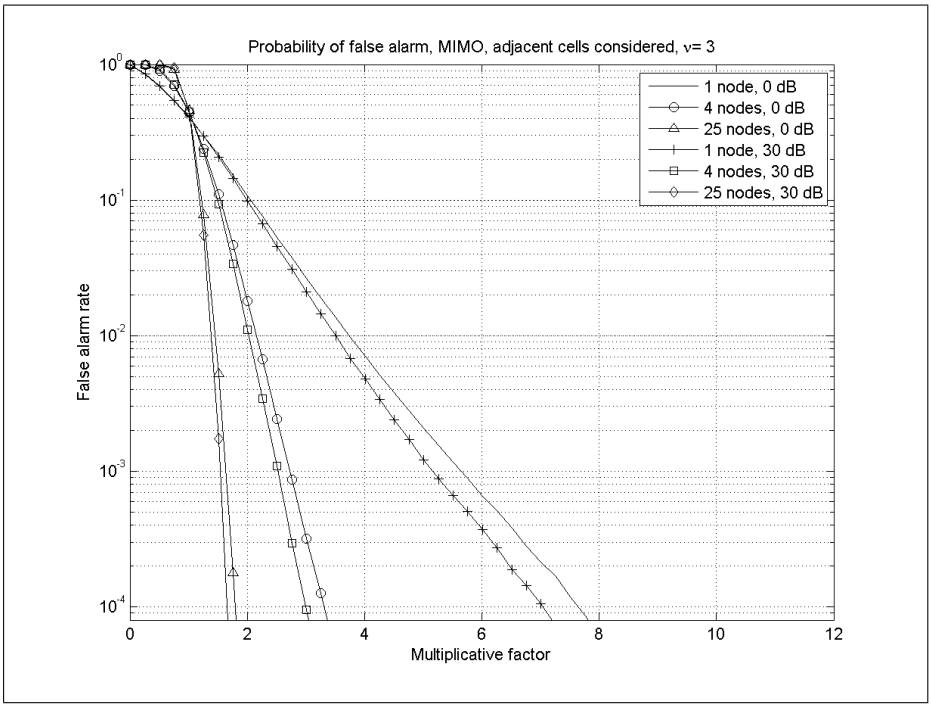

Figure 6.17: FAR performances, MIMO, guard cells, $\tau = 3$

monostatic systems: with spiky and highly correlated clutter, discarding the closest cells can lead to a considerable underestimation that has to be compensated with a bigger value of $\frac{k}{L}$.

However, it is worth noting that multistatic systems manage to make this loss much smaller: with 4 nodes (2 tx, 2 rx), but especially with 25 nodes (5 tx, 5 rx) this is almost negligible. This is due to the increased information carried by the radar network and to the diverse aspect angle of the clutter that allow a better estimation of the characteristics of the area under observation and mitigates the loss of knowledge occurring in disregarding the most meaningful cells. Small differences between curves with the same numbers of nodes, but different CNR, are due to some residuals of thermal noise affecting the processing. Actually the noise samples are independent and therefore its response to the CA algorithm has similar effects to removing the adjacent range cells of a CUT: it decreases the algorithm's accuracy in averaging. Of course the lower the CNR, the higher the thermal noise effect.

Figures 6.19 and 6.20 show the false alarm performance for the RPNR system.

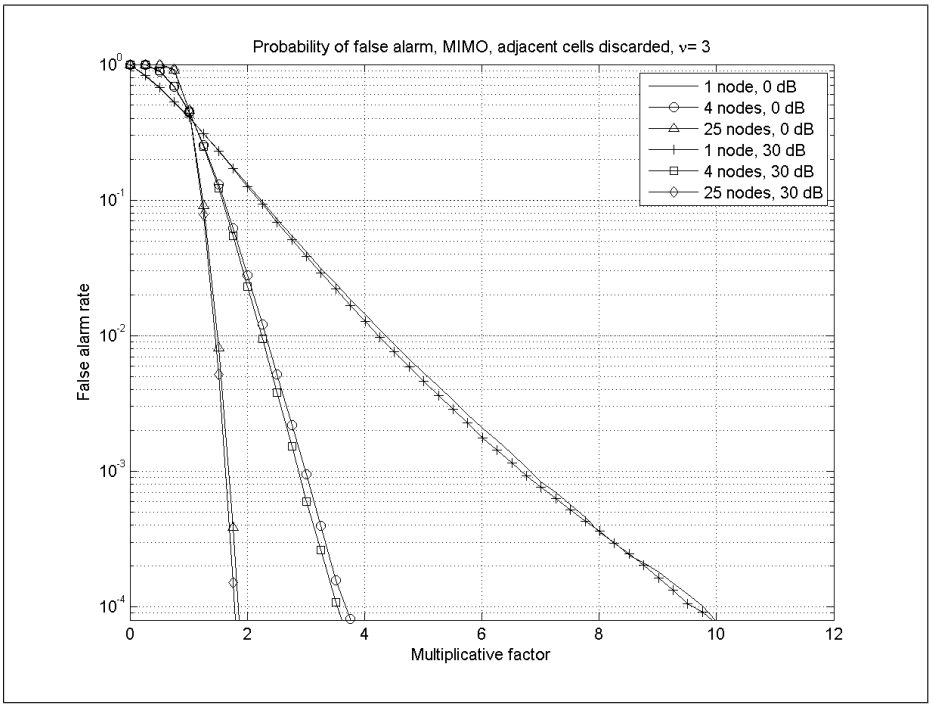

Figure 6.18: FAR performances, MIMO, guard cells discarded, $\tau = 3$

The effects of noise are evident also in Figure 6.19, where guarding cells are present: here, while the curves for high CNR overlap to one another, the residuals of the noise power separate the curves of FAR for CNR = 0 dB. Apart from this difference, variations in the curves are minimum. This is due to the overall disturbance distributions that, in the coherent case, are of the same kind, as it is particularly evident also in Figure 6.20. This is a common feature in coherent processing that has been already observed: increasing the number of nodes and processing data coherently do not modify the shape of the original distribution of the interference and therefore the behavior of the performance is similar to the monostatic case. On the contrary the incoherent processing realized by the MIMO radar systems modifies this distribution. In this figures, as well as in the work produced so far, this modification is propitious to set a lower threshold, when compared to the coherent case, for the false alarm rate.

Figures from 6.21 and 6.24 show the detection rate for a Swerling II target against the overall interference power. There are minor differences between the two versions of the CA CFAR implementation. Once again MIMO systems loose

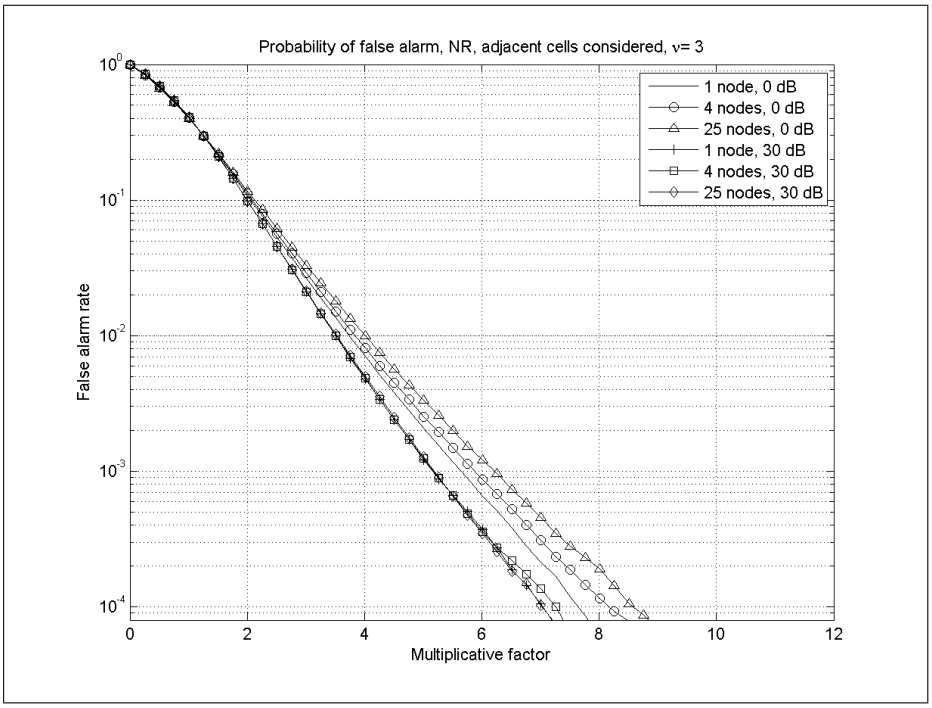

Figure 6.19: FAR performances, RPNR, guard cells, $\tau = 3$

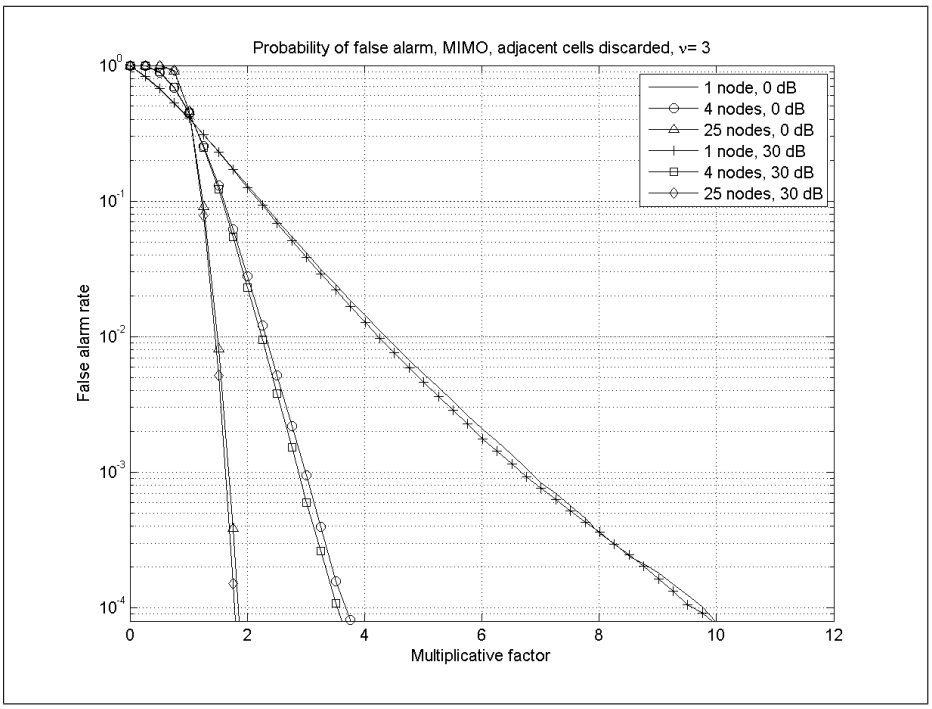

Figure 6.20: FAR performances, RPNR, guard cells discarded, $\tau = 3$

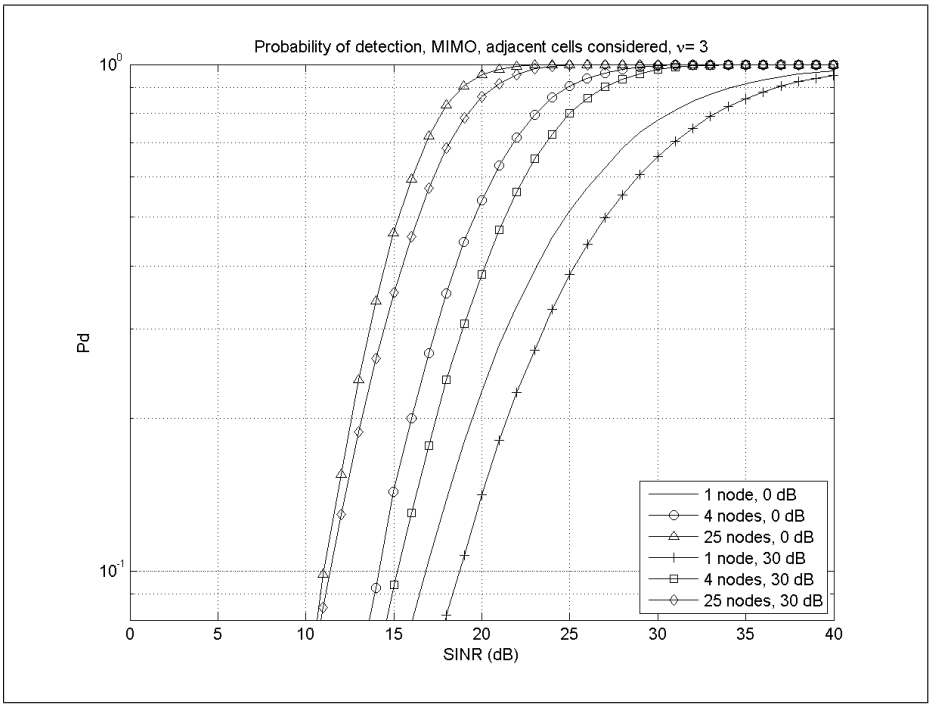

Figure 6.21: P_d performances, RPNR, guard cells, $\tau = 3$

a few dB against the RPNR that works with a-priori knowledge in order to maximize the SINR. As previously, here multistatic systems overcome the monostatic one also when constant power is transmitted: this is due to the lower threshold set for false alarm rate that allows recovering most of the losses due for sub-optimal processing.

The relatively high values of SINR necessary to yield an adequate detection rate can be justified by taking into account the distributions of the models and the integration time ($Q = 16$ pulses) before processing: actually in the time-integration process, whilst the noise and signal's power achieve a gain of Q only, because they are uncorrelated, the power of the clutter, that is highly correlated, is magnified by a much higher factor.

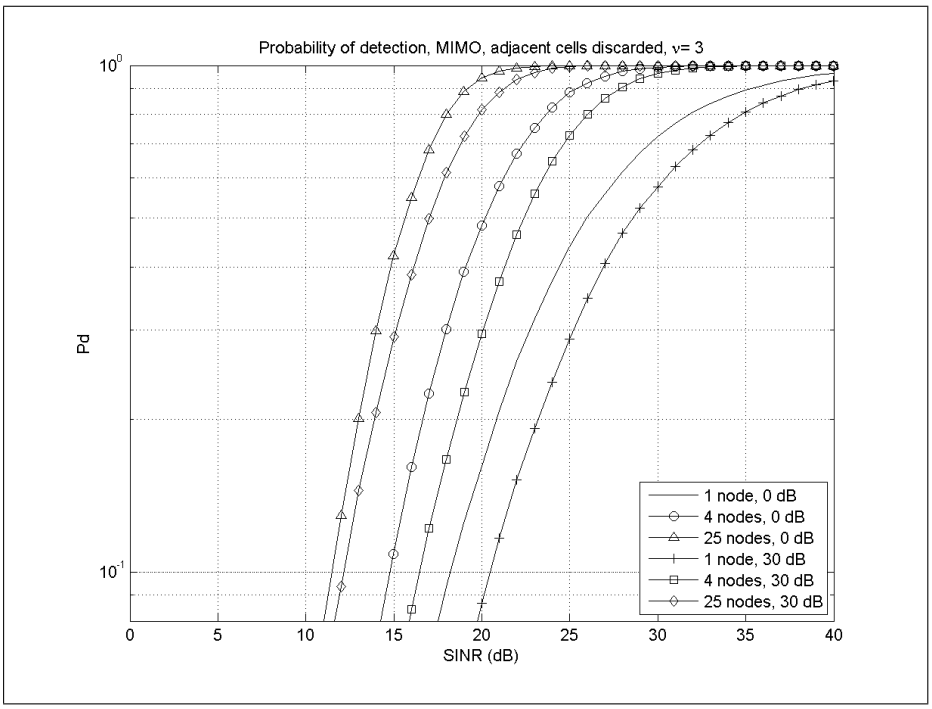

Figure 6.22: P_d performances, RPNR, guard cells discarded, $\tau = 3$

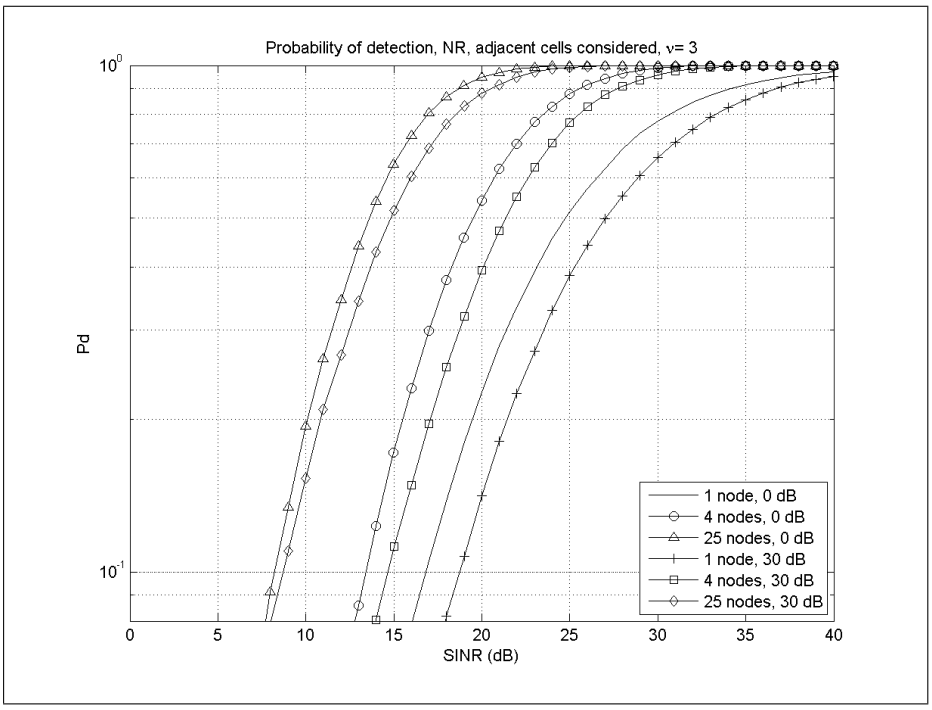

Figure 6.23: P_d performances, RPNR, guard cells, $\tau = 3$

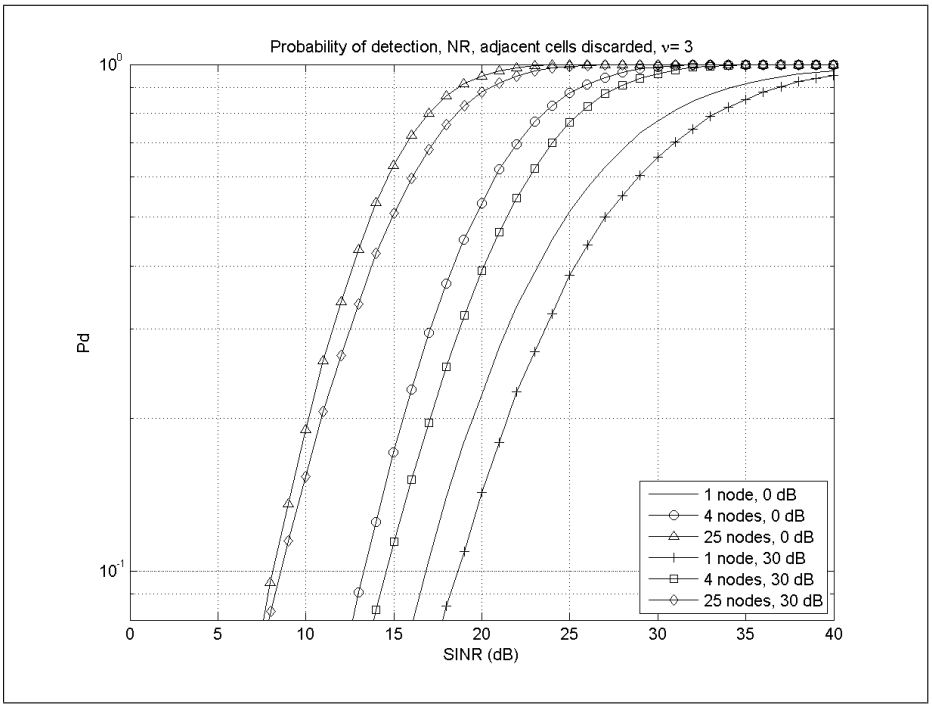

Figure 6.24: P_d performances, RPNR, guard cells discarded, $\tau = 3$

Chapter 7

Decentralized processing

In this section we apply a different sub-optimum algorithm to a radar network. This algorithm is characterized by a double threshold for detection and we report the results for two types of decision rules. The use of this form of processing technique represents an alternative to MIMO processing for radar networks. The radar network operates in the same geometry of MIMO and NR systems. This is a sub-optimum way of processing the incoming signals, where the radar network is considered as being made of all the possible mono/bistatic radars working separately in a first stage and consequently fusing the results together. The processing therefore consists of two parts. Firstly, detection is extracted from the signals for each of the mono/bistatic cases, i.e. in a decentralized pre-processing. Secondly all the decisions are jointly fused, so the system can provide a final output.

We further investigate the increased potential against jamming: we show that this algorithm, although introducing minor losses, provides the network of radars with an increased tolerance to ECM that is achieved without any of the countermeasures commonly adopted. This is due to an extra degree of freedom that can be exploited at least under jamming.

Results are reported for different numbers of transmitters and receivers that, for simplicity, have been co-located. The number varies from 1 (i.e. the monostatic case) to 5. This therefore corresponds to a number of nodes equal to 1, 4, 9, 16 and 25. The total transmit power is kept, as usual, constant.

7.1 Algorithm and statistical background

Here we expose the characteristics of the system under investigation, the model for the signals and the adopted processing. For the sake of simplicity at a first stage we assume that the signal is only affected by the noise: additional effects, such as clutter, are not relevant to understand the capabilities and the overall behaviour of this algorithm. However, we do consider the loss of performance when one of the receivers of the network is jammed with a fully matched transmission, as reported in Section 7.3.

The signal incoming to each receiver is modelled conventionally as

$$r_k(t) = H_{0/1} \sum_{m=1}^{M} \alpha_{k,m}(\sigma)\, s_m\left(t - \frac{R_{m,k}}{c}\right) + n_k(t), \tag{7.1}$$

with symbols as in Section 4.

We assume for the sake of simplicity that the noise after every matched filter has the same statistics. Therefore the thresholds for all the nodes are set to the same value in order to guarantee the same false alarm rate. After each mono/bistatic decision has been taken, a vector $\mathbf{v}$, containing only zeros (i.e. not-detections) and ones (i.e. detections), is available for the second stage of processing. At this point the decision rule assumes the target present when L elements of the vector are set at 1. The number of L can vary according to the specifications of the system. Thus the decision rule is as follows:

$$\sum_{k=1}^{MN} v[k] \geq L. \tag{7.2}$$

From a statistical point of view, if each element of $\mathbf{v}$ is independent from the others and each value '1' occurs with a probability P, the overall probability that equation (7.2) is verified is given by the following binomial function:

$$P\left(\sum_{k=1}^{MN} v[k] \geq L\right) = \sum_{k=L}^{MN} \binom{MN}{k} P^k (1-P)^{MN-k}, \tag{7.3}$$

where

$$\binom{h}{k} = \frac{h!}{k!\,(h-k)!} \tag{7.4}$$

is the binomial coefficient that takes into account all the permutations of the possible positions of '1' in **v**.

From a radar point of view we can therefore express the false alarm rate of the overall system as

$$P_{fa_{global}} = \sum_{k=L}^{MN} \binom{MN}{k} P_{fa}^{k} \left(1 - P_{fa}\right)^{MN-k}, \tag{7.5}$$

and the overall probability of detection as

$$P_{d_{global}} = \sum_{k=L}^{MN} \binom{MN}{k} P_{d}^{k} \left(1 - P_{d}\right)^{MN-k}, \tag{7.6}$$

It is worth of note that, when the false alarm rate of each single node is relatively small (i.e. $1 - P_{fa} \approx 1$), we can write the 7.6 as:

$$\begin{aligned} P_{fa_{global}} &= \sum_{k=L}^{MN} \binom{MN}{k} P_{fa}^{k} \left(1 - P_{fa}\right)^{MN-k} \approx \\ &\approx \sum_{k=L}^{MN} \binom{MN}{k} P_{fa}^{k} \approx \binom{MN}{L} P_{fa}^{L}. \end{aligned} \tag{7.7}$$

No simplified expressions can be written for the probability of detection as we are interested in much higher values of Pd and such approximations cannot be made.

This concept is therefore very close to the 'Moving Window' concept that it is well known in monostatic radar systems ([26]). However an important difference between this and the Moving Window algorithm is that here we gather samples in a space-diversity context only and consequently there is no sliding window in time; in other words we collect in one instant of time all the signals from different aspect angles and we apply a criterion as equation (7.2).

At this stage it would be suggested to use a number L of minimum detections that minimizes the losses. This has been heuristically estimated in ([26])

$$L \approx 1.5\sqrt{MN}. \tag{7.8}$$

This means that overall detection is assumed when respectively 1, 3, 5, 6 and 8 single detections occur.

In the following pages we show how, introducing a different criterion, it is possible to achieve similar performance and at the same time to have an increased tolerance to ECM. Particularly we focus our attention to the results when

$$L = \left\lceil \frac{MN}{2} \right\rceil, \tag{7.9}$$

where $\lceil x \rceil$ is the greater nearest integer of x, i.e. we assume that target is present if at least the 50% of nodes detect the target in a mono/bistatic configuration. This is to increase the jamming rejection of the overall system, as shown in the next section. Given the number of co-located transmitters and receivers we assume to detect a target when 1, 3, 5, 9 and 13 thresholds of the single nodes are passed. The first three numbers are the same for both the decision rules, so there will be no difference in their results. However this indicates that for a reduced number of nodes the two reported criteria are equivalent. On the contrary, when the radar network is made of an increased number of nodes, the two decision rules considerably differ, since there is a difference of roughly 20% of nodes in assuming detection.

Figures 7.1 and 7.2 show the results of the overall false alarm rate achievable by the network of radar against the false alarm rate of a single node respectively using the two criteria in equation (7.8), i.e. the minimum losses one, and in equation (7.9), i.e. the 50% single detections one. Here is particularly evident that the false alarm generated in one node is compensated by all the double-threshold processing and that the FAR achievable by the minimum losses criterion is smaller than the other one, whilst statistical improvement when used in detection is bigger. Furthermore it is evident that with the second criterion considered the curves for networks made of a higher numbers of nodes have an advantage on the corresponding ones of the first criterion. Moreover, whilst in the second case the more

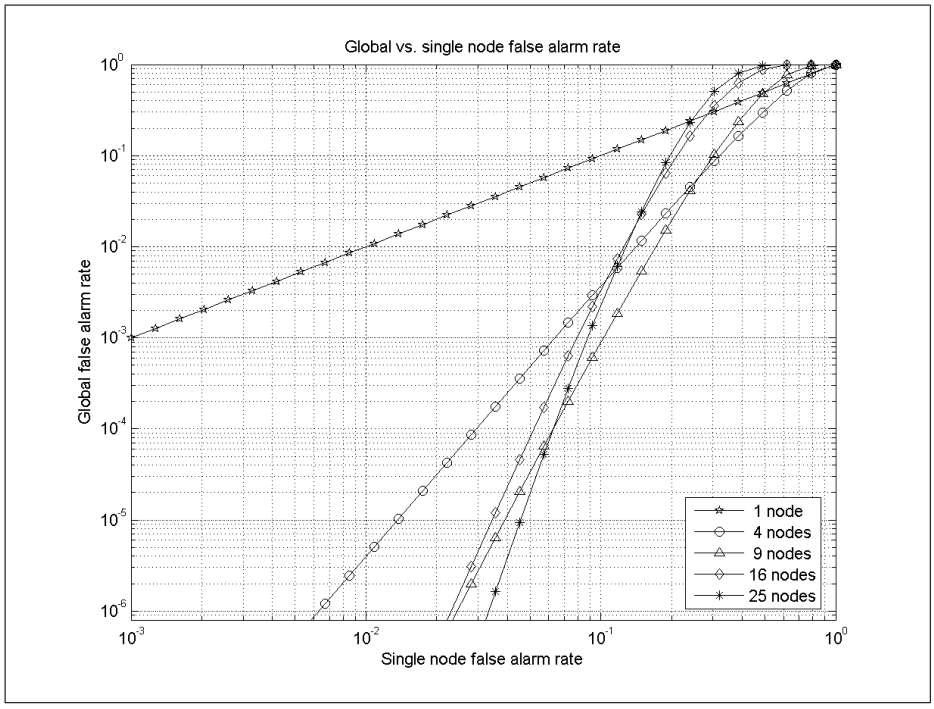

Figure 7.1: Global FAR against single node FAR, minimum losses criterion

the nodes, the better the performance, in the first one networks of 9 and 16 nodes give roughly the same results.

Figure 7.3 and 7.4 show the corresponding gain in detection. Although the first decision rule provides with better results, derived from equation (7.6), it is important to highlight that these curves have been obtained as statistical results since they do not take into account the effects of constant transmitted power as it is reported in the following section.

7.2 Performance in radar application

In this section we report the results of the algorithm described in the previous section when applied to the radar network considered. As in Section 5.2 we modelled the backscatter coefficient as a Gaussian random variable with expected value zero and variance given by the SNR times the noise power, i.e. we assume a Swerling II space-time model for the RCS of the target. Figure 7.5 shows the false alarm rate achieved by this system against the single node threshold. If compared

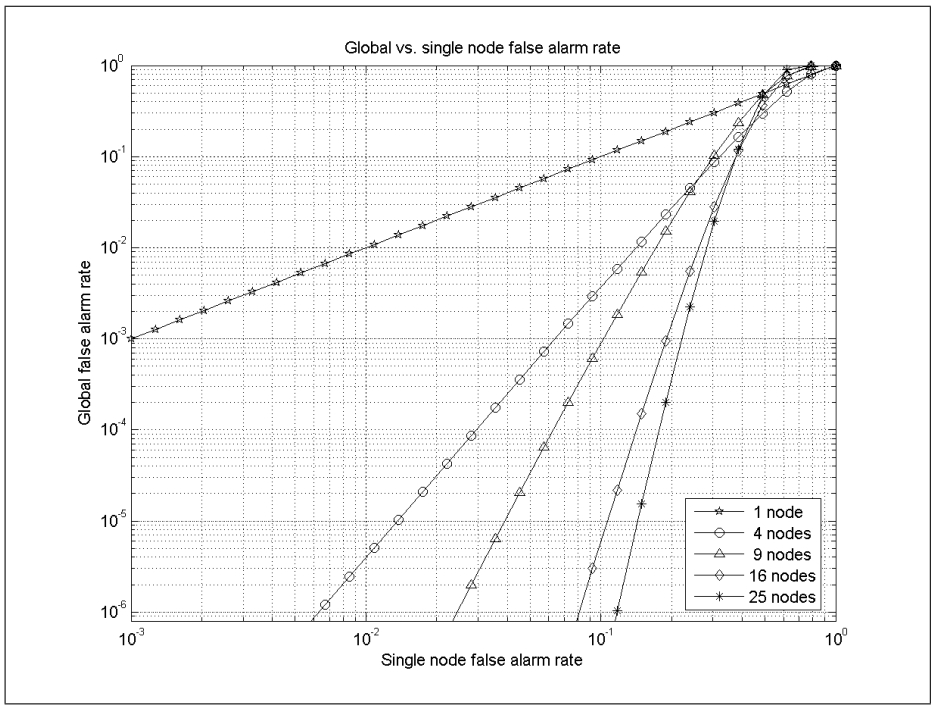

Figure 7.2: Global FAR against single node FAR, 50% criterion

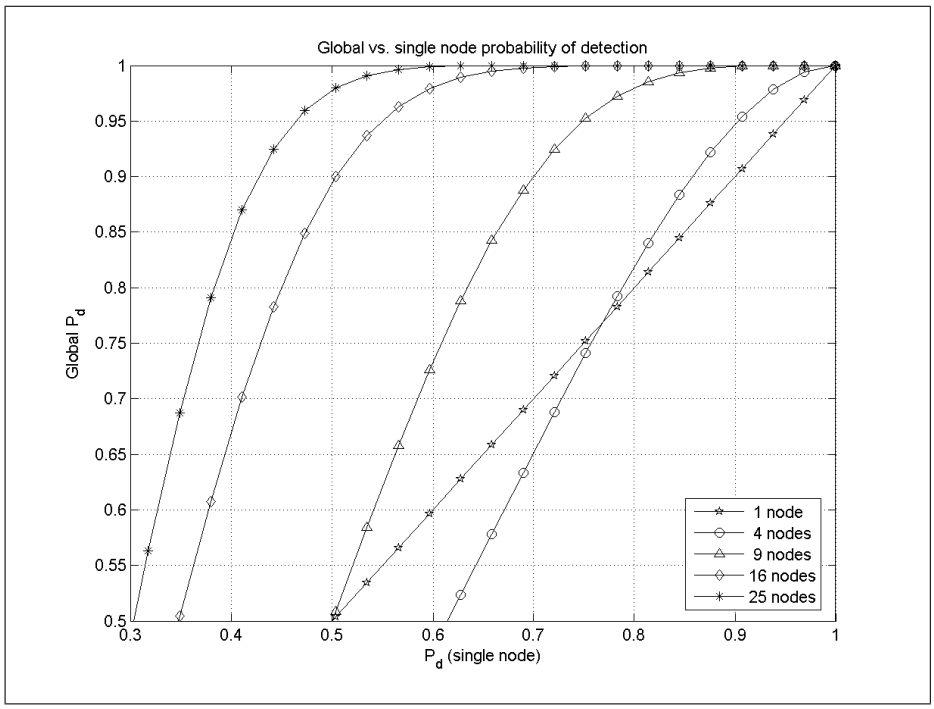

Figure 7.3: Global P_d against single node P_d, minimum losses criterion

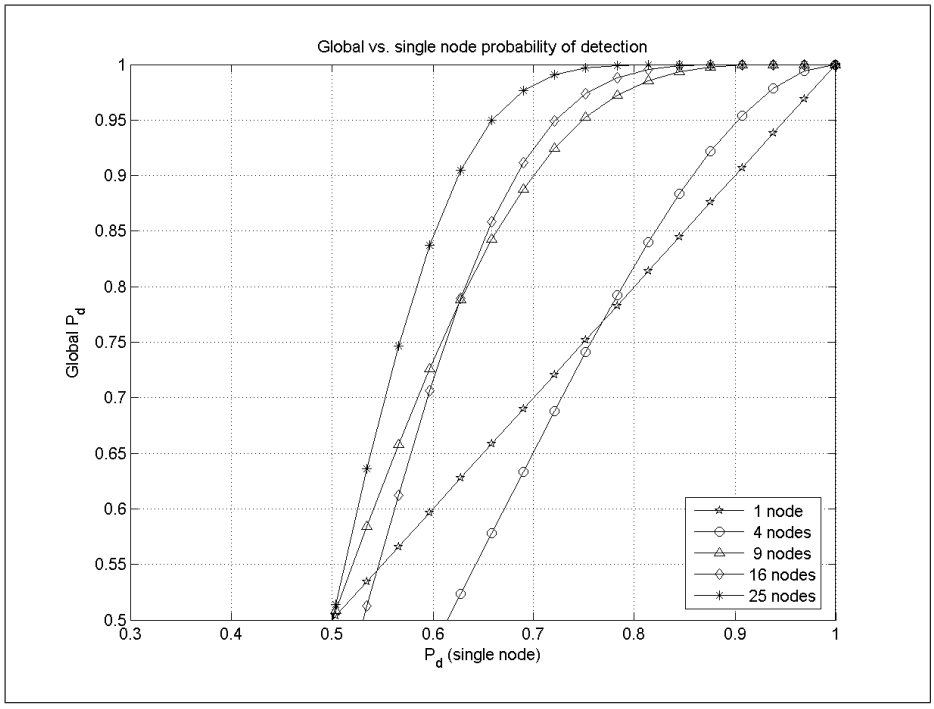

Figure 7.4: Global P_d against single node P_d, 50% criterion

to Section 5.2, it is evident that, whilst for MIMO and NR systems the higher the number of nodes, the higher the threshold, the opposite happens when using a decentralized algorithm. However it has to be highlighted that here the threshold is set at the single node, while in the centralized case it was determined for the overall set of received signals.

Figure 7.6 shows the results for the probability of detection of the single nodes, taking into account the effects of constant transmitted power. The false alarm rate of the overall system is set at 10^{-6} as in Section 5.2, in order to enable a direct comparison. Since for 16 and 25 signals the false alarm rate on the single node is relatively high, here we can distinguish, for low SNR, these curves of Pd approaching the corresponding values of FAR. For high values of detection, all the curves are close to one another. This is due to two opposing factors: (i) the lower threshold allows networks with a high number of nodes to have increased performance and (ii) the bound on the total power in transmission provides networks with a lower number of nodes with an increased energy that allows recovering most of the gap.

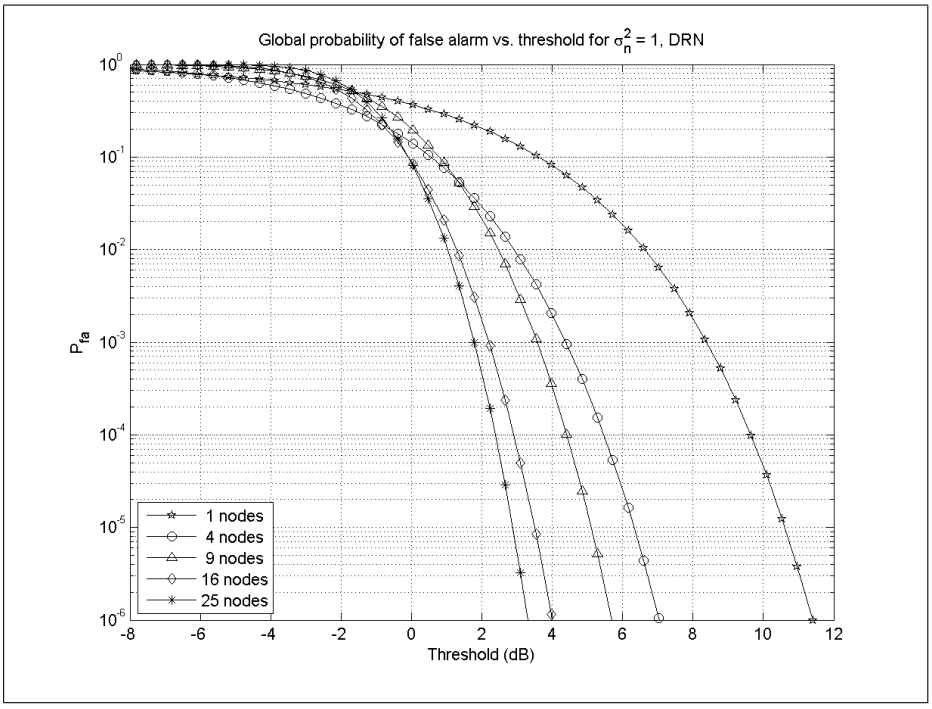

Figure 7.5: Global FAR against single node threshold, 50% criterion

Figures from 7.7 to 7.10 report the results in detection when all the signals are taken into account. Particularly Figures 7.7 and 7.8 show the results for the two criteria introduced in this Chapter, whilst the 7.9 and 7.10 report in a more compact structure the same results obtained in Section 5.2 (this Figures have been introduced to help a quick comparison between the performance). The first two clearly demonstrate that, for high values of P_d, after the second-threshold processing, the more the signals, the better the performance, as it can be expected. However it is worth noting that for low SNR (roughly below 1 dB) detection with a monostatic system is greater than the multi-node one.

Losses in SNR, for $P_d = 80\%$, are overall reasonable and can be estimated in roughly 1 to 4 dB against MIMO and in 2 to 5 dB against coherent NR, when respectively from 4 to 25 signals are processed. These losses can be considered as due to distributed processing and, indeed, they could be expected, due to two main reasons:

- ▷ since the received power is a function of the measured RCS, this is system

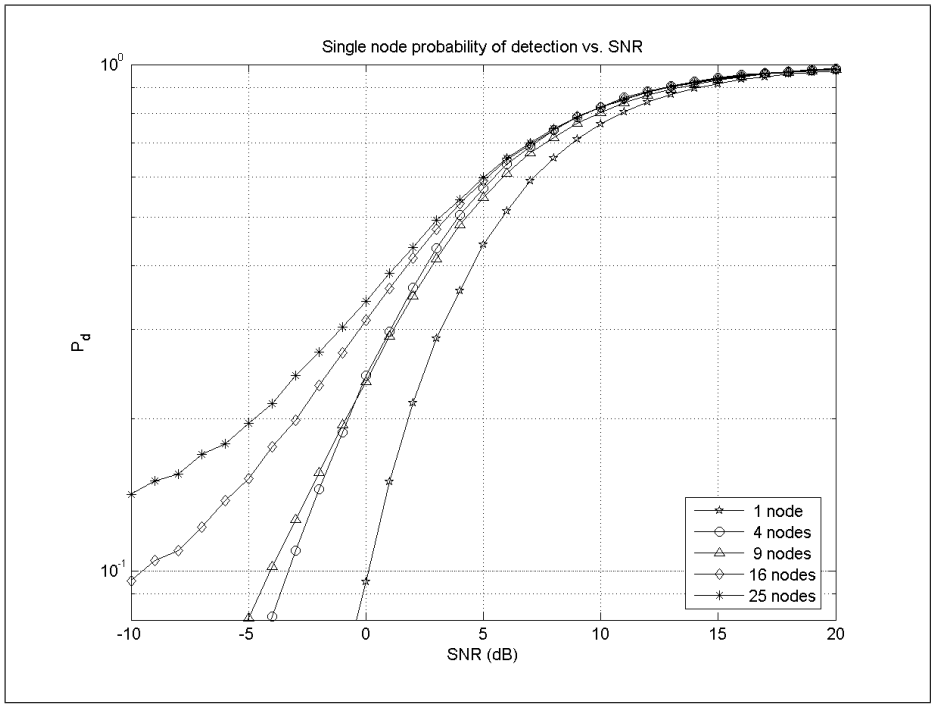

Figure 7.6: Single node P_d against SNR, global FAR= 10^{-6}, 50% criterion

is not able to detect a target when just a few echoes are large and the others relatively small. This is a drawback of this algorithm that does not affect centralized processing algorithms.

▷ Furthermore, for relatively low SNR, while MIMO and NR systems sum up every signal incoming into the receiver, this sub-optimum algorithm considers only the signals with a power greater than the first threshold. So, whilst in centralized processing every received signal contributes to the output power, here only a number of them are taken into account. This can be considered as a loss of power or sensitivity introduced into the second stage of processing and consequently in a loss of performance.

7.3 Jamming tolerance

In this section we consider the effects on performance when one of the receivers of the network is jammed with a fully matched transmission, i.e. when the received

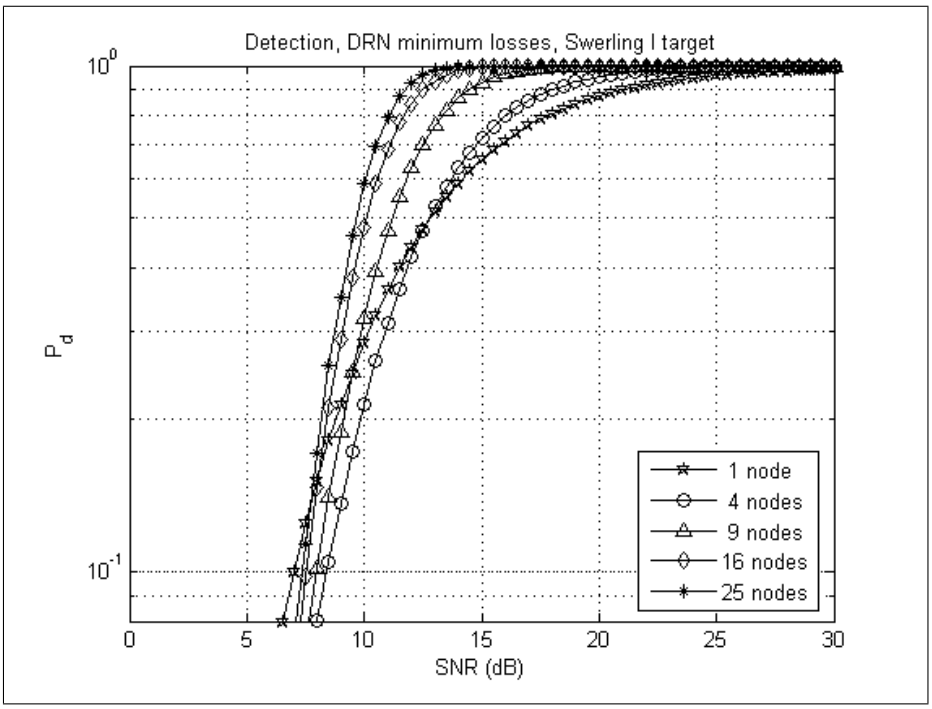

Figure 7.7: Global P_d against SNR, FAR= 10^{-6}, minimum losses criterion

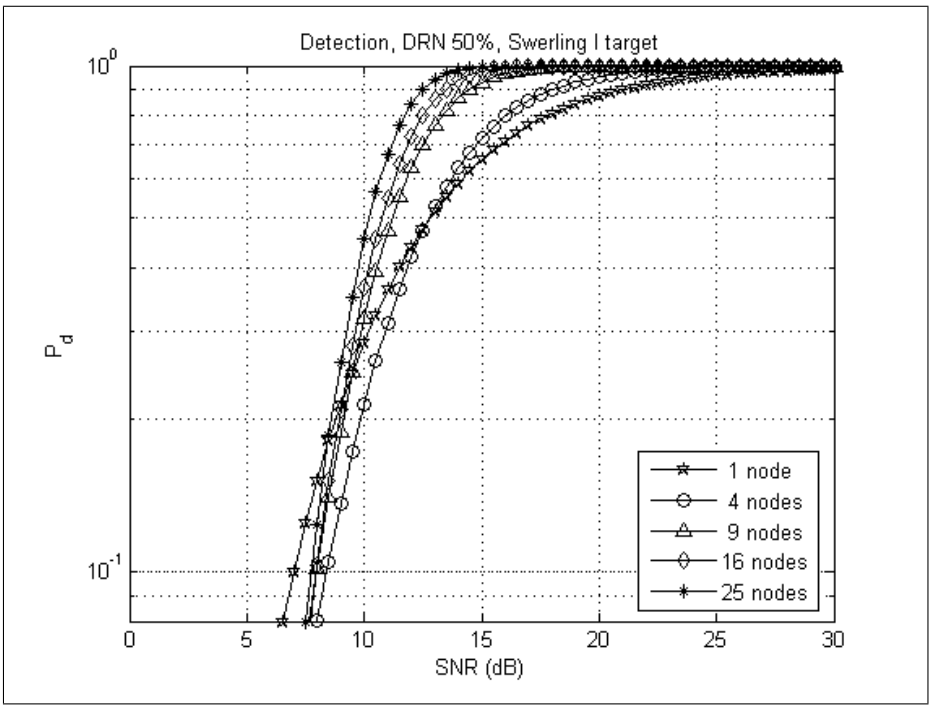

Figure 7.8: Global P_d against SNR, global FAR= 10^{-6}, 50% criterion

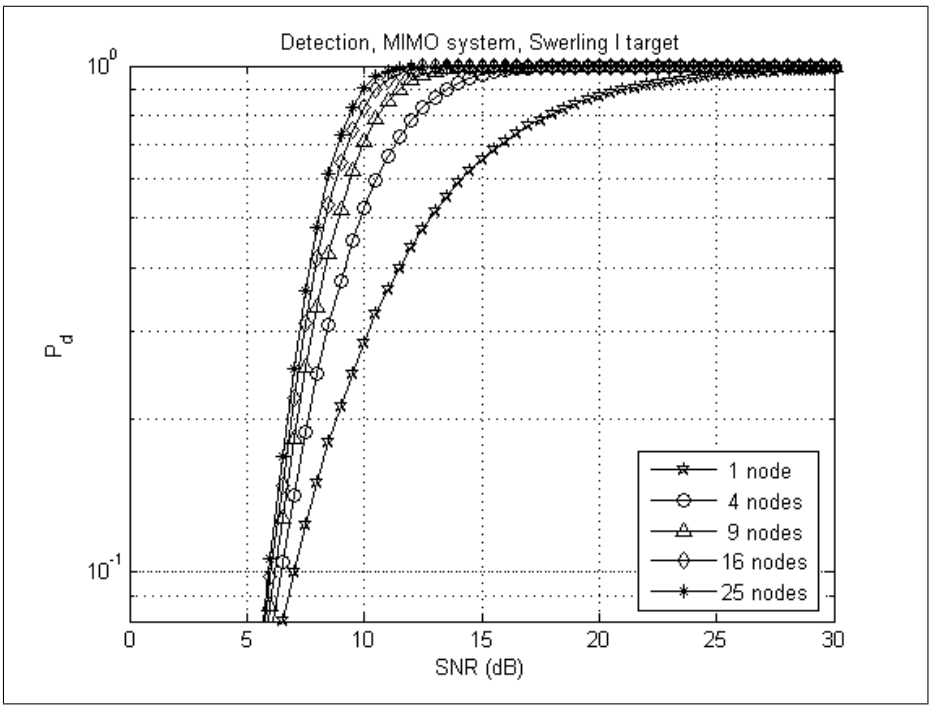

Figure 7.9: MIMO P_d against SNR, global FAR= 10^{-6}

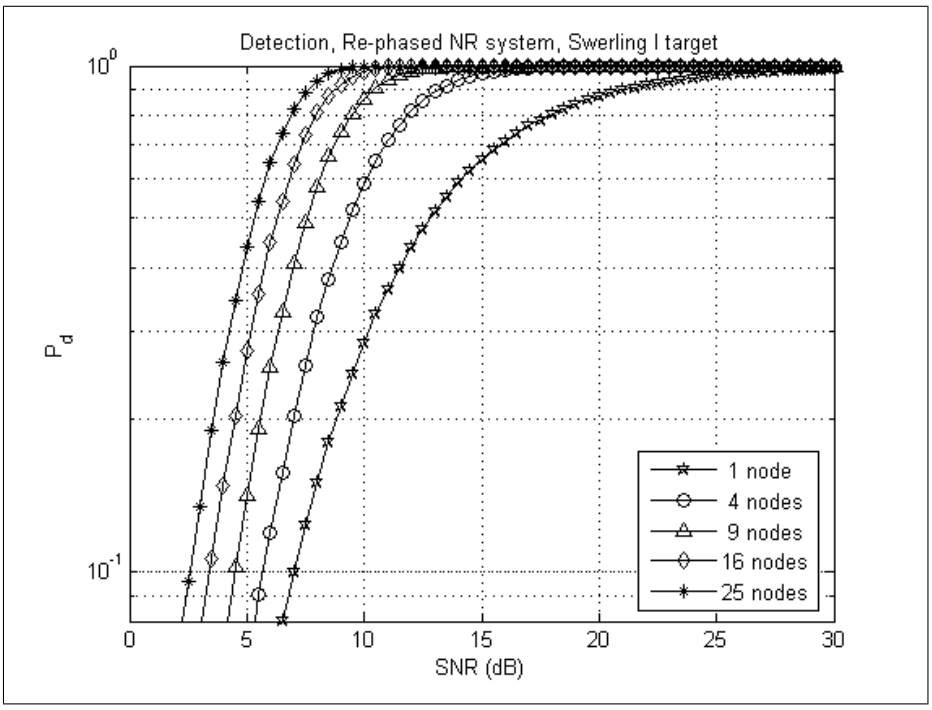

Figure 7.10: re-phased NR P_d against SNR, global FAR= 10^{-6}

signal at the q^{th} receiver is expressed as

$$r_q(t) = H_{0/1} \sum_{m=1}^{M} \alpha_{q,m}(\sigma) s_m \left(t - \frac{R_{m,q}}{c} \right) + n_q(t) + \sum_{m=1}^{M} \beta_{q,m}(\sigma) s_m \left(t - \tau_m \right), \quad (7.10)$$

with symbols as in Section 4 and

$$\begin{cases} |\beta|^2 \gg |\alpha_{q,m}|^2 \\ |\beta|^2 \gg \sigma_n^2 \\ |\beta|^2 \gg \lambda_{q,m} \end{cases} \quad (7.11)$$

and $\lambda_{q,m}$ is the threshold after matched filtering of for the m^{th} waveform at the q^{th} receiver.

Figures 7.11 and 7.12 show the performance of the false alarm rate when one of the N receivers is jammed. This means that, due to the co-location of transmitters and receivers, M nodes (from 1 to 5 respectively) are being jammed. As expected there is a significant loss in FAR for all the systems. In this scenario the monostatic radar system totally loses its capacity for detection and it is evident that the higher the number of nodes, the lower the losses. No ECCM has been considered and thresholds are kept fixed at nodes, so applying any sort of ECCM algorithm will provide an ulterior tolerance. Here it is evident the minimum losses criterion has much worse performance when jammed. That is the reason why a criterion as the 50% one, that introduces roughly just one dB of extra losses, should be preferable for a decentralized processing in a radar network.

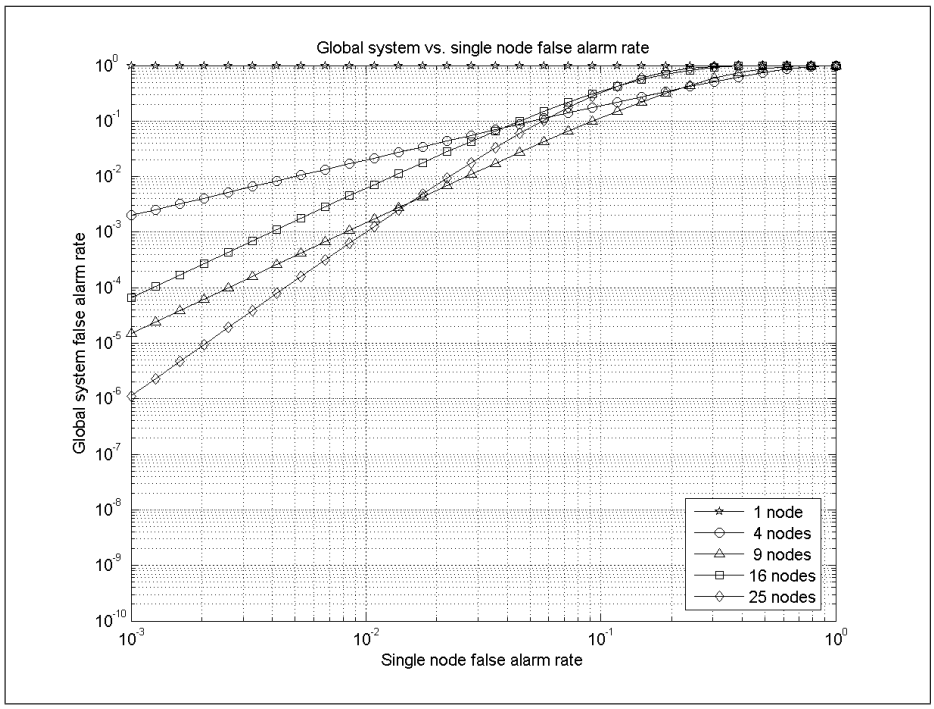

Figure 7.11: Global FAR against single node FAR, 1 jammed receiver, ML criterion

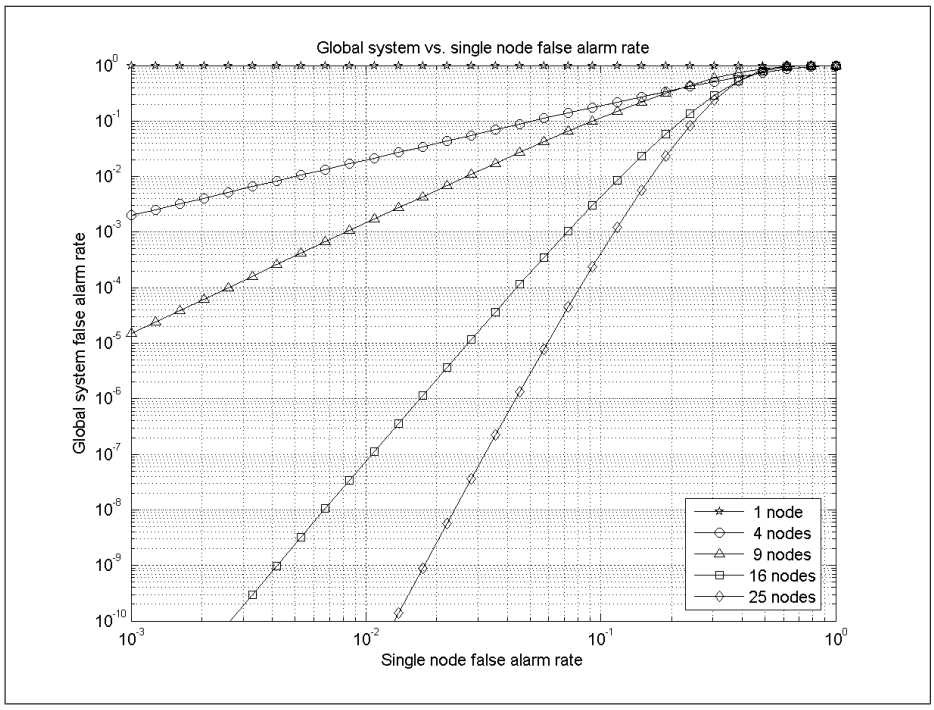

Figure 7.12: Global FAR against single node FAR, 1 jammed receiver, 50% criterion

Chapter 8

Coverage

In this section the sensitivity of each processing approach and subsequent coverage is computed as a function of the number of nodes in the radar network. Therefore, the received power and the SNR levels for a target in a particular geometry can be examined. We may recall that a constant transmit power is supplied to the radar network regardless of the number of transmitters. This allows for a straightforward comparison of performance.

8.1 Sensitivity

From the bistatic radar equation the power received $P_r(m,k)$ from a target at a distance R_m from the transmitter and R_k from the receiver is given by

$$SNR(m,k) = \frac{P_0}{M}\frac{G_T(m)G_R(k)\lambda^2\sigma(\theta_{m,k},\phi_{m,k})}{(4\pi)^3R_m^2R_k^2LKTBF} = \frac{P_r(m,k)}{KTBF}, \tag{8.1}$$

where $P_r(m,k)$ is the received power of the useful signal, K is Boltzmann's constant, T is the receiver temperature in Kelvin degrees, B is the bandwidth of the system and F is the noise figure and the rest of the symbols are defined in Section 4. This reduces to the monostatic case when $R_m = R_k$.

All the parameters with no dependency on distance, number of nodes or RCS are grouped and give the symbol $\rho_{m,k}$ (where m refers to the transmitter and k to the receiver). Thus:

$$\rho_{m,k} = P_0 \frac{G_T(m) G_R(k) \lambda^2}{(4\pi)^3 L}. \tag{8.2}$$

Therefore the dependency of the power at a single node of the network system on the range and on the number of transmitters is:

$$SNR(m,k) = \frac{1}{M} \frac{\rho_{m,k} \sigma(\theta_{m,k}, \phi_{m,k})}{R_m^2 R_k^2} \frac{1}{KTBF}. \tag{8.3}$$

In the rest of this section, for simplicity and to allow an immediate comparison, it is assumed that $P_0 = 5$ kW, $G_T(m) = G_R(k) = 30$ dB, $\lambda = 12.5$ cm, $L = 1$, $T = 290°K$, $F = 2$, $B = 10$ MHz, $M = 5$, i.e. $\rho_{m,k}$ is a constant, say ρ_0. We still assume the RCS $\sigma(\theta_{m,k}, \phi_{m,k})$ to be Swerling I distributed with 0 mean value and variance $\sigma_0 = 10$ m^2.

8.2 Covered area

The coverage resulting from the differing processing approaches is evaluated as a function of the average SNR. A value of SNR is chosen so that the overall detection rate, for each system, is 80% with a FAR equal to 10^{-6}. This means, given the differences in the underlying statistics of the overall incoming noise (Section 9), the chosen SNR value for a single pulse at each node is different in every system. This is (approximately) 18 dB in the monostatic case, 7 dB in the RPNR case, 25 dB in the simple NR case, 9.5 dB in the MIMO system and finally 11.75 dB in the DRN one (Figure 9.6 and 5.2 for the monostatic case).

8.2.1 Monostatic case

In the monostatic case the coverage (in two dimensional space) is circular and the maximum covered radius can be recovered inverting equation 8.3 and setting $R_m = R_k = R$ and $M = 1$:

$$\max\{R\} = \sqrt[4]{\frac{\rho_0 \sigma_0}{KTBF} \frac{1}{\min\{SNR_{mono}\}}}. \tag{8.4}$$

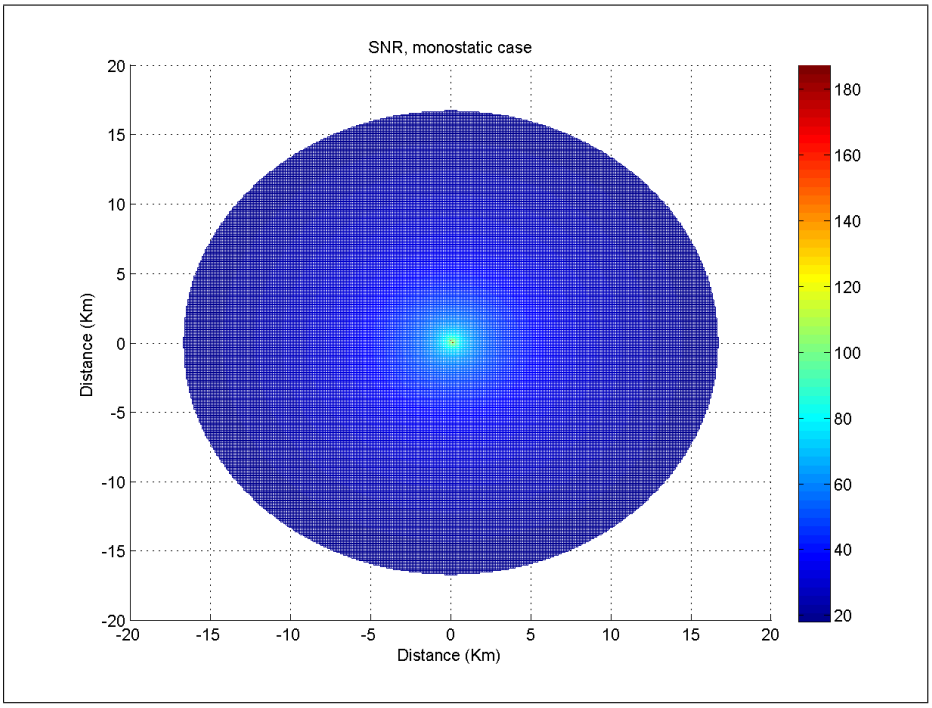

Figure 8.1: SNR and coverage, monostatic case

With $\frac{\rho_0\sigma_0}{KTBF} = 186.9$ dB $\cdot$ m^4 and $\text{SNR}_{mono} \approx 18$ dB, we find that $R_{max} \approx 16.7$ Km. Figure 8.1 shows the coverage under these assumptions.

8.2.2 Re-phased NR

Here the RPNR is examined. In this case it is convenient not to consider power as these systems operate coherently, but the amplitude and phase of all incoming signals. The global received power, after the appropriate alignment of the phases from all the signals, can be expressed as

$$P_r = \left| \sum_{m=1}^{M} \sum_{k=1}^{N} \frac{1}{R_m^2 R_k^2} \sqrt{\frac{\rho_{m,k}\sigma(\theta_{m,k}, \phi_{m,k})}{M}} \exp\{j\phi_0\} \right|^2, \tag{8.5}$$

where the phases of all the signals have been realigned to ϕ_0. On average and in the far field, where $R_m \approx R_k = R$, the received power can be expressed as

$$P_r \approx \frac{1}{R^4} E\left\{\left|\sum_{m=1}^{M}\sum_{k=1}^{N}\sqrt{\frac{\rho_{m,k}\sigma(\theta_{m,k},\phi_{m,k})}{M}}\exp\{j\phi_0\}\right|^2\right\} = \\ = \frac{\rho_0}{MR^4} E\left\{\left|\sum_{m=1}^{M}\sum_{k=1}^{N}\sqrt{\sigma(\theta_{m,k},\phi_{m,k})}\right|^2\right\}, \tag{8.6}$$

where $\sqrt{\sigma(\theta_{m,k},\phi_{m,k})}$ is Rayleigh distributed. Therefore equation 8.6 can be reduced to:

$$P_r \approx \frac{\rho}{MR^4} MN\left[1+(MN-1)\frac{\pi}{4}\right]\sigma_0{}^1. \tag{8.7}$$

The computation of the average SNR after re-phased coherent summation of all the signals is therefore:

$$SNR_{RPNR} = \frac{\frac{\rho_0}{MR^4} MN\left[1+(MN-1)\frac{\pi}{4}\right]\sigma_0}{MNKTBF} = \\ = \frac{\rho_0}{MR^4}\frac{\sigma_0}{MNKTBF}\left[1+(MN-1)\frac{\pi}{4}\right], \tag{8.8}$$

where the noise power is increased by a factor MN because of the coherent summation of all the noise samples.

Here, compared to the monostatic case, there is a gain $\left[1+(MN-1)\frac{\pi}{4}\right]$ in the global SNR. This can be approximated to $\frac{N\pi}{4}$ as the number of nodes increases. The coverage from the centre of each device is approximately 45 Km. The increase of coverage is huge when compared to the monostatic case and this is

[1] If x_k and y_k are Gaussian RV with 0 mean value and σ^2 and $\xi_k = |x_k + jy_k|$ is their corresponding Rayleigh-distributed envelop, the following applies:

$$E\left\{\left|\sum_{k=1}^{L}\xi_k\right|^2\right\} = E\left\{\sum_{k=1}^{L}\xi_k^2 + \sum_{k=1}^{L}\sum_{\substack{h=1\\h\neq k}}^{L}\xi_h\xi_k\right\} = E\left\{\sum_{k=1}^{L}\xi_k^2\right\} + E\left\{\sum_{k=1}^{L}\sum_{\substack{h=1\\h\neq k}}^{L}\xi_h\xi_k\right\} = \\ = 2L\sigma^2 + \sum_{k=1}^{L}\sum_{\substack{h=1\\h\neq k}}^{L} E\{\xi_h\xi_k\} = 2L\sigma^2 + \sum_{k=1}^{L}\sum_{\substack{h=1\\h\neq k}}^{L} E\{\xi_h\}E\{\xi_k\} = 2L\sigma^2 + \sum_{k=1}^{L}\sum_{\substack{h=1\\h\neq k}}^{L}\frac{\pi}{2}\sigma^2 = \\ = 2\sigma^2 L\left[1+(L-1)\frac{\pi}{4}\right].$$

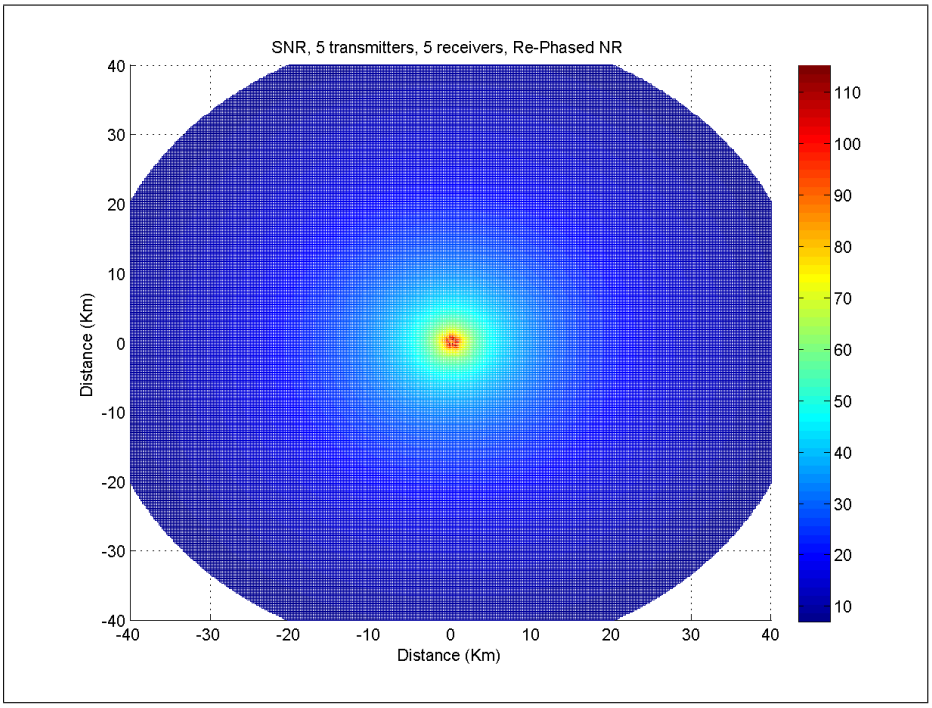

Figure 8.2: SNR and coverage, RPNR case, d= 500 m

due to the increased global SNR after processing and the reduced minimum SNR required at each single node (from 18 to 7 dB). Again, when compared to MIMO and the DRN processing, this gives us the upper bound limit for performance. Figure 8.2 shows the coverage for this kind of radar when devices are spaced 0.5 km away from the original position in the monostatic case when the system is made of 5 transmitters and 5 receivers (co-located devices). This network configuration will be the same for the other processing approaches. As shown, in both cases the coverage is increased and can be further improved by locating the nodes further away from each other (at least until the limit on sensitivity starts to be exceeded).

8.2.3 Coherent NR

Here we discuss the simple not re-phased NR system. For the same conditions as used previously the received power is given by:

$$P_r = \frac{1}{R^4}\left|\sum_{m=1}^{M}\sum_{k=1}^{N}\sqrt{\frac{\rho_{m,k}\sigma(\theta_{m,k},\phi_{m,k})}{M}}\exp\{j\phi_0\}\right|^2 \approx$$
$$\approx \frac{1}{M}\frac{\rho_0}{R^4}\left|\sum_{m=1}^{M}\sum_{k=1}^{N}\sqrt{\sigma(\theta_{m,k},\phi_{m,k})}\exp\{j\varphi_{m,k}\}\right|^2, \tag{8.9}$$

where $\varphi_{m,k}$ takes into account the phase-shift due to the path. On average this quantity can be expressed as

$$P_r \approx \frac{1}{M}\frac{\rho_0}{R^4}\left|E\left\{\sum_{m=1}^{M}\sum_{k=1}^{N}\sqrt{\sigma(\theta_{m,k},\phi_{m,k})}\exp\{j\varphi_{m,k}\}\right\}\right|^2. \tag{8.10}$$

It is well known that the coherent sum of Gaussian distributed white RV achieves a gain equal to MN in power, therefore the global SNR on the far field can be written as:

$$SNR_{NR} \approx \frac{1}{M}\frac{\rho_0}{R^4}\frac{MN\sigma_0}{MNKTBF} = \frac{1}{M}\frac{\rho_0}{R^4}\frac{\sigma_0}{KTBF}. \tag{8.11}$$

As a consequence in this system the overall SNR is of a factor M smaller than the monostatic case and in addiction the threshold on the single node is bigger (from 18 to 25 dB). This explains the reduced coverage in Figure 8.3.

8.2.4 Spatial MIMO

When spatial MIMO processing is applied, the received power is computed from the signals as

$$P_r \approx \frac{1}{M}\frac{\rho_0}{R^4}\left|E\left\{\sum_{m=1}^{M}\sum_{k=1}^{N}\sqrt{\sigma(\theta_{m,k},\phi_{m,k})}\exp\{j\varphi_{m,k}\}\right\}\right|^2. \tag{8.12}$$

On average and in the far field this can be approximated by

$$SNR_{MIMO} \approx \frac{MN\frac{1}{M}\frac{\rho_0}{R^4}}{MNKTBF} = \frac{1}{M}\frac{\rho_0}{R^4}\frac{1}{KTBF} = \frac{1}{M}SNR_{MONO}. \tag{8.13}$$

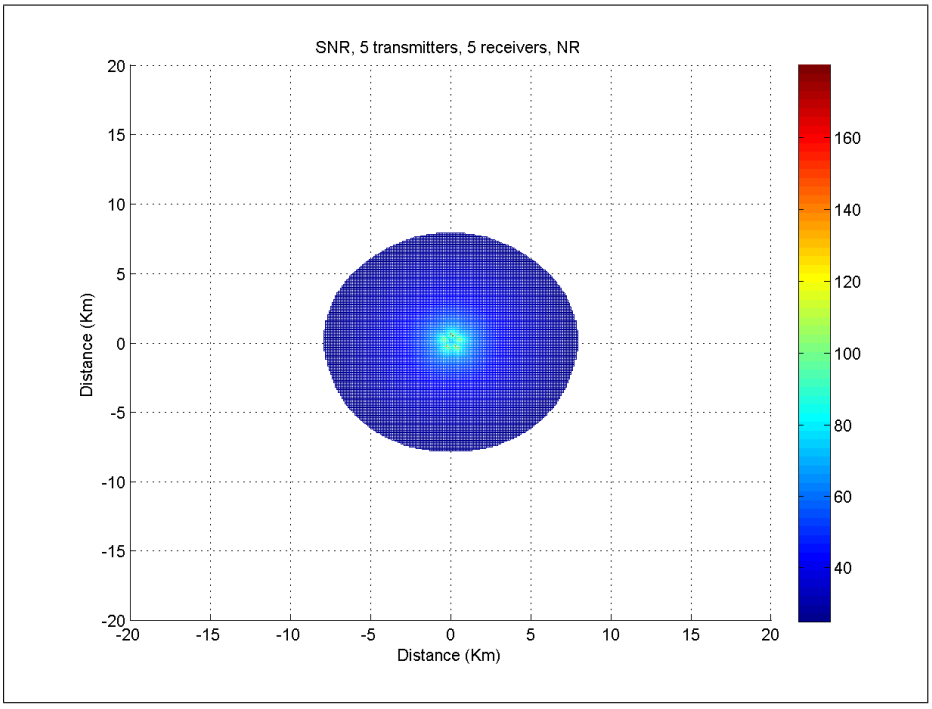

Figure 8.3: SNR and coverage, NR case, d= 500 m

Therefore in the MIMO case decreased SNR and hence reduced coverage might be expected when compared to the re-phased case. Figure 8.4 show the coverage for MIMO processing. Here the maximum covered distance is approximately 18 Km. However it is worth noting that in this case the coverage is still more extensive than in the monostatic case. This reinforces the hypothesis that in real cases, when the RCS has a complex multistatic behaviour, the angular diversity provided by MIMO radar systems can exploit scintillation of the target to outperform a monostatic system.

8.2.5 DRN

In DRN processing each node of the system operates as a single mono/bistatic radar system and in a second stage the gathered information is fused together. Under this assumption, when each device works in a monostatic configuration, it can assumed that the SNR is M times smaller than the monostatic case (due to the reduced transmitted power), thus the maximum area covered can be obtained

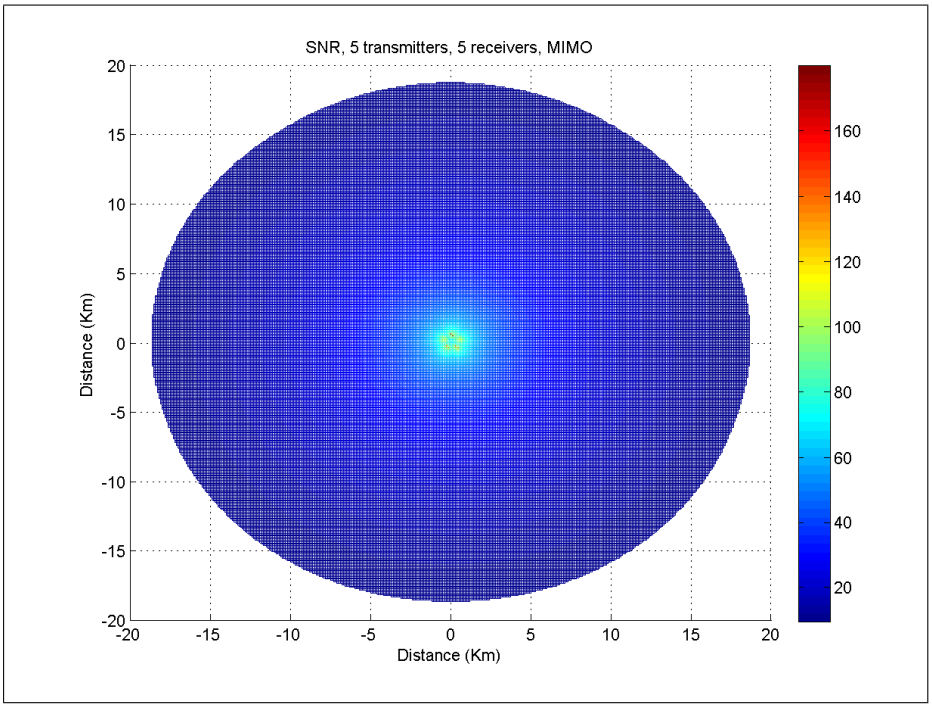

Figure 8.4: SNR and coverage, RPNR case, d= 500 m

from equation (8.4). In the far field this assumption is valid including when the receivers work in a bistatic configuration.

Figure 8.5 shows that with this form of processing the minimum SNR required at 80% of Pd is approximately 11.75 dB, against 18 dB for the monostatic case (i.e. with a gain of approximately 6 dB), but has a loss of M (= 5, i.e. $\approx$ 7 dB) due to the bound on the total transmitted power. Therefore the actual loss of this system in SNR, compared to the monostatic case is approximately 0.75 dB and the subsequent loss on the covered distance is $\approx$ 4.2%. However this loss in coverage could be fully recovered by spacing the devices in a more optimum fashion. Indeed, in realistic scenarios this will be dictated by the terrain.

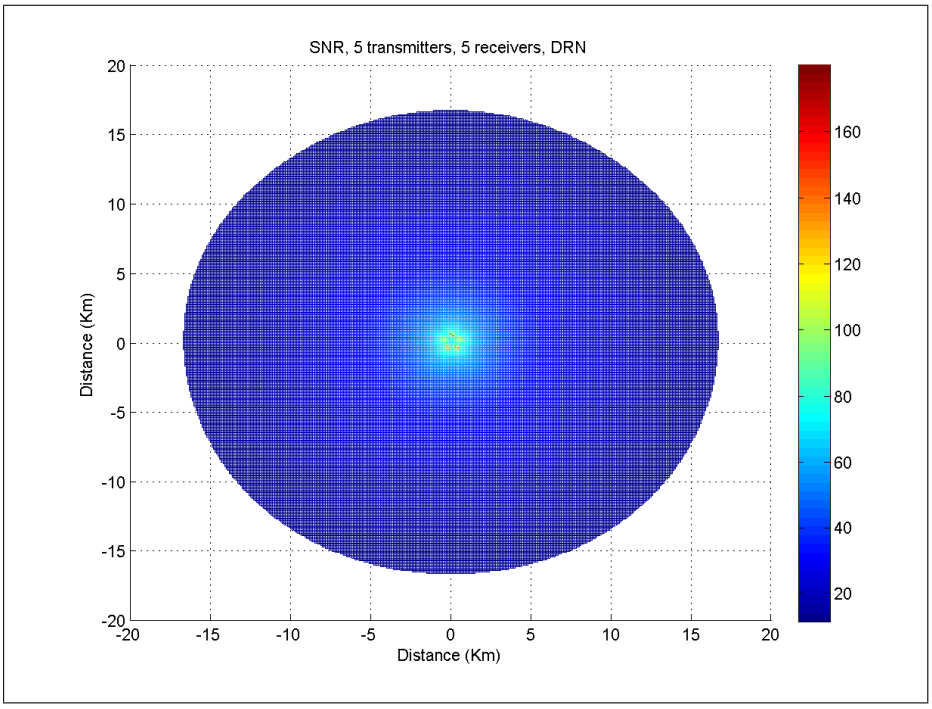

Figure 8.5: SNR and coverage, RPNR case, d= 500 m

Chapter 9

Discussion

Here consideration of the systems and their performance are reported. The aims are (i) to explain briefly the meaning of the achieved results, (ii) to understand the conditions that make a MIMO radar system to perform not far from the theoretical upper bound limit and consequently (iii) to recognize the main characteristics of the MIMO systems and to recommend improvements in the simulation and possible experiments as part of future work.

9.1 Gaussian noise and P_{fa}

In 5 we showed that MIMO systems achieve better performance than netted radars when white Gaussian noise is incoming into the receivers. This can be seen comparing Figures 5.1 and 5.2. In this section we provide a further explanation about this topic, as this is a fundamental achievement for a better understanding of the actual capabilities of this concept. In those Figures it is evident that, to reach the same values of P_{fa}, a higher value of the threshold is requested by the NR: it means that the noise power after processing is greater in this system than in both MIMO cases.

From a mathematical point of view, given the complex noise n_k at the output of any of the matched filters, according to the expression of the receiver when no target is present, the overall noise power affecting the MIMO processing can be written as

$$\sigma^2_{n,MIMO} = \|\mathbf{n}\|^2 = \mathbf{n}^H\mathbf{n} = \\ = \sum_{k=1}^{MN} |n_k|^2 = \sum_{k=1}^{MN} \sigma_k^2 \tag{9.1}$$

and the one affecting the NR processing as

$$\sigma^2_{n,NR} = \left|\sum_{k=1}^{MN} n_k\right|^2 = \sum_{k=1}^{MN} n_k^H \sum_{k=1}^{MN} n_k = \\ = \sum_{k=1}^{MN} |n_k|^2 + \sum_{k=1}^{MN} n_k^H \sum_{k=1}^{MN} n_k = \\ = \sum_{k=1}^{MN} \sigma_k^2 + 2\mathrm{Re}\left\{\sum_{k=1}^{MN-1} \sum_{h=k+1}^{MN} n_k^H n_h\right\} = \\ = \sigma^2_{n,MIMO} + 2\mathrm{Re}\left\{\sum_{k=1}^{MN-1} \sum_{h=k+1}^{MN} n_k^H n_h\right\}, \tag{9.2}$$

where MN is the number of processed signals. It is then mathematically clear that, even when the NR's noise samples are statistically independent and the mean values of noise are the same in both systems, an extra variance has to be considered in the PDF of the noise power of the NR. This extra variance leads to lower performance of the NR systems for low false alarm rates.

Looking to the problem from a statistical point of view, an even deeper understanding can be provided. It is convenient to proceed step by step. First of all, we term x and y the I&Q noises each one independently Gaussian-distributed with mean value 0 and standard deviation σ. Consequently the pdf of n can be expressed as the joint pdf $p(x, y)$ and it will be:

$$p(n) = p(x, y) = p(x)p(y) = \\ = \frac{1}{\sqrt{2\pi\sigma^2}} \exp\left\{-\frac{x^2 + y^2}{2\sigma^2}\right\}. \tag{9.3}$$

This originates in amplitude a Rayleigh distribution $\rho = \sqrt{x^2 + y^2}$ with pdf:

$$p(\rho) = \frac{\rho}{\sigma^2}\exp\left\{-\frac{\rho^2}{2\sigma^2}\right\}, \tag{9.4}$$

that in power $w = \rho^2$ becomes an exponential:

$$p(w) = \frac{1}{2\sigma^2}\exp\left\{-\frac{w}{2\sigma^2}\right\}, \tag{9.5}$$

For the sake of simplicity, we modify this expression in the simpler

$$p(t) = \exp\{-t\}\, u(t), \tag{9.6}$$

i.e. we apply the transformation

$$t = \frac{w}{2\sigma^2} \tag{9.7}$$

to equation (9.5) and we introduce the function $u(t) = \begin{cases} 0, & t < 0 \\ 1, & t \geq 1 \end{cases}$. This is equivalent to considering each noise having unit power.

Under this premise, when the netted radar processing is applied, the pdf resulting from the coherent summation of MN noise-variables will be a complex Gaussian with variance MN times bigger than the original one. Consequently the pdf of the resulting power can be expressed as:

$$p(\hat{t}) = \frac{1}{MN}\exp\left\{-\frac{t}{MN}\right\} u(t), \tag{9.8}$$

where $\hat{t} = \left|\sum_{k=1}^{MN} n_k\right|^2$.

This expression of the pdf of the overall noise explains therefore perfectly why the curves in Figure 5.2 have exactly the same shape and the only difference is a shift on the x-axis. Actually they are the realization of the same pdf apart from a different variance. Furthermore the distance, measured on the x-axis, between a certain curve and the monostatic one is exactly MN converted to dB.

When the MIMO processing is applied, the sum of the random variables is in power and not any more in amplitude and phase. This means that the pdf of the power of 2 signals, say $\tau = |n_1|^2 + |n_2|^2$, can be expressed from equation (9.6) as

$$\begin{aligned} p(\tau) &= p(t) * p(t) = \\ &= \int_{-\infty}^{+\infty} p(t)p(\tau - t)\, dt = \\ &= \int_{-\infty}^{+\infty} \exp\{-t\}u(t)\exp\{-(\tau - t)\}u(\tau - t)\, dt = \\ &= \int_{0}^{\tau} \exp\{-t\}\exp\{t - \tau\}\, dt = \\ &= \int_{0}^{\tau} \exp\{-\tau\}\, dt = \\ &= \tau\exp\{-\tau\}u(\tau), \end{aligned} \tag{9.9}$$

where $*$ is the operator of convolution. Therefore the distribution resulting from the sum of the power of two noises is a Rayleigh. Applying this process MN times, the pdf of the sum of MN noise power $\tau = \sum_{k=1}^{MN} |n_k|^2$ is distributed as follows:

$$p(\tau) = \frac{\tau^{MN-1}}{(MN-1)!}\exp\{-\tau\}\, u(\tau), \tag{9.10}$$

i.e. with a Poisson distribution. This distribution of power, as in many works published so far, can be intended as a chi-squared with $2MN$ degrees of freedom:

$$p(\zeta) = \frac{\zeta^{n/2-1}}{2^{n/2}\Gamma(n/2)}\exp\left\{-\frac{\zeta}{2}\right\} u(\zeta), \tag{9.11}$$

with $n = 2MN$. Introducing this value in equation (9.11), it becomes

$$\begin{aligned} p(\zeta) &= \frac{\zeta^{MN-1}}{2^{MN}\Gamma(MN)}\exp\left\{-\frac{\zeta}{2}\right\} u(\zeta) = \\ &= \frac{\zeta^{MN-1}}{2^{MN}(MN-1)!}\exp\left\{-\frac{\zeta}{2}\right\} u(\zeta). \end{aligned} \tag{9.12}$$

Finally the two expressions in equations (9.10) and (9.11) are exactly the same

when the change of variables $\tau = \frac{\zeta}{2}$ is applied. This transformation is necessary in order to reduce the mean value of the equations (9.12) from $2MN$ to MN that is the expected value, since we sum MN noise samples with unit variance (power).

Comparing equations (9.8) and (9.10), it is clear that asymptotically whilst the distribution of the power in a MIMO system decays with an exponential coefficient, the distribution of the power in NR systems decays with the same coefficient divided by the number of nodes, i.e. more slowly. Therefore fixing a certain threshold for both systems, say λ, we can express the NR's and the MIMO probabilities of false alarm respectively as:

$$\begin{aligned} p_{fa_{NR}} &= \int_{\lambda}^{+\infty} \frac{1}{MN} \exp\left\{-\frac{t}{MN}\right\} dt = \\ &= \exp\left\{-\frac{\lambda}{MN}\right\}, \end{aligned} \tag{9.13}$$

and

$$\begin{aligned} p_{fa_{MIMO}} &= \int_{\lambda}^{+\infty} \frac{t^{MN-1}}{(MN-1)!} \exp\{-t\} = \\ &= \exp\{-\lambda\} \sum_{k=0}^{MN-1} . \frac{\lambda^k}{k!} \end{aligned} \tag{9.14}$$

Figures from 9.1 to 9.4 show the distributions in equations (9.8) and (9.9) for 4 and 25 nodes and Figures 9.5 and 9.6 report the probability of false alarm, i.e. the cumulative distribution function, for the same number of nodes. From them it is possible to discriminate the different slopes of the decay of the power and consequently that, from a particular value of the threshold forward, the probability of false alarm generated by a MIMO system is smaller than the one of NR. These values of thresholds are, roughly, 7 dB for 4 signals processed and 14.5 for 25 with corresponding values of overall false alarm greater than 0.1, so much higher than values of interest in radar systems. Finally it is worth noting that the curves in the last Figures match exactly the corresponding ones in Section 5.

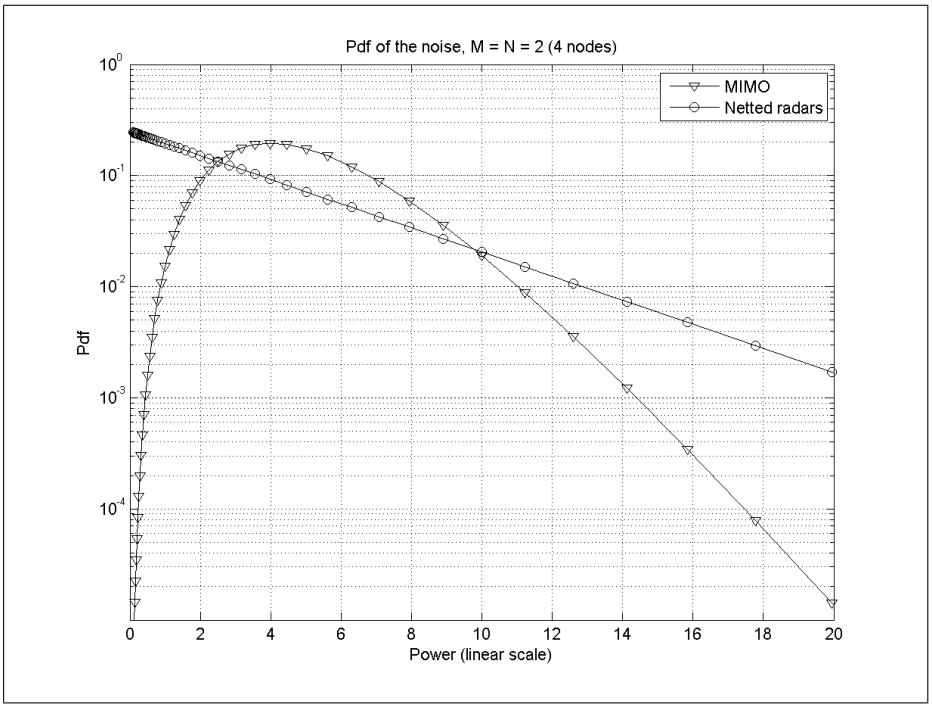

Figure 9.1: pdf of the noise power in MIMO and NR, 4 nodes

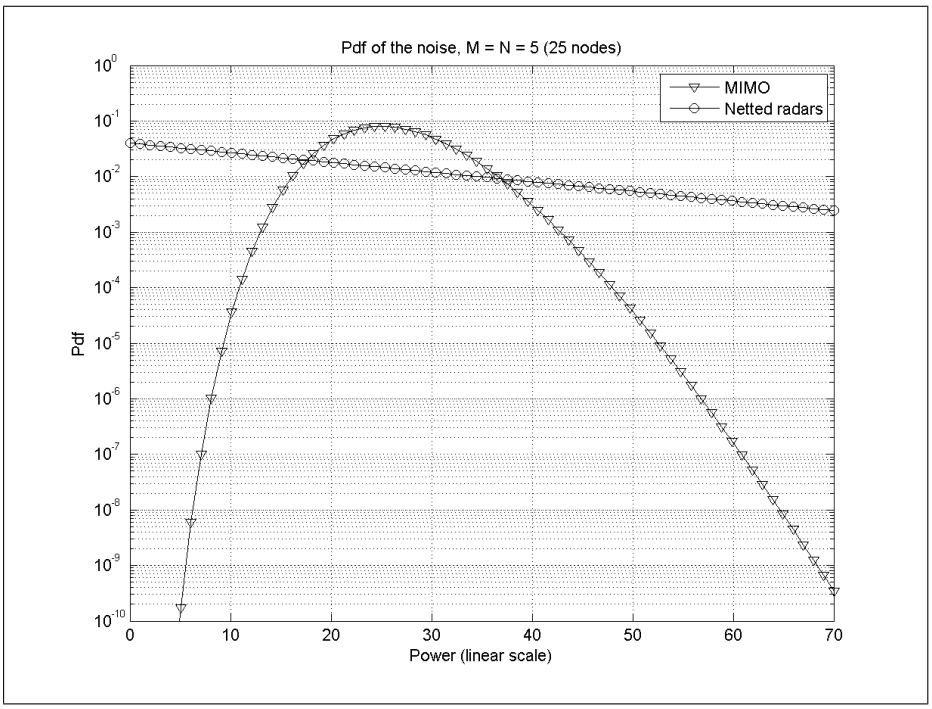

Figure 9.2: pdf of the noise power in MIMO and NR, 25 nodes

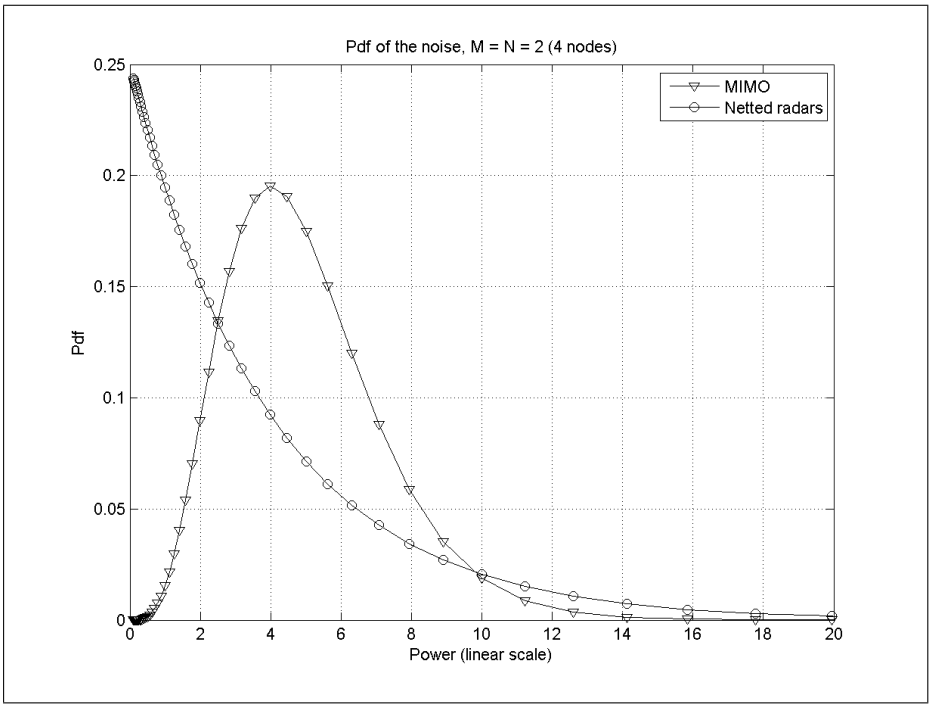

Figure 9.3: pdf of the noise power in MIMO and NR, 4 nodes

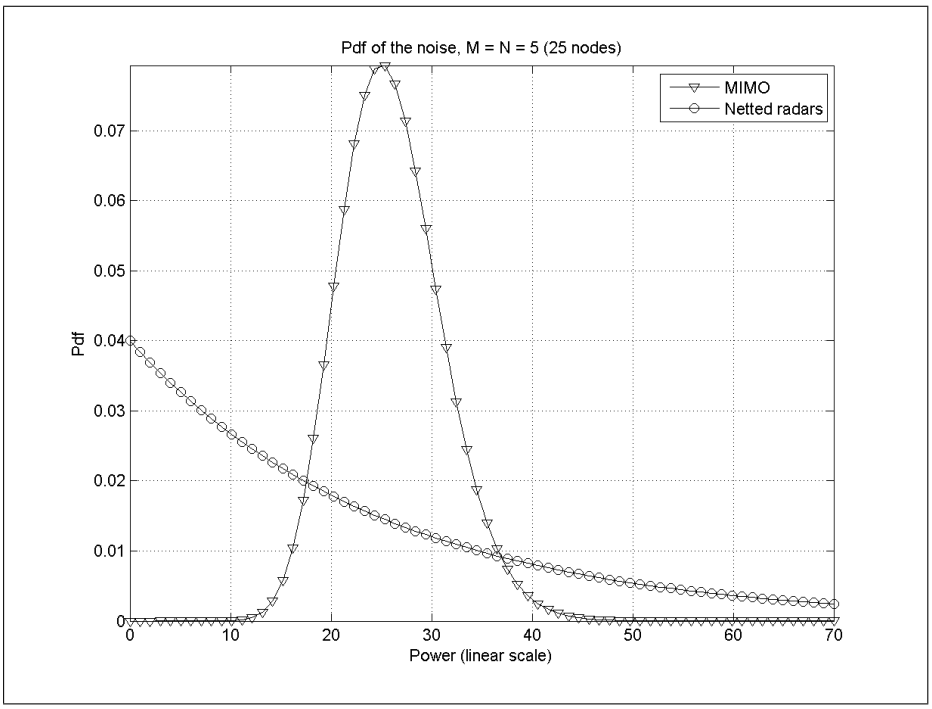

Figure 9.4: pdf of the noise power in MIMO and NR, 25 nodes

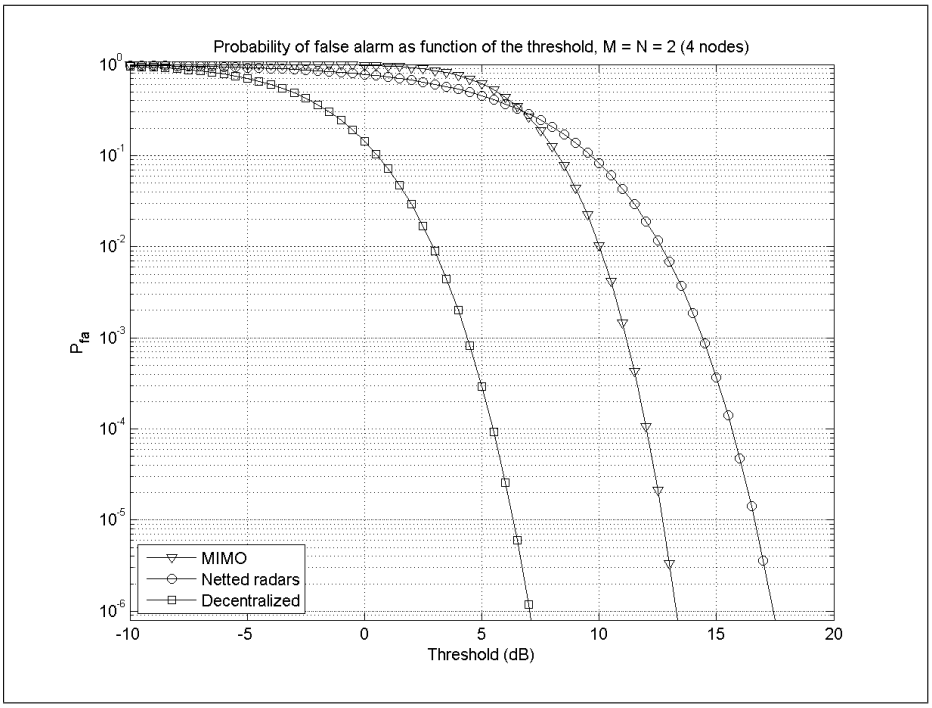

Figure 9.5: probability of false alarm in MIMO, NR and DRN, 4 nodes

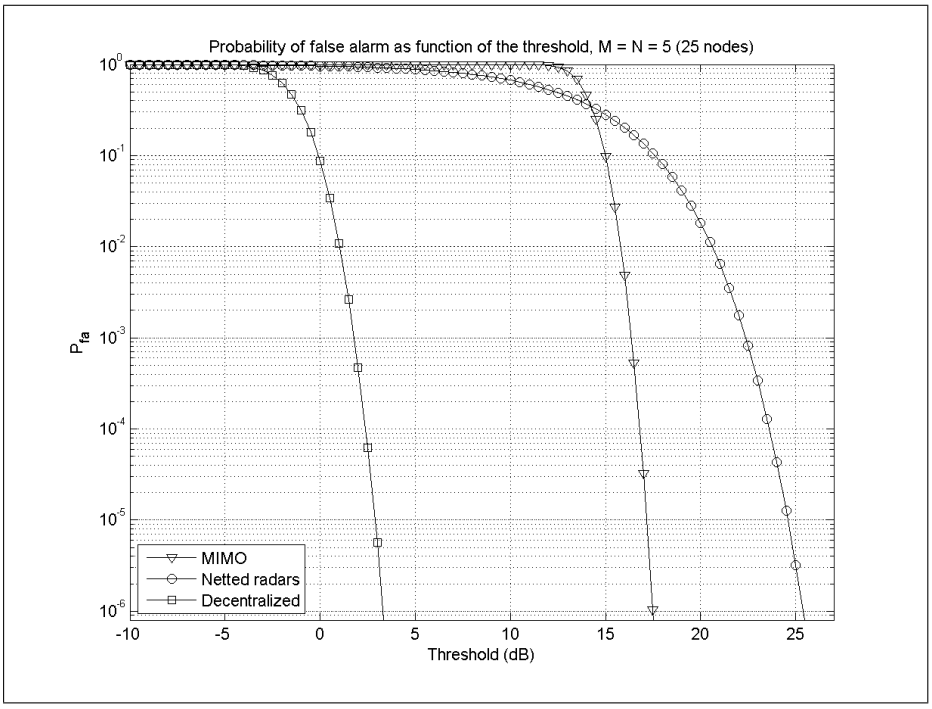

Figure 9.6: probability of false alarm in MIMO, NR and DRN, 25 nodes

9.2 P_d for Swerling targets

For Swerling distributed targets MIMO's performance is much better than the NR's one. This is mainly due to the coherent processing realized by this system that, without a-priori information and an algorithm for re-phasing the incoming signals, is not able to exploit all its potential. The figures show if coherent processing is not able to be accurately implemented the MIMO system achieves better performance and has the advantage of relative simplicity of hardware and processing.

9.3 P_d for spherical targets

The performances achieved in this case are extremely interesting as they show differences when comparing spatial and frequency MIMO systems. The spherical target doesn't yield independent samples for spatial MIMO but it does to a certain extent when the frequency variant is employed. Figures from 5.12 to 5.17 indicate that it is not possible to predict the best performer a priori between the frequency and the spatial MIMO cases and might be more indicative when considering real targets.

In Figure 5.12 the performance achieved by frequency MIMO is even better than the one of the NR where an algorithm for re-phasing the received signals has also been applied. This is due to the frequency diversity permitting at least one measurement of the target's RCS in the resonance zone of the curve in Figure 5.11 $0.5 \leq \frac{2\pi r}{\lambda} \leq 1.5$ that introduces some extra signal strength into the signal power, hence enhancing detection. It is then evident that the frequency MIMO's performances are affected by the ratio $\frac{r}{\lambda}$, as theoretically expected. For a small number of transmitted signals, the frequency MIMO seems to perform better than the corresponding spatial MIMO; on the contrary the higher the number of processed signals, the more similar the achieved results.

Significant is the loss of performance of frequency MIMO for $\frac{2\pi r}{\lambda} = 1$: in this case all the spatial MIMO's and NR's signals operate in peak of the resonance zone of Figure 5.11; on the contrary, the frequency diversity of the other MIMO

system allows at least one signal to operate in that zone, while all the others are in the Rayleigh or optical regions.

As soon as the ratio $\frac{2\pi r}{\lambda}$ reaches the optical zone of Figure 5.11, the frequency MIMO cannot exploit the extra signal strength so it performs worse than the re-phased NR. As expected, the spatial MIMO P_d curve always performs worse than the re-phased NR as the phase-shifting maximizes the received SNR.

9.4 Multipath

The improvement in detection in MIMO systems depends only on the statistical increase of the amplitude of the received signal, due to the incoherent way of processing. It should be noted that even re-phased NR system's performances can be improved by the injection of multipath into the model of the signal. This is even the case if the coherent sum processed by these systems has a reduced gain on the SNR compared to the MIMO systems.

In the case of a smooth surface this gain can be easily explained: given the Swerling I model target, the coherent sum in equation 6.1 statistically increases the variance of the measured RCS by a factor of 4. In the case of rough-surface multipath a similar effect occurs and the variance of the signals increases, although less than in the previous case. The sum of s_0 and s_1 gives rise to a Rice random variable with a pdf given by

$$p(\rho) = \frac{\rho}{\sigma^2}\exp\left\{-\frac{\rho^2 + m^2}{2\sigma^2}\right\} I_0\left(\frac{\rho m}{\sigma^2}\right); \tag{9.15}$$

at the same time also the sum of s_2 and s_3 is the realization of a Rice random variable with a PDF as in equation (9.15), even if its amplitude, compared to the previous one, is statistically reduced by a factor m. The received signal is then the sum of two Rician-distributed variables and consequently its PDF can be expressed as their convolution. These pdfs have been reported in Figure 9.7, together with the one related to the initial RCS (i.e. without multipath effect); comparing the first PDF (original RCS) to the last one (signal plus all kinds of multipath), the changes in terms of mean value and variance of the received signal, and then in terms of achieved performance, are evident.

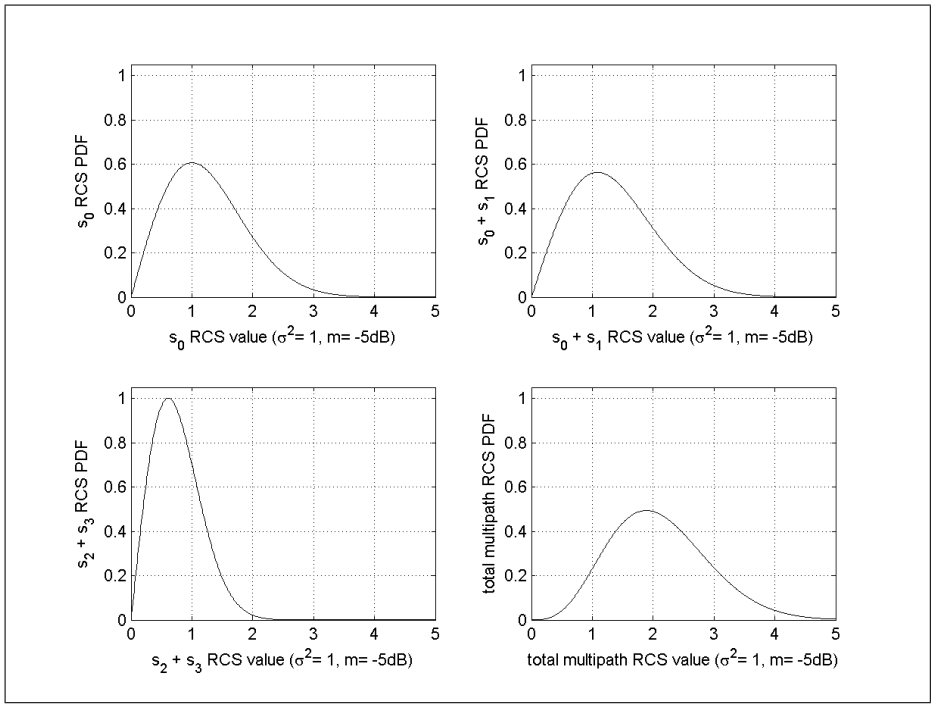

Figure 9.7: RCS (amplitude) pdf for a multipath received signal

9.5 Clutter

9.5.1 Fixed threshold

Theoretically, the threshold of the NR system processing MN data, after respectively time and couples tx-rx whitening, can be computed as follow: the sum of MNQ independent complex Gaussian RV with variance $\tau_{i,q} + \sigma_n^2$ is, again, a complex Gaussian RV, say w, with variance

$$MNQ\sigma_n^2 + \sum_{i=1}^{MN}\sum_{q=1}^{Q}\tau_{i,q} = \hat{\sigma}_n^2 + \hat{\tau}, \tag{9.16}$$

where $\hat{\tau}$ is Γ-distributed with shape parameter ν and mean value $MNQ\mu$. Thus, given a threshold λ_{NR}, the probability of false alarm will be given by

$$P_{fa} = \int_{\lambda_{NR}}^{+\infty}\int_{0}^{+\infty} p\left(r|\hat{\tau},\hat{\sigma}_n^2\right) p(\hat{\tau})\, d\hat{\tau}\, dr, \tag{9.17}$$

where $r = |w|^2$, so $p\left(r|\hat{\tau}, \hat{\sigma}_n^2\right)$ is an exponential pdf. Thus

$$P_{fa} = \int_0^{+\infty} p(\hat{\tau}) \left[\int_{\lambda_{NR}}^{+\infty} p\left(r|\hat{\tau}, \hat{\sigma}_n^2\right) dr \right] d\hat{\tau} =$$
$$= \int_0^{+\infty} p(\hat{\tau}) \left[\int_{\lambda_{NR}}^{+\infty} \frac{1}{2\left(\hat{\tau} + \hat{\sigma}_n^2\right)} \exp\left\{ -\frac{r}{2\left(\hat{\tau} + \hat{\sigma}_n^2\right)} \right\} dr \right] d\hat{\tau} =$$
$$= \int_0^{+\infty} \exp\left\{ -\frac{\lambda_{NR}}{2\left(\hat{\tau} + \hat{\sigma}_n^2\right)} \right\} p(\hat{\tau})\, d\hat{\tau}. \tag{9.18}$$

Under the same hypothesis, the pdf of the received power of clutter and noise, when processing data in MIMO systems, can be expressed as the convolution of MN identical pdfs $p(r)$ where

$$p(r) = \frac{1}{2\left(\sigma'^2_n + \tau'\right)} \exp\left\{ -\frac{1}{2\left(\sigma'^2_n + \tau'\right)} \right\} p(\tau') \tag{9.19}$$

where σ'^2_n and τ' are RV generated as in equation (9.16) but performing the summation only on the time domain. It is clear then that expressing the false alarm rate in a closed form is hard and quite meaningless. Prediction in a closed form of the results in detection is not possible for both netted radar and MIMO systems as well.

The overall results achieved show a loss of performance for both NR and MIMO systems when the correlation is present. This is consistent with the results of monostatic systems.

9.5.2 CA CFAR

In this section we briefly describe the modification of the statistics of the received signals during the processing itself. From a statistical point of view, in a monostatic system using a CA CFAR algorithm as in equation (6.11) we consider the random variable z_m, given τ:

$$z_m = |x_m|^2 - \frac{k}{L}|y_m|^2. \tag{9.20}$$

Detection occurs when $z_m \geq 0$. This infers that, given its pdf $p_z(z_m|\tau)$, the system yields detection with a rate equal to $\int_0^{+\infty} p_z(z_m|\tau)\, dz_m$.
$p_z(z_m|\tau)$ can be written as function of x_m and y_m:

$$p(z_m|\tau) = p(|x_m|^2 - \frac{k}{L}|y_m|^2|\tau). \tag{9.21}$$

This expression is obviously a function also of the noise power and of the correlation properties of the clutter.

If we assume that the samples x_m in equation (6.11) are statistically independent and they have an almost constant texture, the final expression of the pdf is much simpler and clearer. Whilst the second assumption can be considered fairly close to reality, as the texture is almost constant in the interval of few range cells, the first assumption is usually not realistic, unless a pre-processing of data is realized in order to remove the correlation between range cells. In any case, the statistical modifications that follow and their consequences are useful to get a better understanding also when the correlation between the samples of clutter is reintroduced. Under the hypotheses above, we can write:

$$\begin{aligned} p(z_m|\tau) &= p_{x^2}(|x_m|^2|\tau) * p_{y^2}\left(-\frac{k}{L}|y_m|^2|\tau\right) = \\ &= p_{x^2}(|x_m|^2|\tau) \otimes p_{y^2}\left(\frac{k}{L}|y_m|^2|\tau\right). \end{aligned} \tag{9.22}$$

Particularly, when no target is present, we write $p_{x^2}(|x_m|^2|\tau)$ as an exponential pdf function of power $w|\tau$, i.e.:

$$\begin{aligned} p_{x^2}(|x_m|^2|\tau) &= p_{wx}\,(w|\tau) = \\ &= \frac{1}{\tau + \sigma_n^2} \exp\left\{-\frac{w}{\tau + \sigma_n^2}\right\}, \end{aligned} \tag{9.23}$$

and $p_{y^2}(|y_m|^2|\tau)$ as a gamma, i.e. as the result of L convolutions of the distribution in equation (9.23) with itself:

$$p_{y^2}(|y_m|^2|\tau) = p_{wy}(w|\tau) =$$
$$= p_{wy}(w|\tau) * p_{wy}(w|\tau) * \cdots * p_{wy}(w|\tau) =$$
$$= \frac{1}{(L-1)!}\frac{1}{\tau+\sigma_n^2}\left(-\frac{L}{k}\frac{w}{\tau+\sigma_n^2}\right)^{L-1}\exp\left\{-\frac{L}{k}\frac{w}{\tau+\sigma_n^2}\right\}, \tag{9.24}$$

Considering $p_{y^2}\left(\frac{k}{L}|y_m|^2|\tau\right)$, as in equation (9.24), we should take into account the factor $\frac{k}{L}$. Consequently this pdf can be expressed as:

$$p_{y^2}(|y_m|^2|\tau) =$$
$$= \frac{L}{k}\frac{1}{(L-1)!}\frac{1}{\tau+\sigma_n^2}\left(-\frac{L}{k}\frac{w}{\tau+\sigma_n^2}\right)^{L-1}\exp\left\{-\frac{L}{k}\frac{w}{\tau+\sigma_n^2}\right\}, \tag{9.25}$$

Figure 9.8 shows the pdf in equation (9.21) (in a logarithmic scale on the vertical axis) for several values of $k\left(\frac{16}{3}, 16, 48\right)$, $L = 16$ and $\tau + \sigma_n^2 = 1$. Since we assumed no target present, the area of the curves for $z \geq 0$ represent the probability of false alarm; as expected, the lower the ratio $\frac{k}{L}$ (i.e. the lower averaging coefficient of the power from the all the secondary data), the bigger FAR.

In a multistatic incoherent radar system, such as a MIMO, we have to develop the distributions starting from the decision rule, equation (6.12), and the mono/bistatic distributions, as in equations (9.24) and (9.25). Working in analogy with the monostatic case, we find curves for $p(z_m|\tau)$ as in Figure 9.9.

These curves have been obtained considering a multistatic system made of 2 tx and 2 rx and they confirm that, also in this case, the smaller the ratio $\frac{k}{L}$, the bigger the FAR. From a comparison with Figure 9.8 a modification of the pdf is observed: particularly, it is worth mentioning that the false alarm rate increases for small values of $\frac{k}{L}$, whilst it decreases for greater values of this ratio. This is consistent with the results presented in the following section.

Statistics in the coherent case (RPNR) are similar to the monostatic case since

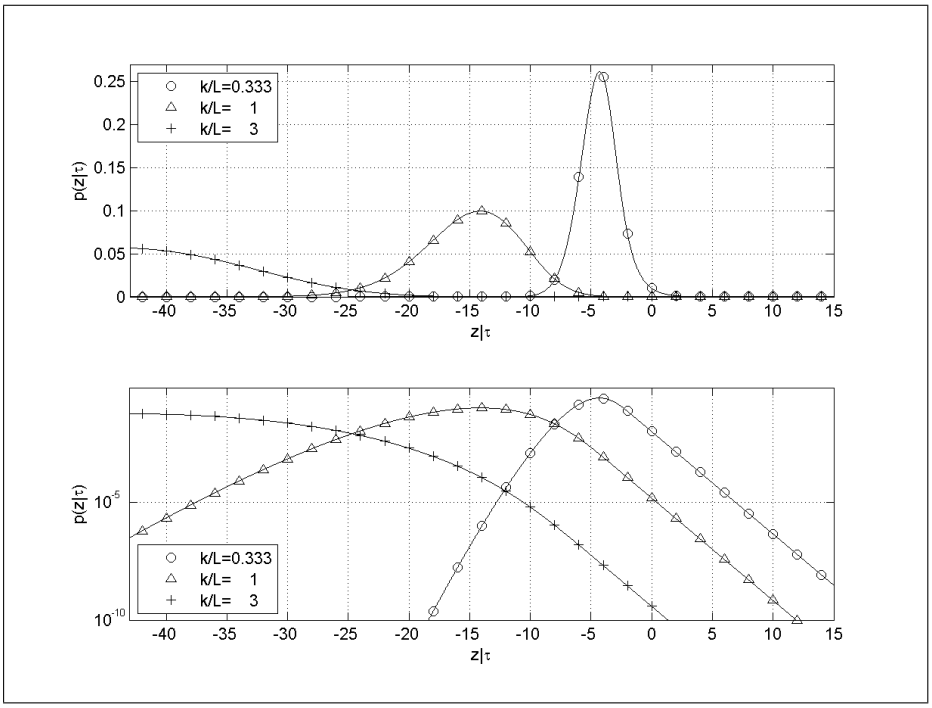

Figure 9.8: Pdf of $z_m|\tau$, monostatic case

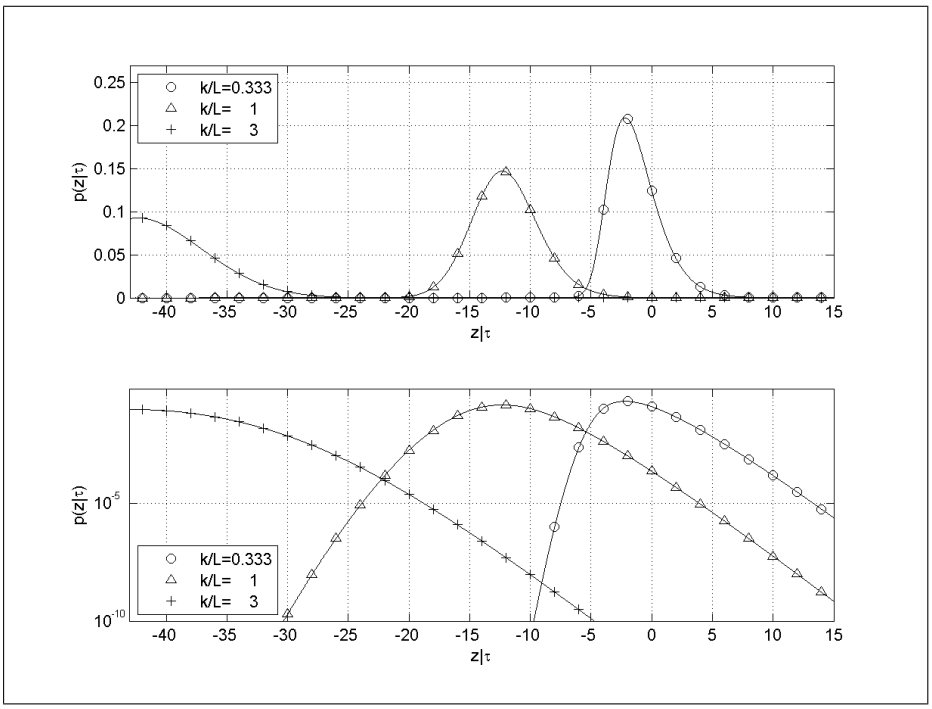

Figure 9.9: Pdf of $z_m|\tau$, multistatic case (MN= 4)

one CA CFAR is present at the end of coherent summation of all the components, as in equation (6.13). In this case, and under the same assumptions of the MIMO case (i.e. uncorrelated samples of clutter and constant texture in range), the only difference with the monostatic case is that the coherent pre-summation of all the contributes originates two distributions identical to equations (9.24) and (9.25) apart from a multiplicative factor for the variance $\tau + \sigma_n^2$: this is due to the effects of summing coherently MN independent random variables. For brevity the corresponding curves are not reported.

Chapter 10

Experiment setup

In this chapter we introduce the radar system used for acquiring data and consequently we describe the experiment setup and show the processing of the data. Through the acquired data we aim to validate the concepts developed so far and provide a more realistic scenario of the potential of a radar network.

In particular, in this section we show

- ▷ the hardware configuration,
- ▷ the experiment setup,
- ▷ the noise and clutter characteristics,
- ▷ the multistatic data characteristics for a moving target (person) and clutter,
- ▷ a range-Doppler analysis of the acquired data,
- ▷ the detection approach and the consequent false alarm rate,
- ▷ ways for localizing a target.

10.1 Hardware

Figures 10.1 and 10.2 show one pair tx-rx used for the experiment.

The beam pattern of each tx or rx antenna has been chosen to be quite wide (20° el. ×30° az. one way beamwidth, as in Figure 10.6). Such a beam pattern

Figure 10.1: tx-rx external outlook

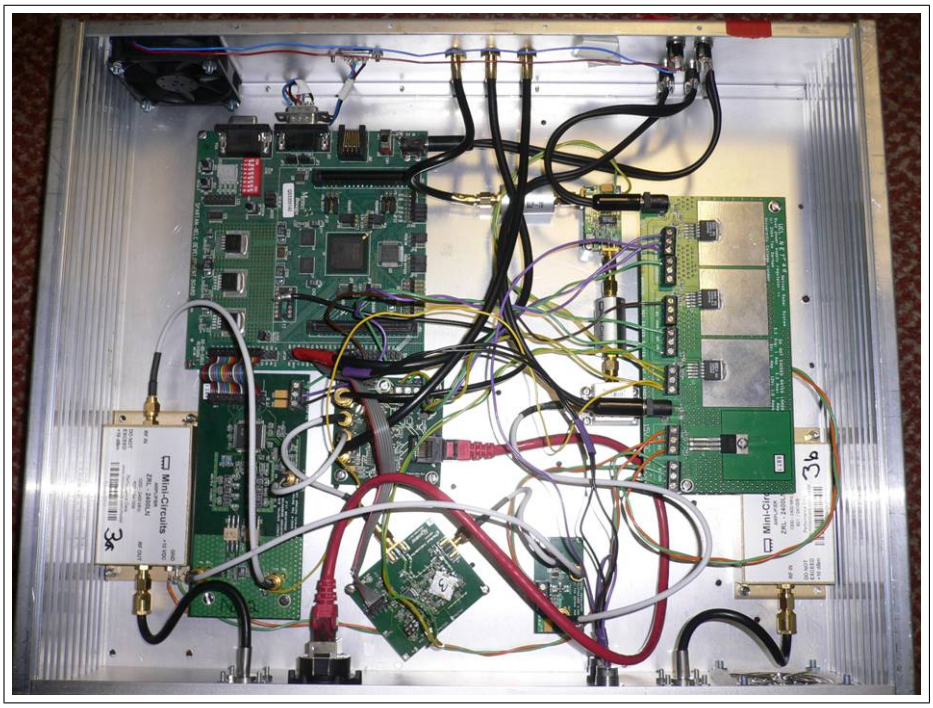

Figure 10.2: tx-rx internal outlook

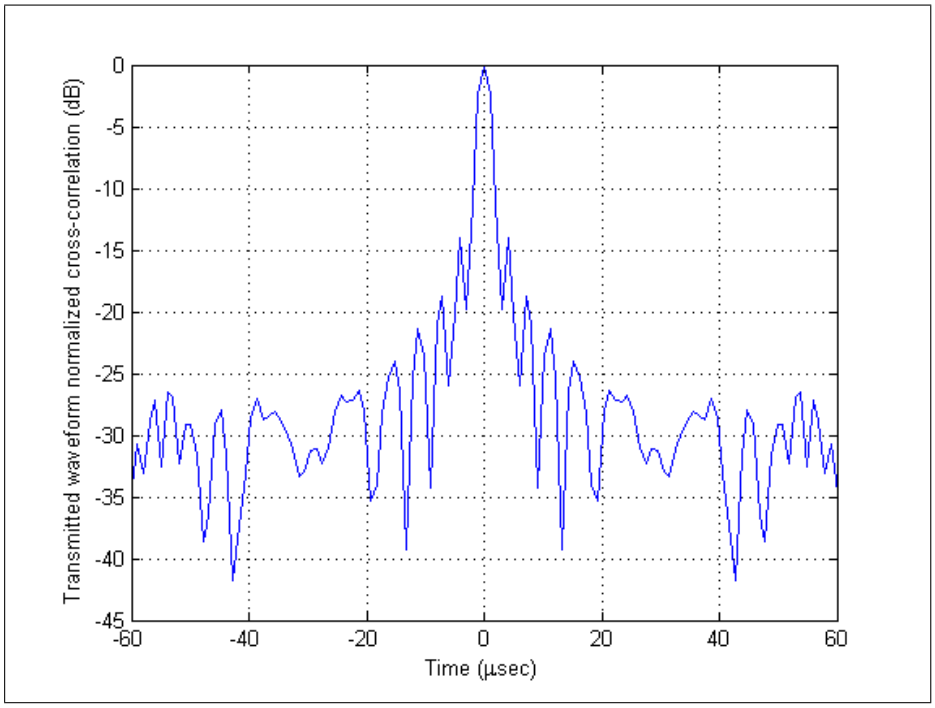

Figure 10.3: cross-correlation of the transmitted waveform

has been chosen in order to illuminate an area wide enough to allow the target movements, even though the clutter component in the received signal will be greater.

The one-way gain of each antenna is $\approx$ 15 dB. The two transmitters have been set to a *PRF* of 10 kHz each. An interleaved transmission strategy has been used to provide good isolation of the receivers, hence enabling full recovery of each of the tx-rx signals. The transmitted waveform is an up-chirp with 40 MHz effective radiofrequency bandwidth and duration $T = 0.6\ \mu$s. The carrier frequency has been set at 2.4 GHz and the *IF* at 20 MHz. The A/D converter emits 100 MSamples/s, each one quantized to 14 bits. The nominal transmitted power for the data presented here is $\approx$ 23 dBm ($\approx$ 0.2 W). The crosscorrelation of the transmitted waveform is reported in Figure 10.3.

10.2 Experimental setup

The experiment configuration is shown schematically in Figure 10.4. The experiment was conducted at the UCL Shenley Sports Ground, London, Colney in Hertfordshire (UK). Although the system is comprised of 3 devices each of them able to transmit and receive, the second device has been configured as a silent receiver only. As a consequence, with $M = 2$ transmitters and $N = 3$ receivers, the system's output O is comprised of 6 multistatic signals, that can be schematically represented as

$$O = \begin{bmatrix} tx1 - rx1, & tx1 - rx2, & tx1 - rx3 \\ tx3 - rx1, & tx3 - rx2, & tx3 - rx3 \end{bmatrix}. \tag{10.1}$$

The antennas were fixed, i.e. during the acquisition of the data they were not scanning, and pointed to the initial position of the target. The transmitting and the receiving antennas of the first and third devices were separated by a small distance ($\approx$ 90 cm), although for simplicity they have been represented as one in Figure 10.4. Here this is referred to as either "monostatic signals" or "monostatic configuration" or "quasi-monostatic". In Chapter 11 it is seen that the different location of the tx and rx antennas affects the observations.

It is worth highlighting that there is a symmetry between the bistatic signals of the first and the third devices and therefore a very high correlation has to be expected between $r_{1,3}$ and $r_{3,1}$, where we term $r_{h,k}$ the signal after matched filtering when the h-th device transmits and the k-th receives. This acts also a simple test of the system and the experimental method. The target presented in the following figures is a person walking radially towards the first device starting from a range of (approximately) 120 m.

10.2.1 Reference signal and matched filtering

This will be shown in the final report.

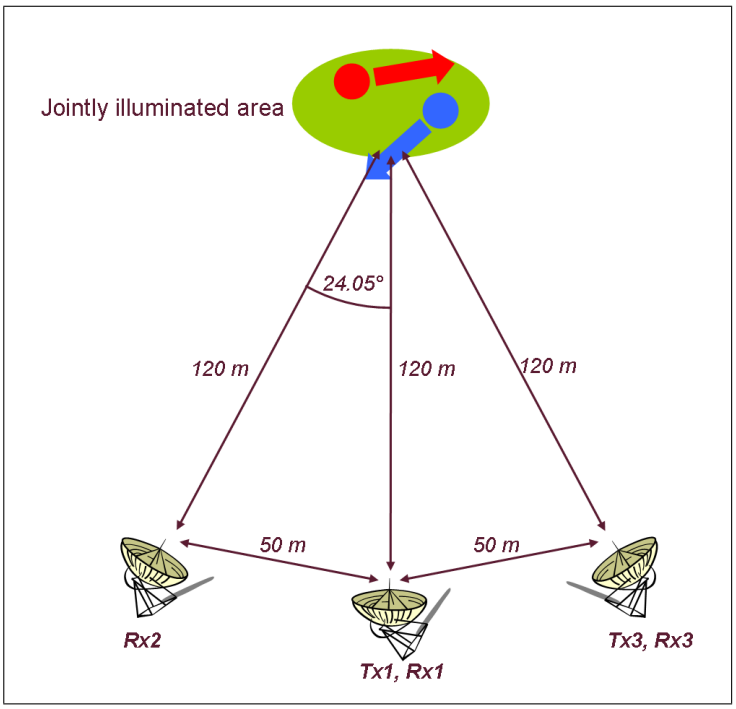

Figure 10.4: Schematics of the radar network configuration

Figure 10.5: Actual radar network configuration

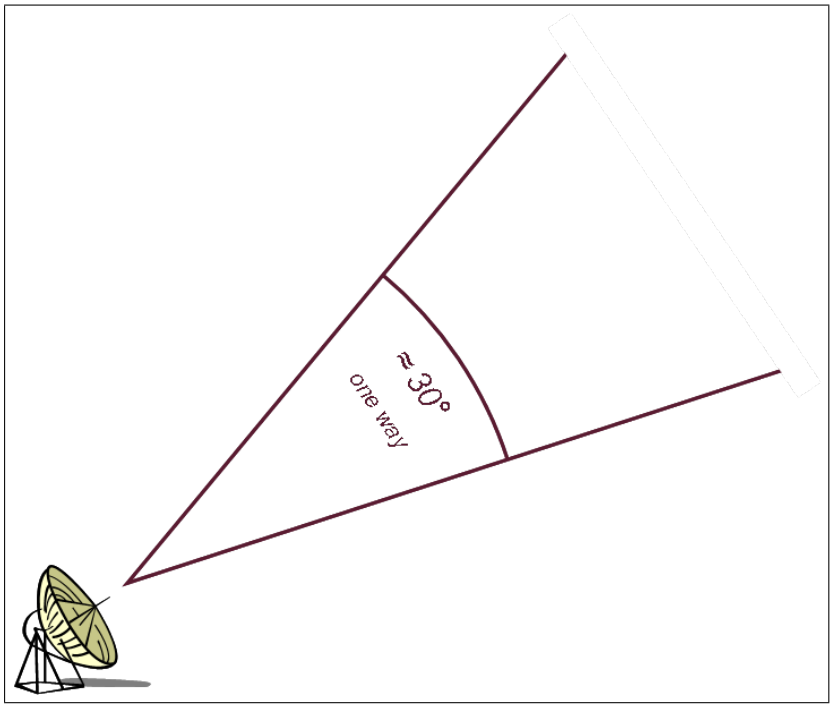

Figure 10.6: Antenna pattern

10.3 Received signals and clutter removal

The signal to each receiver after matched filtering is expected to be made of (i) target (when present), (ii) clutter, (iii) multipath and (iv) thermal noise, i.e.

$$r_{k,m}(t) = \sum_{m=1}^{M} H_{0/1}\left[\alpha_{k,m} s_m\left(t-\tau_s\right) + \beta_{k,m} s_m\left(t-\tau_s-\Delta\tau_s\right)\right] + \\ + c_{k,m}\left(t-\tau_c\right) + n_k\left(t\right), \tag{10.2}$$

where $k = 1..N$ and $m = 1..M$ (N and M are respectively the numbers of receivers and transmitters), $H_{0/1}$ is 0 or 1 according to the absence or presence of the target and $c_{k,m}$ is the clutter, n_k is the noise and $\alpha_{k,m}$ and $\beta_{k,m}$ are the backscatter coefficients, inclusive of the phase terms determined by the parameters of the radar equation and due, respectively, to the direct path and the multipath. The dependency of the delays $\tau_{s/c}$ and $\Delta\tau_s$ on the indexes k and m have been omitted for brevity.

In the acquisitions completed to date, the time between two interleaved transmissions of the reference chirp and the distance of the target allows the echoes from the target to be separated in time. Thus it is possible to write equation (10.2) in a simplified form as:

$$\begin{aligned} r_{k,m}(t) = H_{0/1}\left[\alpha_{k,m} s_m\left(t-\tau_s\right) + \beta_{k,m} s_m\left(t-\tau_s-\Delta\tau_s\right)\right] + \\ + n_k\left(t\right) + c_{k,m}\left(t-\tau_c\right). \end{aligned} \tag{10.3}$$

In more complex systems, covering greater distances, it will be necessary to exploit code diversity or other properties to minimize the mutual interference between the transmitted signals. This argument is not considered in this report.

10.3.1 Clutter removal

In this section we provide a brief description of the processing adopted to remove the clutter and its effects on the received signals. Figures 10.7 and 10.8 show the signals arriving at all the receivers, after matched filtering but before clutter suppression, when tx1 and tx3 are transmitting.

From the a-priori knowledge of the experiment, the moving target is expected to be at a mono/bistatic range of 125 m. This is graphically confirmed from the visual analysis of some signals in Figures 10.7 and 10.8, 10.11 and 10.12.

It is clear that the transmitted waveform directly feeds the receiver, due to the presence of sidelobes in the pattern of the tx/rx antennas. From the experimental setup in Figure 10.4, it can be inferred that the path from tx3 to rx2 is the maximum distance affected by this direct interference and it measures $\approx$ 91.32 m (one way). As a consequence, we disregard the corresponding acquired samples to avoid this kind of interference in all the following processing and the corresponding analysis.

Whereas the clutter is expected to be due to the backscattering from the soil, and consequently without a particularly spread Doppler, it has been cancelled using a high-pass filter with a cutoff frequency of 10 Hz. Figure 10.10 shows its amplitude response. The filter cutoff has been designed to attenuate the clutter as much as possible while preserving the Doppler response of even slow-moving

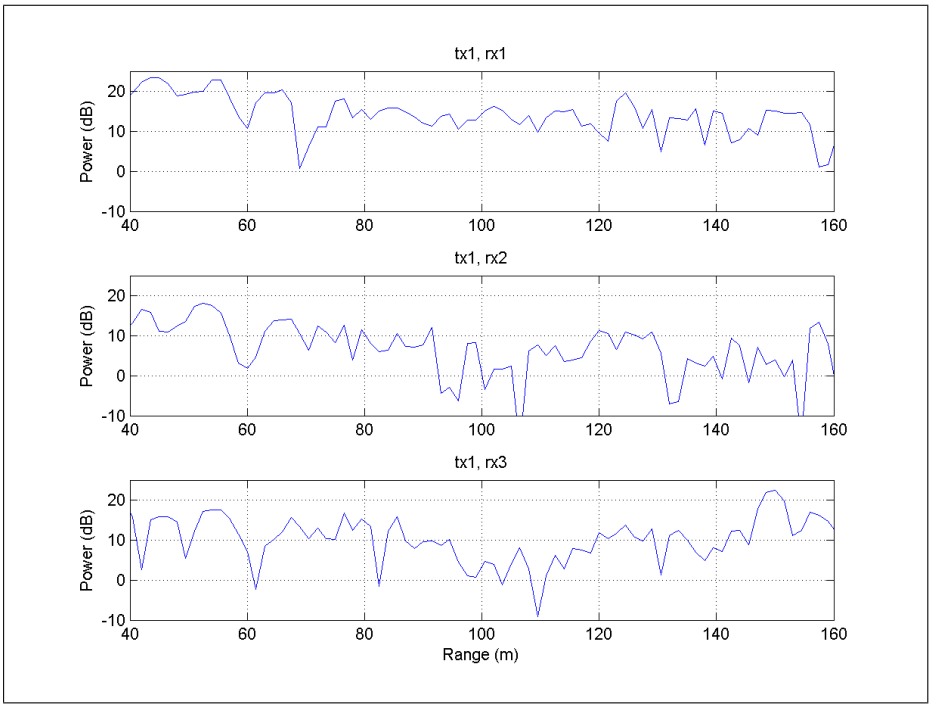

Figure 10.7: Signals from tx1 to all receivers

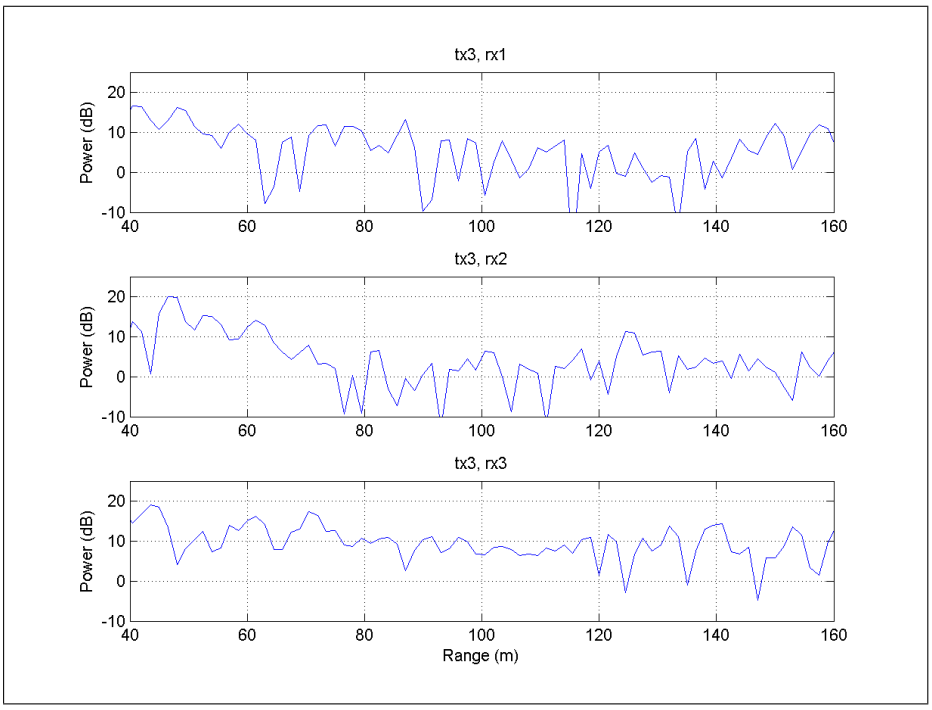

Figure 10.8: Signals from tx3 to all receivers

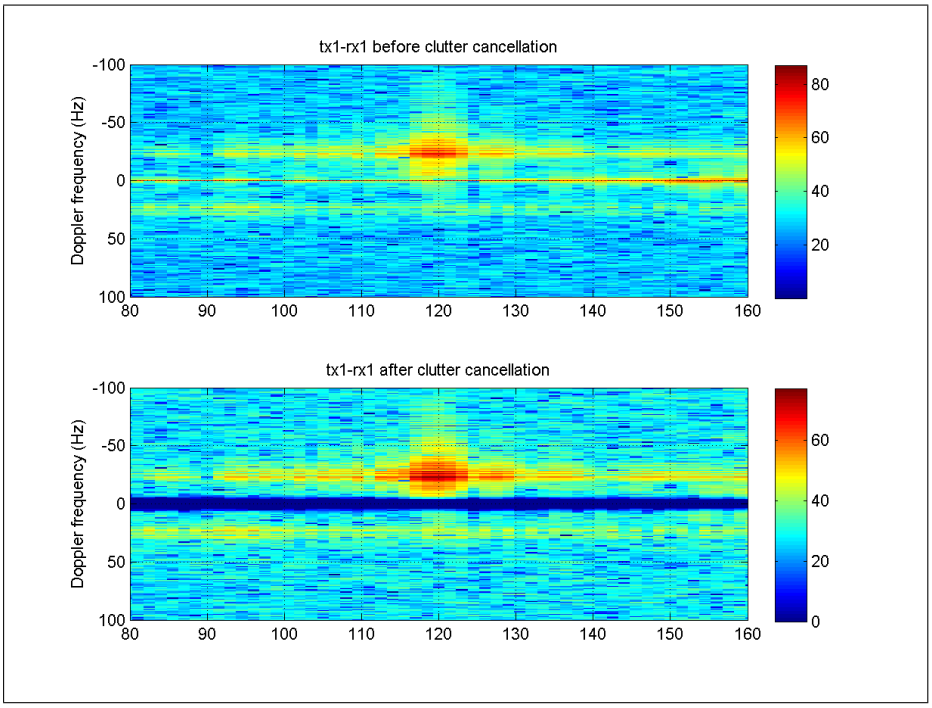

Figure 10.9: Range-Doppler plots before and after clutter removal

targets such as a walking person. The effectiveness of filtering in saving the Doppler information of a walking person is also shown in Figure 10.9. Here a range-Doppler plot of the monostatic signal tx1-rx1 is reported before and after clutter removal. The integration time is here 1 second. Although this is too high for an actual processing (range cell migration of the target is observed), as also discussed in Section 12.2.2, it allows to evaluate the clutter removal. As it can be easily seen, after the clutter removal the signal stands out much more clearly than before.

10.3.2 Target, noise and clutter signals

In this section we deepen the analysis regarding the effects of high-pass filtering the signals as described in Section 10.3.1. Particularly, we focus the attention on the echoes from two different range cells only: the first is the target's and the second contains only clutter and noise. Moreover, we consider echoes related to

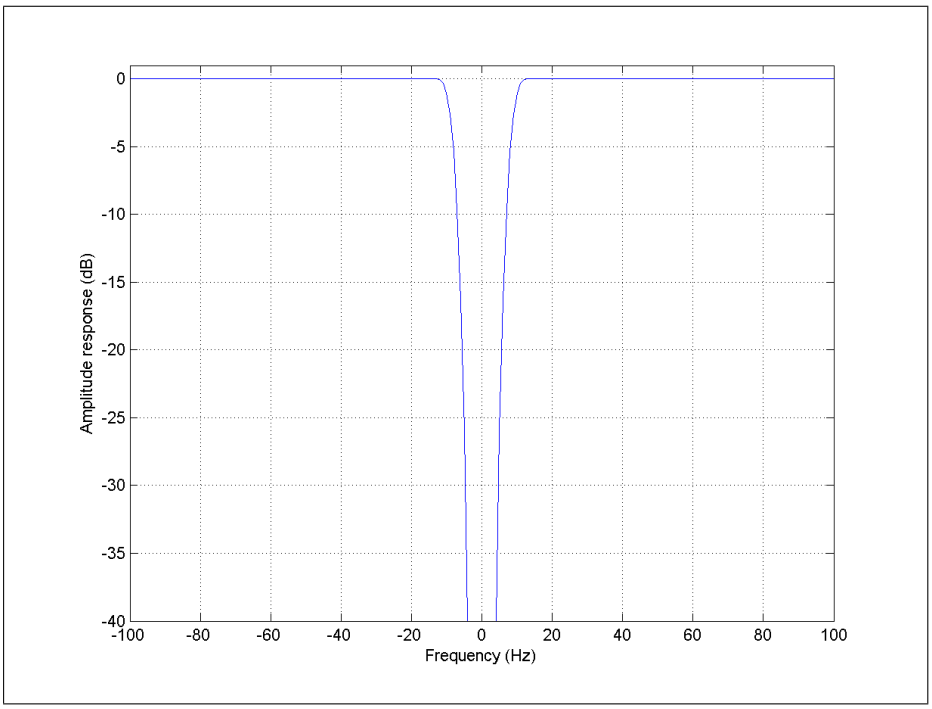

Figure 10.10: Signals received from tx1 after clutter removal

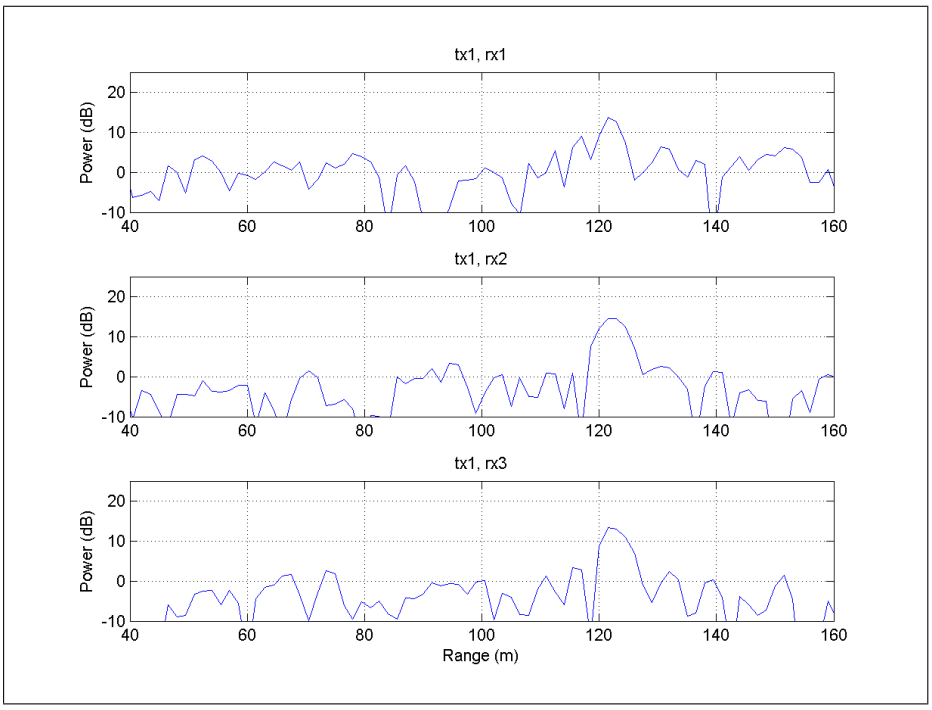

Figure 10.11: Signals received from tx1 after clutter removal

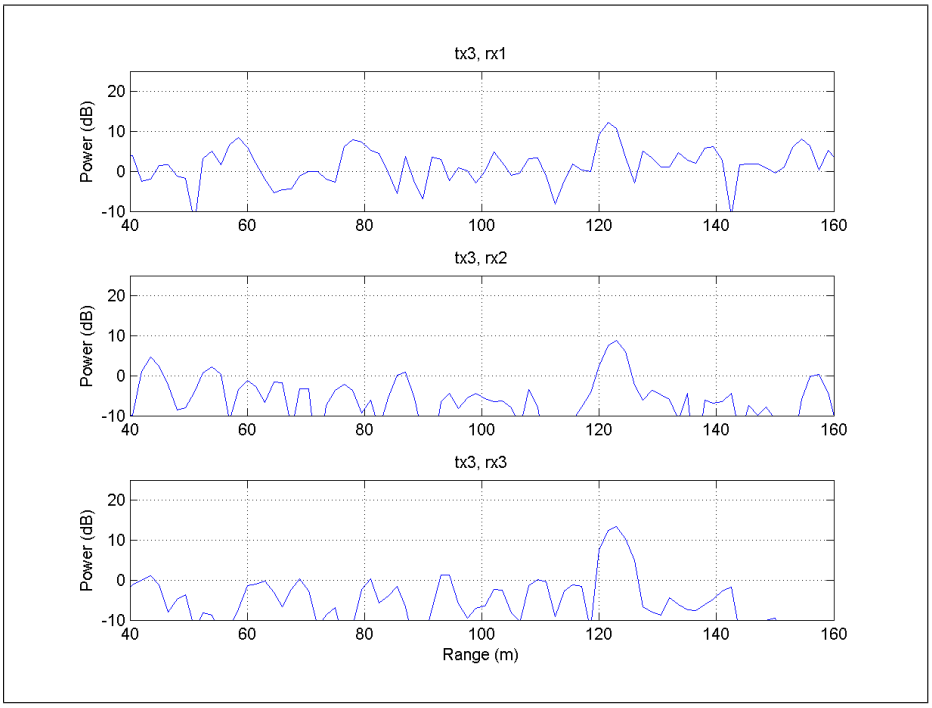

Figure 10.12: Signals received from tx3 after clutter removal

the pair tx1-rx1 only: the signals from the remaining pairs have similar behaviours and therefore for brevity are not reported.

Figure 10.13 shows the power (in dB) and the phase (in degrees) of the received signal for a series of pulses for the range cell where the target is present. One second of acquired data at 10 KHz are reported here (i.e. 10000 pulses). After removing the clutter by filtering, the signal appears cleaner as shown in Figure 10.14. It is worth highlighting that for relatively high SNR the linear(after filtering) behaviour of the phases is clearly evident, whilst it is partially or totally lost for low SNR, e.g. between pulses 6000 and 7000. In other words, for high SNR a quite strong correlation of the phases from pulse to pulse for the target is observed. This might be expected considering that the target is a walking person (therefore with a modest velocity) and the radar has a relatively high PRF and hence there is little change from pulse to pulse.

Figures from 10.15 to 10.17 refer to the a range cell at 105 m where clutter and noise only are present. As it is possible to observe, whilst the noise has an uncorrelated phase, the phase of the clutter has a degree of correlation, that will

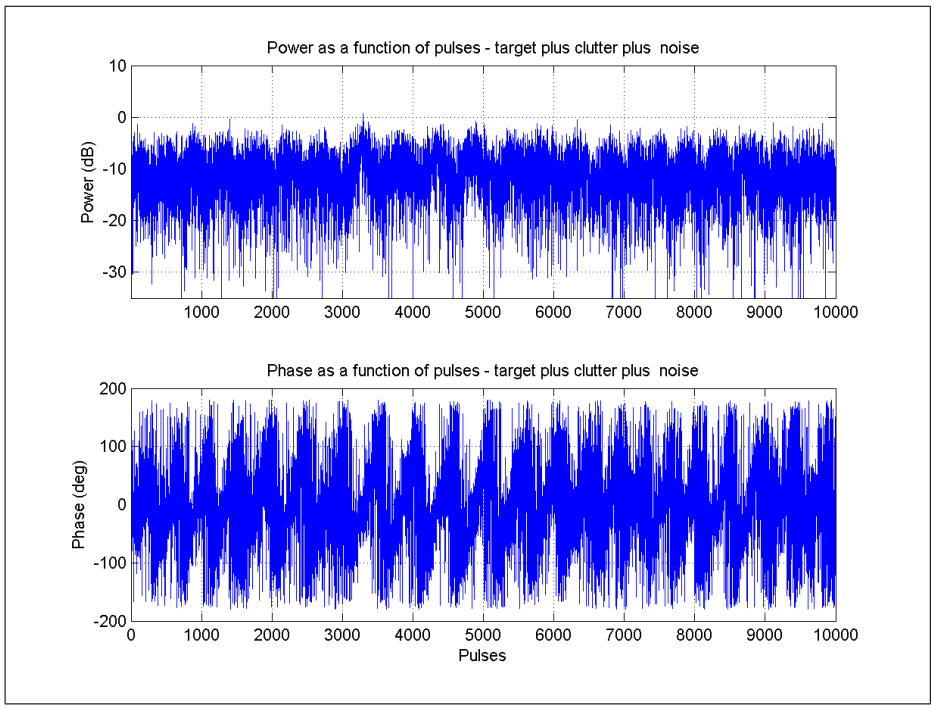

Figure 10.13: Signal and interference as a function of pulses – tx1-rx1

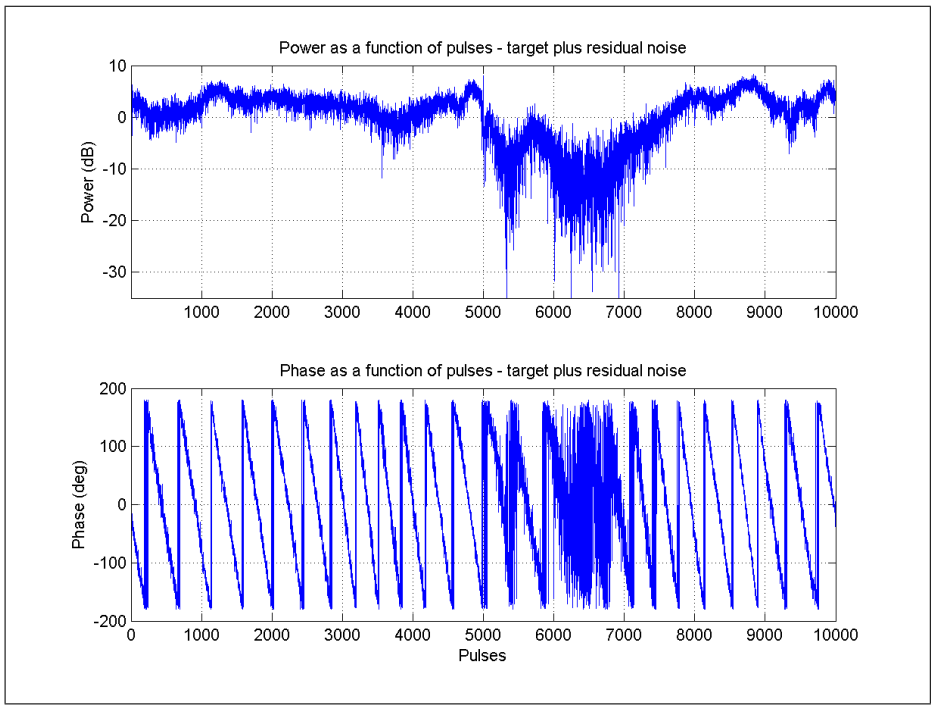

Figure 10.14: Signal and residual noise as a function of pulses – tx1-rx1

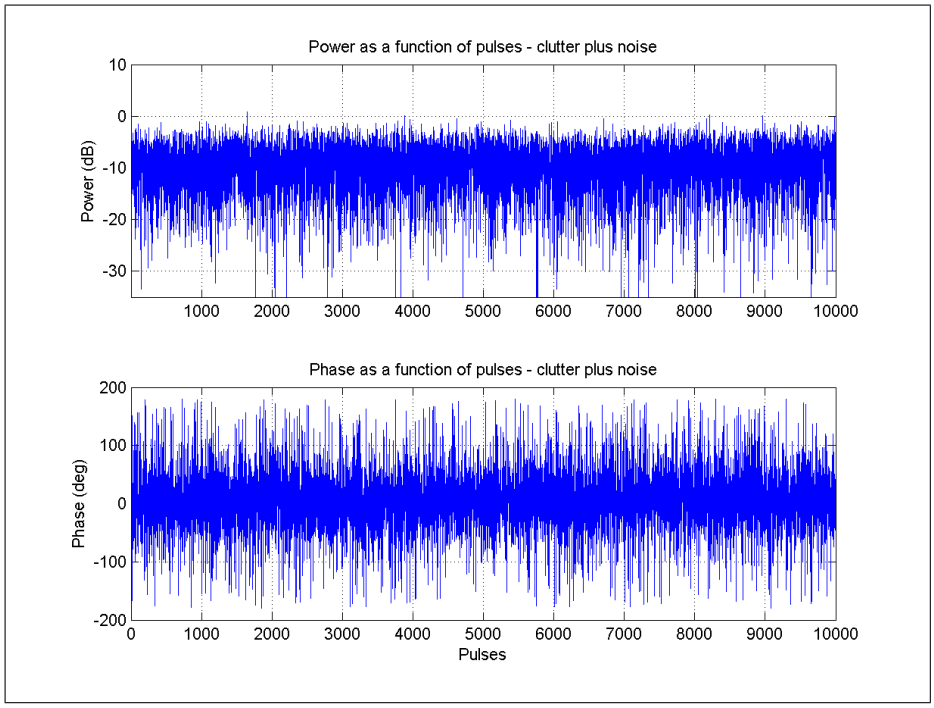

Figure 10.15: Clutter and noise as a function of pulses – tx1-rx1

be deepened in future. Future work will include also a statistical analysis of the characteristics of the clutter and noise power for the acquired data.

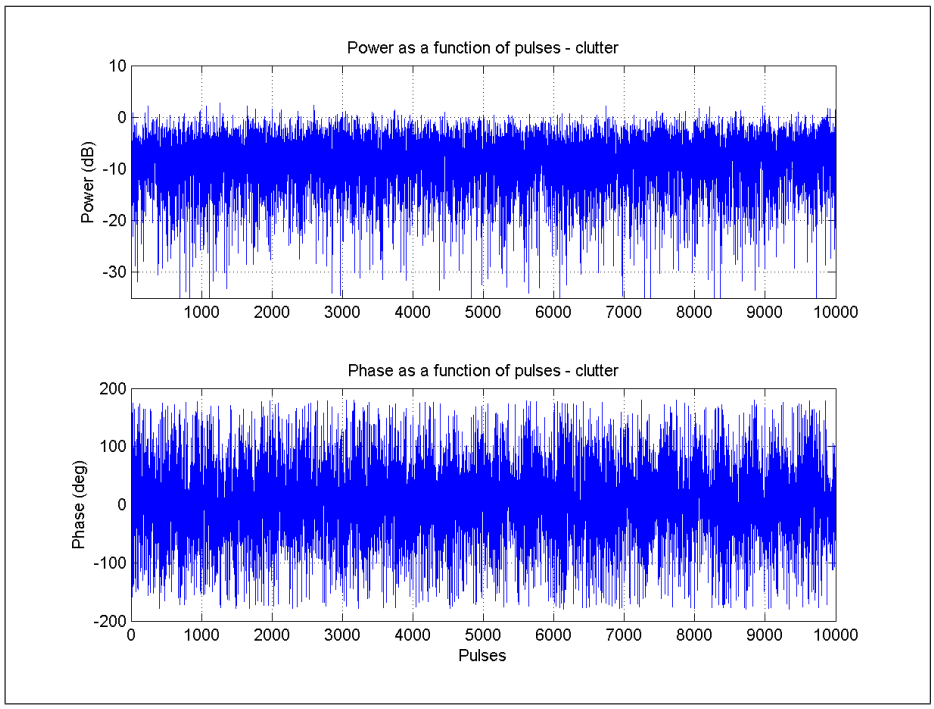

Figure 10.16: Clutter as a function of pulses – tx1-rx1

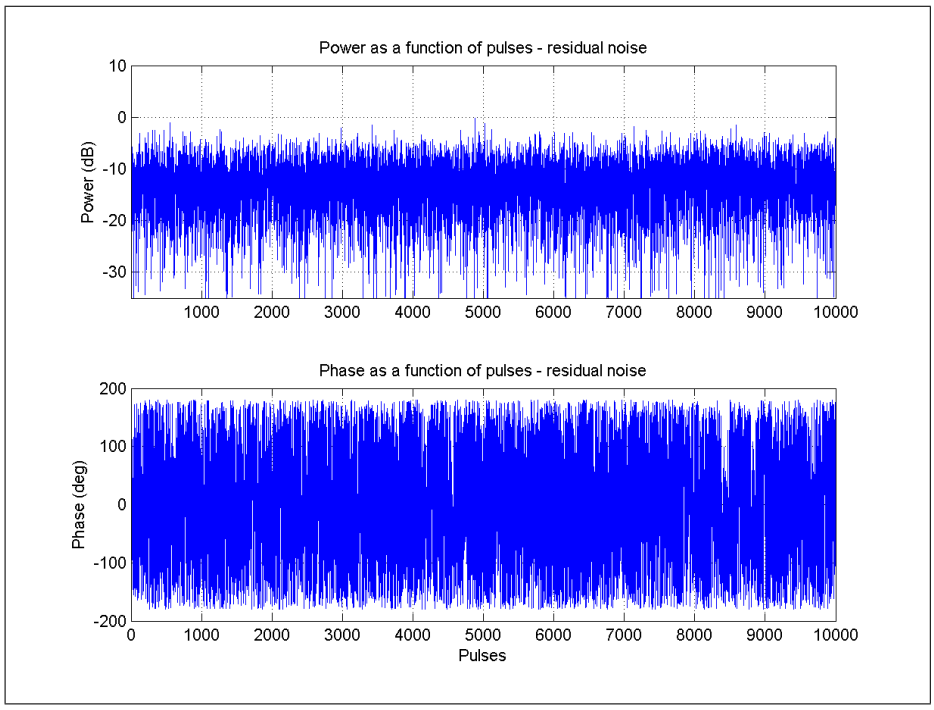

Figure 10.17: Residual noise as a function of pulses – tx1-rx1

Chapter 11

Multistatic data characteristics

In this section we investigate some properties of the set of the acquired signals. This is a preliminary analysis to provide background knowledge to assist with appropriate processing of the data. Particularly here we focus our attention on the cross-correlation characteristics of the received signals.

These correlations have been computed taking into account the data either in their complex format or their amplitude alone or their phase alone in order to best understand all the possible existing relationships. In particular, the phase correlation, although unusual, has been computed to highlight a possible redundancy between the bistatic paths tx1-rx3 and tx3-rx1. We examined the signals over a period of 1 second. Correlations have been computed on single pulses and then averaged. Figures 11.1 to 11.4 show the same correlation properties just when a window of 3 range cells around the target is taken into account. These 2 guard range cells around the nominal cell of the target have been introduced to take into account the oversampled data rate and therefore the fact that the cell with the highest SNR could not be the nominal one.

11.1 Clutter and noise only

Figures from 11.1 to 11.4 show (the absolute value of) the average cross-correlation of a number of received signals with all the others available.

Generally in this entire set of figures, although the amplitudes are quite similar to one another, the phases can be considered almost independent, so that the overall complex level of average correlation is quite low. However there are exceptions to this general behaviour that stand out: first of all, Figures 11.1 and 11.2 show a remarkable correlation between the monostatic measurements. This is quite unexpected, given the different aspect angles of illumination of the clutter patch, which is basically confirmed from the low correlation of the phases, therefore this relatively high level of correlation may be explained by a similarity of the monostatic clutter backscattering from the same area. It is also true that in this particular case the clutter is made of terrain that can have a more homogeneous behaviour than other kinds of clutter, such as that from the sea surface, that is characterized by a spiky echoes rapidly varying in time. As it should be expected, Figure 11.3 shows a quite high correlation between tx1-rx3 and rx3-tx1. This is due to the (quasi) symmetrical configuration of these devices. Finally Figure 11.4 does not show any particular correlation for the clutter and noise case.

Whereas in section 10.3.2 it has been shown that the noise affects the properties of the clutter, it is then clear why in Figure 11.3 the cross-correlation of the symmetrical signals falls to 61%.

Finally Figures from 11.5 to 11.7 show the distribution of the amplitude of the clutter. Most of these distributions have in common a Gaussian texture, which is reflected in the Rayleigh-shaped pdfs. As seen in Section 3.5, the Gaussian distribution is quite common for the texture in the case of ground clutter. In particular Figure 11.5 shows that the two monostatic measurements have two Rayleigh-distributed pdf with different standard deviation. As expected, the two symmetrical signals tx1-rx3 and tx3-rx1 have similar distributions (Figure 11.6) and the difference here can be explained in the extra figure of noise of the first receiver. Finally Figure 11.7 reports the clutter distribution of the remaining two bistatic signals. Whilst the one from tx3 to rx2 has a quite expected shape, that from tx1 to rx2 has a tail which does not match the expectations. At this point, it is worth recalling that the relationships between multistatic clutter returns from the same area are being under investigation only recently, having received so far limited attention. The particular long tail of the distribution in the latter Figure

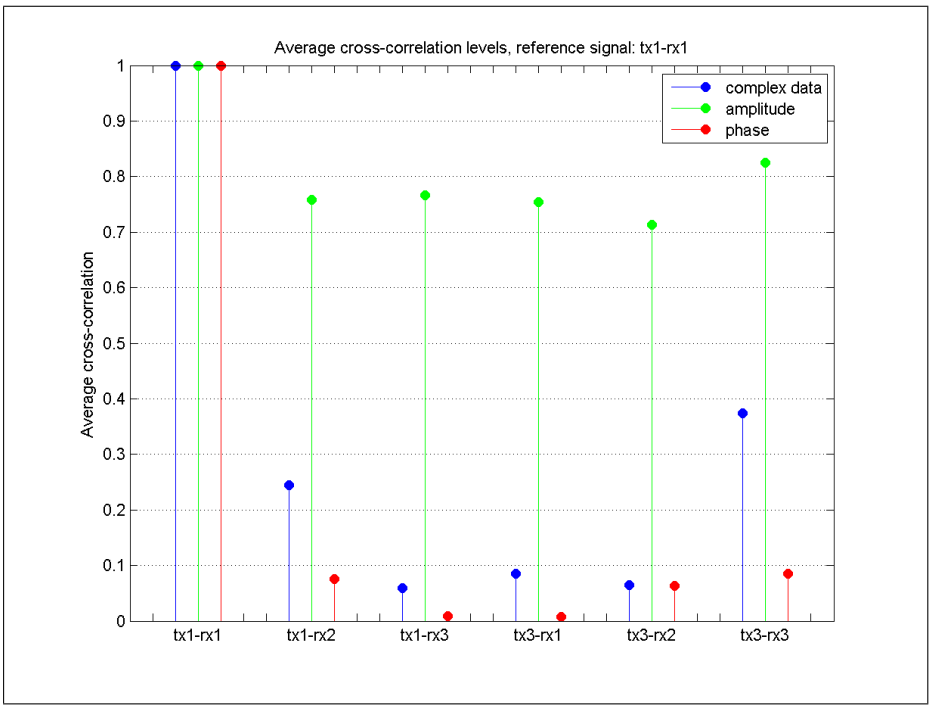

Figure 11.1: Cross-correlation levels with tx1-rx1 – clutter

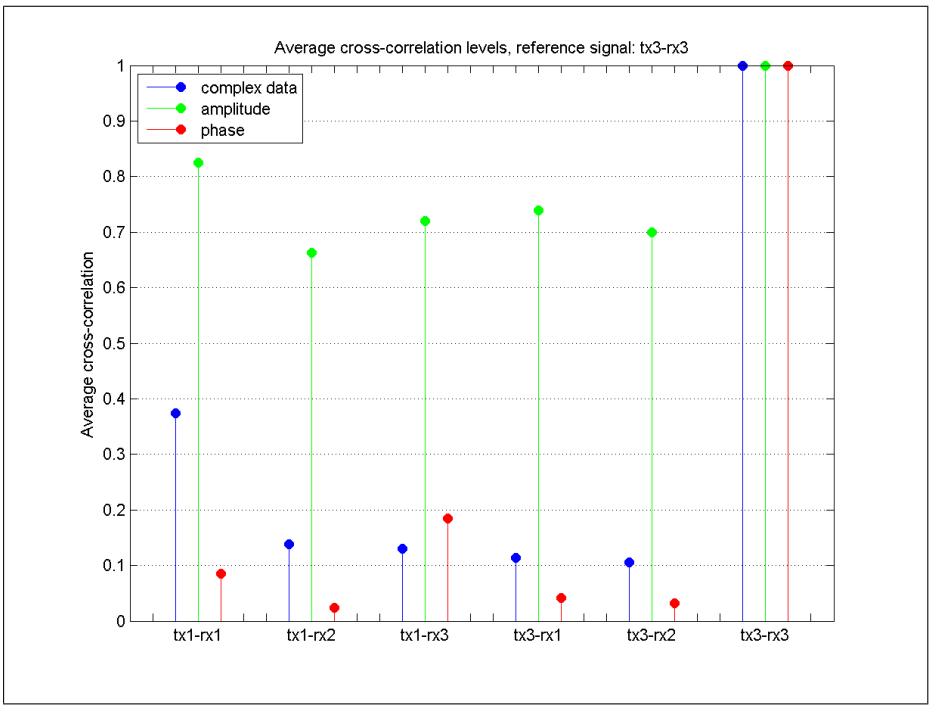

Figure 11.2: Cross-correlation levels with tx3-rx3 – clutter

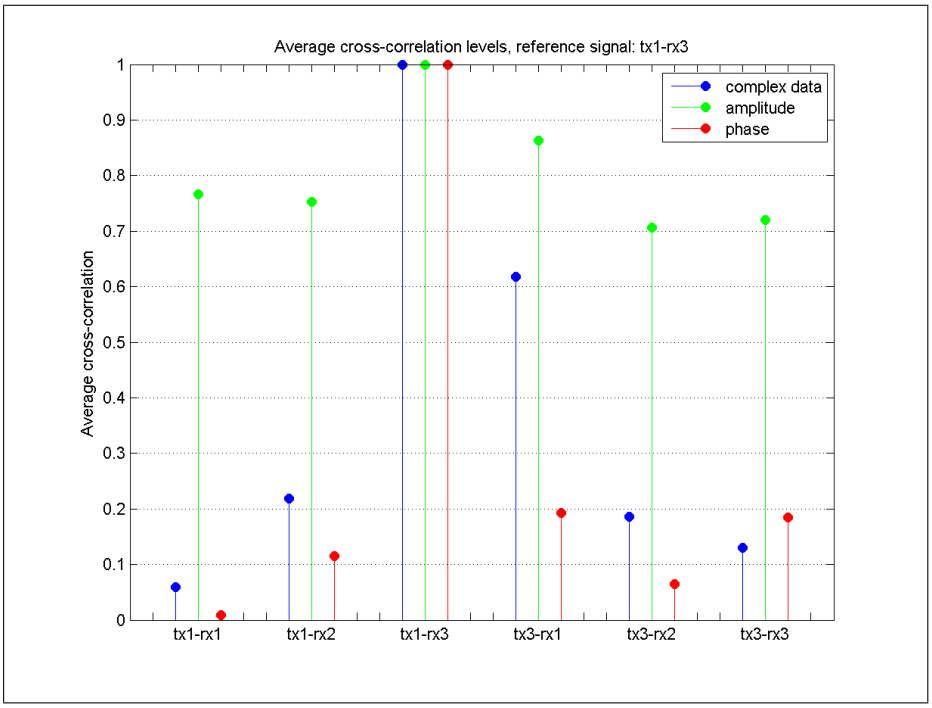

Figure 11.3: Cross-correlation levels with tx1-rx3 – clutter

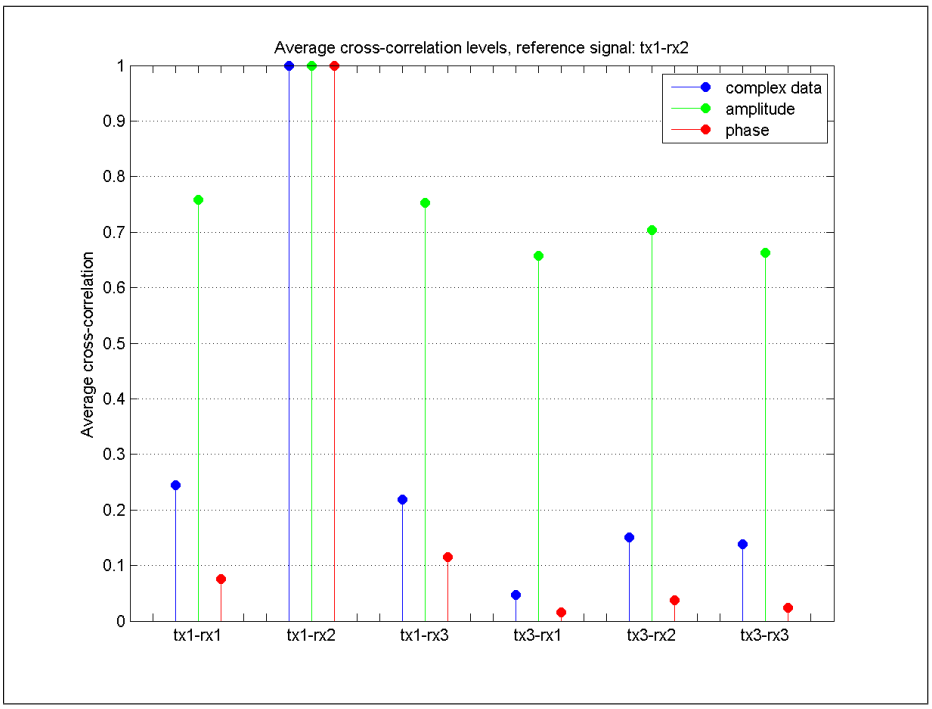

Figure 11.4: Cross-correlation levels with tx1-rx2 – clutter

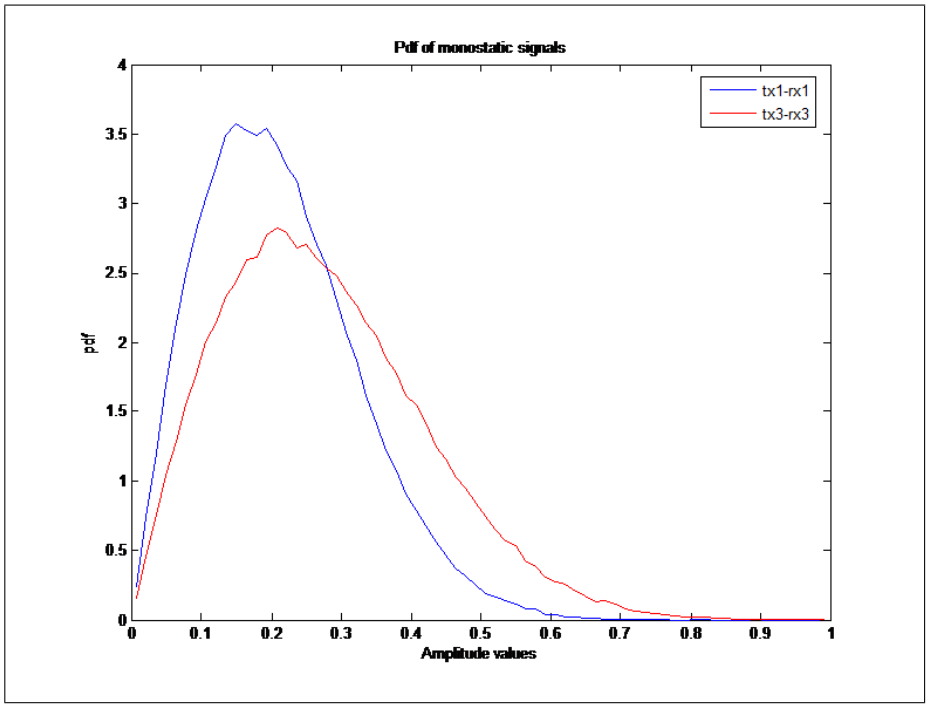

Figure 11.5: Multistatic pdf of the amplitude of the clutter, monostatic signals

can be an indicator of a change in the clutter distribution, not only in its statistics. Therefore, the complex backscattering from even a fairly simple kind of clutter, i.e. from a flat grass field (as in this case), can provide a variety of reflected signals with different properties, as much as it happens in more structured targets.

11.2 Moving target - person

The examination of the set of Figures from 11.8 to 11.11 highlights a different correlation behaviour from that observed in section 11.1 when only the target is examined. In these case the amplitudes are extremely correlated in all the results shown. However, when considering the correlation between the phases and the entire complex data, different characteristics from those in Figures from 11.1 to 11.4 arise. In Figure 11.8 it is quite evident that in this case the monostatic measurements are less similar to one another. On the contrary the monostatic measurements from tx3 to rx3 (Figure 11.9) are quite similar to the one from tx1 to tx2. This is quite unexpected and does not match what found in the clutter

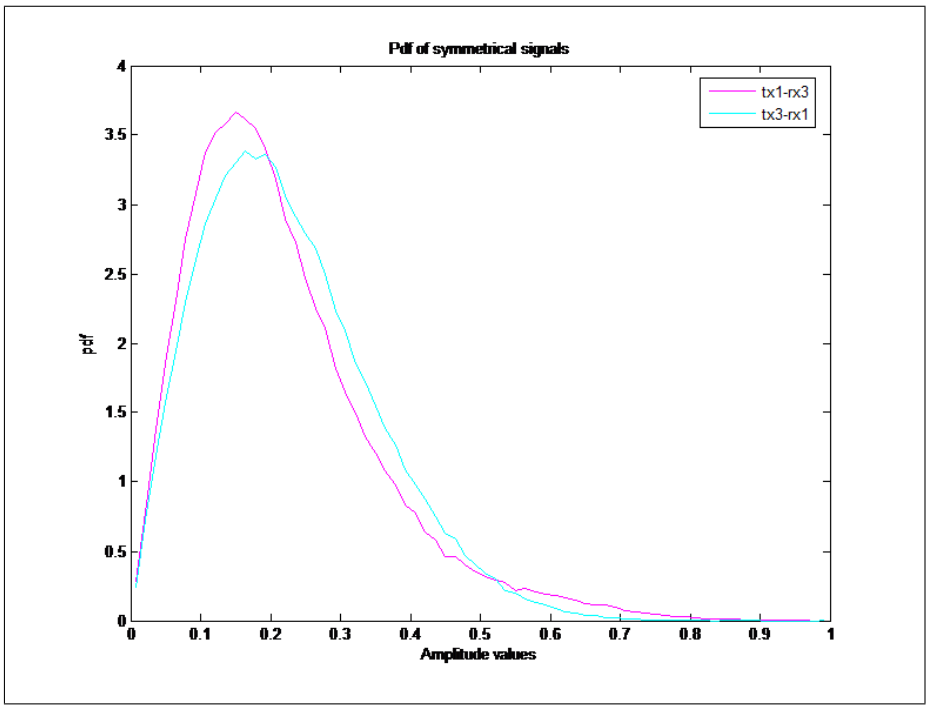

Figure 11.6: Multistatic pdf of the amplitude of the clutter, symmetrical signals

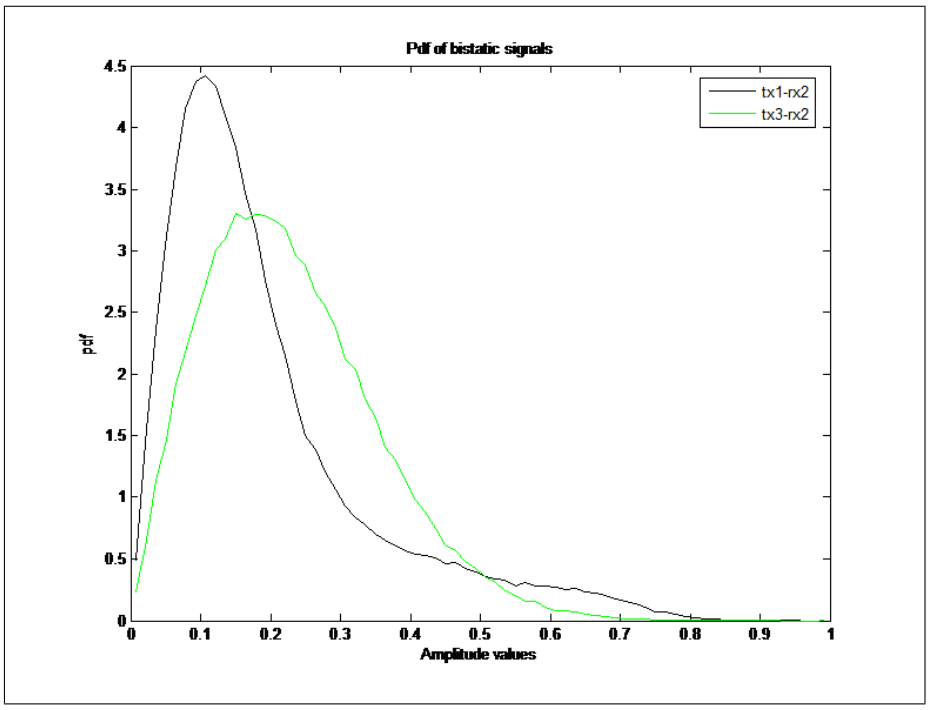

Figure 11.7: Multistatic pdf of the amplitude of the clutter, bistatic signals

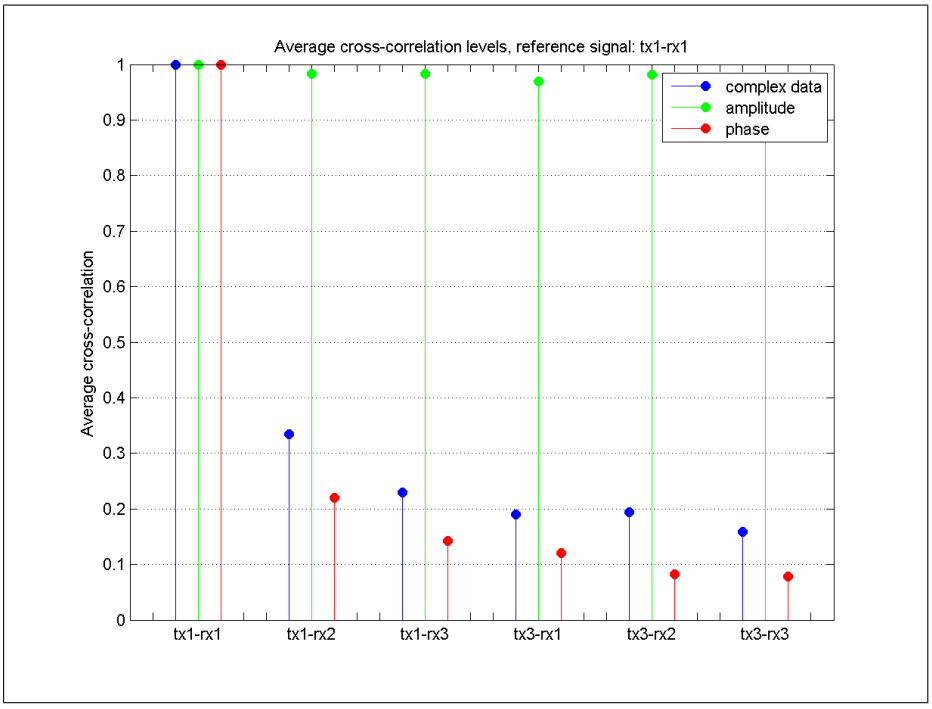

Figure 11.8: Cross-correlation levels with tx1-rx1 – target

cases and may be explained by the backscattering properties of the target. Figure 11.10 shows an interesting result that validates the a-priori expectations about the experiment: here the properties of the symmetrical configuration are extremely clear. There is a similarity at all levels between tx1-rx3 and tx3-rx1 highlights (the average cross-correlation on complex data is $\approx$ 88%) and also a quite high correlation is observed between tx1-rx3 and tx1-rx2, as it might be expected since the target is a person moving towards the central node. This due, again, to the symmetry in carrying out the experiment. Even the phases, which are extremely sensitive to minor mismatches and to low SNR, have a correlation up to almost 50% in one case and 40% in the other. These considerations are basically confirmed by Figure 11.11.

Figures 11.12 and 11.13 shows the signals received from pairs tx1-rx3 and tx3-rx1 respectively. As it can be seen, the overall shape of the signals is very similar, although the signal in Figure 11.13 has a greater contribution of noise, as it can be confirmed as well from an analysis of the phases.

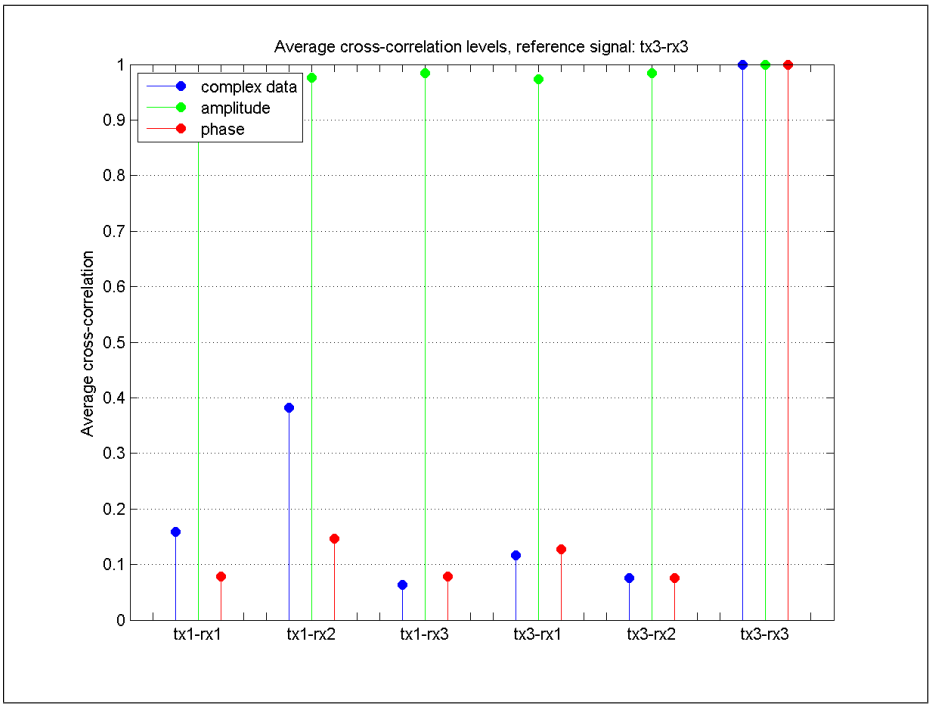

Figure 11.9: Cross-correlation levels with tx3-rx3 – target

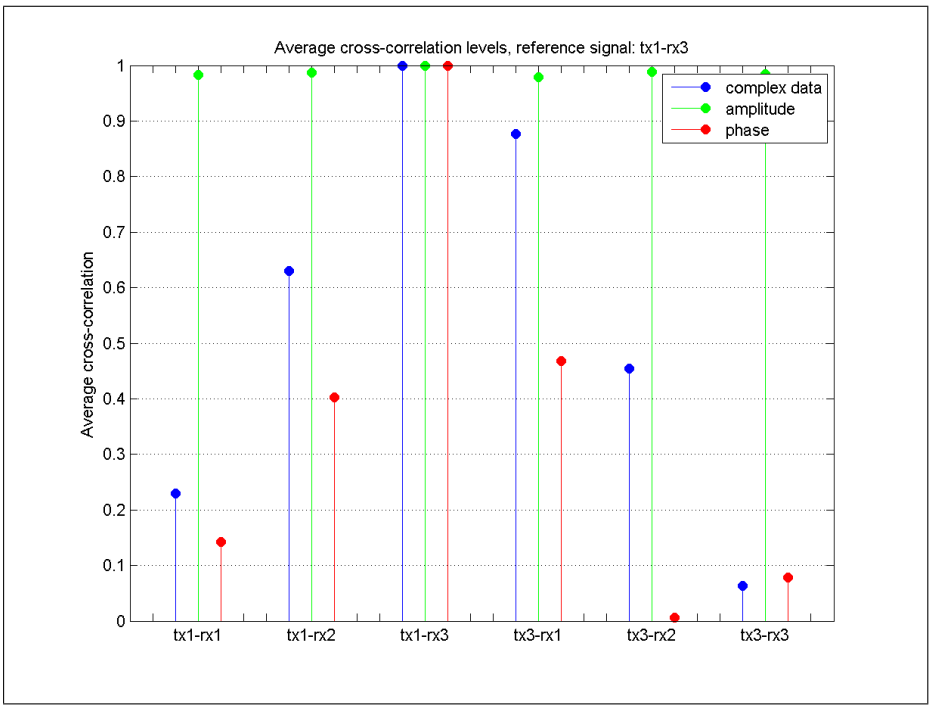

Figure 11.10: Cross-correlation levels with tx1-rx3 – target

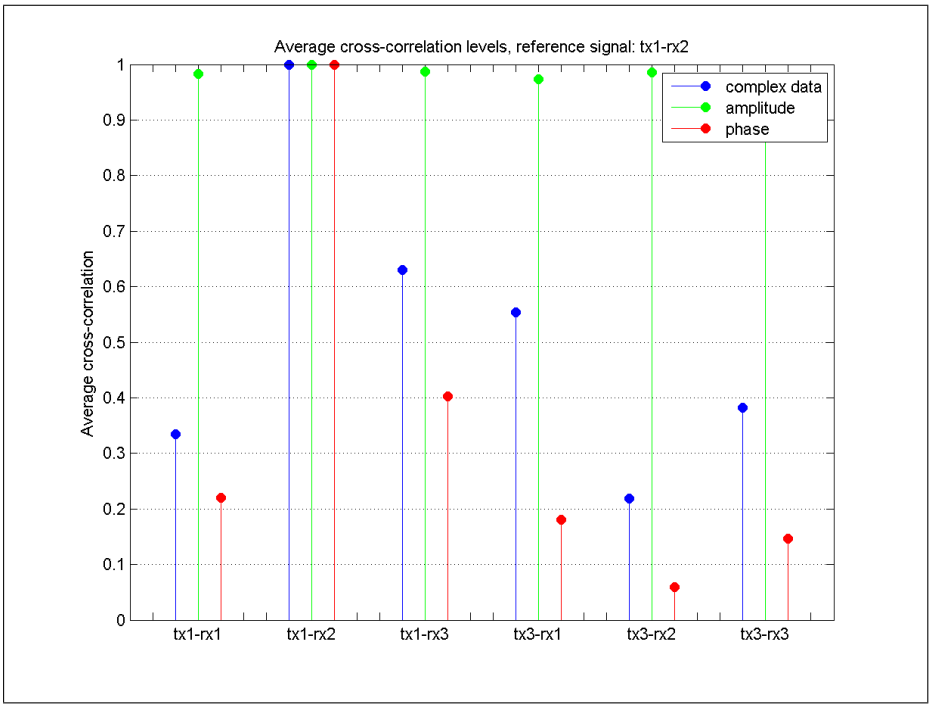

Figure 11.11: Cross-correlation levels with tx1-rx2 – target

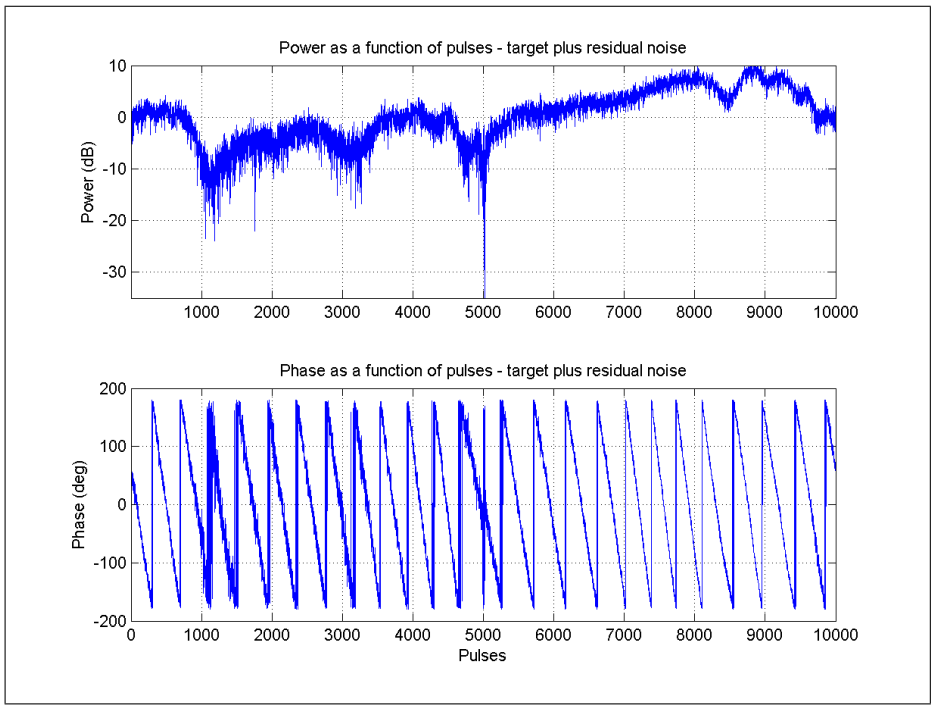

Figure 11.12: tx1-rx3

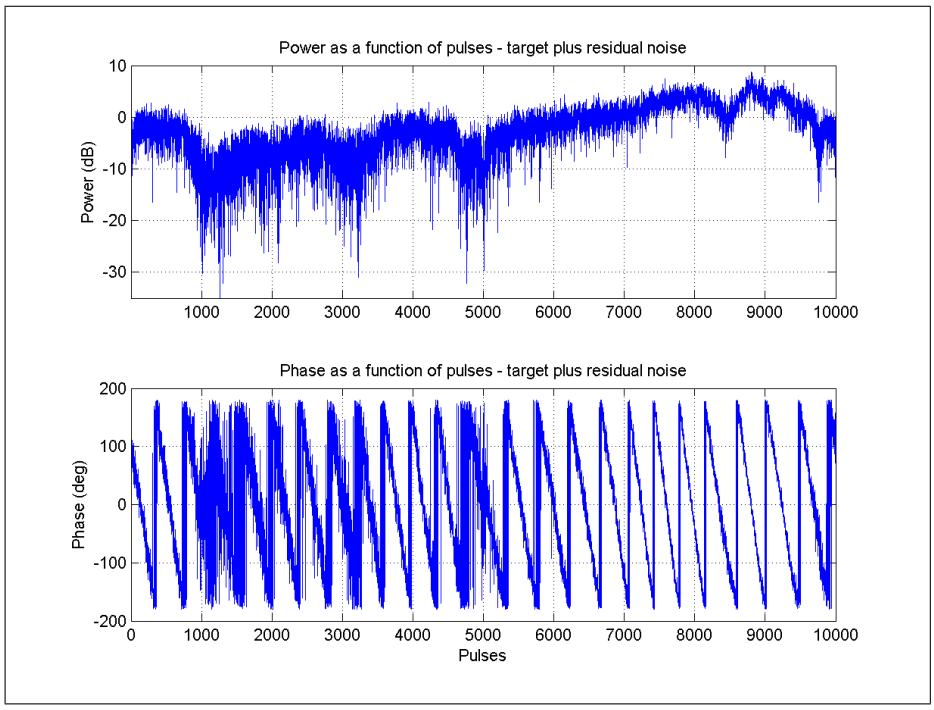

Figure 11.13: tx3-rx1

Chapter 12

Localization

In this Chapter we describe a method of processing data from a chosen area as surveyed by a multistatic system for the localization of a target. Experiment description and pre-processing of the signals have already been discussed in Chapter 10. In particular, we report two ways for localization. The first is a graphical method, whilst the second is numerical. It is clear that numerical minimization of specific functions has to be applied when the estimated target location is used in a tracking algorithm, so we also report an easy and immediate method to localize one (or more) target which expands the domain of potential application. For this purpose, apply to the received data an easy and very fast sub-optimal algorithm to improve the estimation of the measures of the Doppler shifts and the range positions of the target.

Figure 12.1 shows a representation of 25 integrated received signals, as a function of range, spread over the antennas' aperture (assuming no sidelobes). The first transceiver has been taken as the origin of the grid and consequentially the other two devices are located at (−48.96 m, 10.28 m) and (48.96 m, 10.28 m), respectively. As it can be seen from this Figure, the SNR is generally quite high, varying roughly from 15 to 30 dB. From the a-priori knowledge of the experiment, the moving target is expected to be $\approx$ 120 m far from the first device and walking away from it radially.

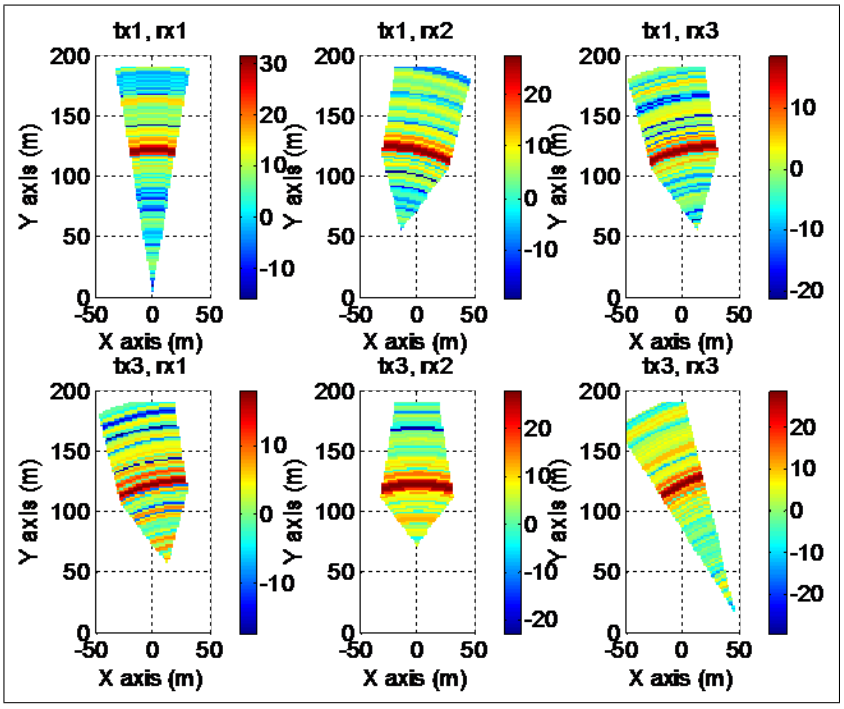

Figure 12.1: Graphical representation of acquired signals

12.1 Visual localization

In this Section the diagrams in Figure 12.1 are summed up together into a single plot only, according to different strategies. These are, in order, in analogy with what examined in the previous Chapters: (*i*) coherent centralized summation (NR), (*ii*) coherent centralized summation with phase correction (RPNR), (*iii*) incoherent centralized summation (MIMO) and (*iv*) incoherent decentralized summation (DRN). For the sake of simplicity, given the high SNR, in the RPNR it has been assumed that

$$\angle(s_{ta}) \approx \angle(s_{ta} + n_{ta}) \tag{12.1}$$

where $\angle x$ is the phase of x, and t_{ta} is the time of reception of the echo from the target. This is not as re-aligning the phases according to the real position of the target, but still gives a good approximation of the best performance available. However, as in the rest of this work, the first two systems are reported only as terms of comparison.

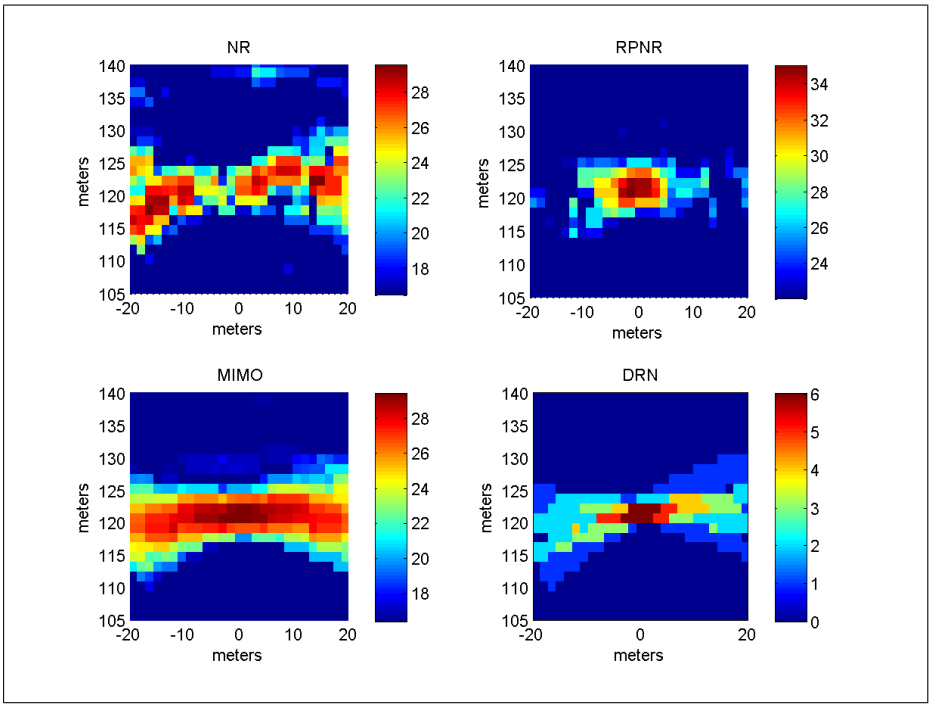

Figure 12.2: Graphical approach to localization, start of acquisition

Figures 12.2 and 12.3 show the graphical approach to localization in the area around the target at the beginning and at the end of the acquisition, respectively. The integration time was 2.5 msec, i.e. equal to 25 pulses. Generally, the coherent uncorrected summation performs worst, as expected, whereas coherency is not achieved in the location of the target, but in other regions, whilst as expected, the re-phased coherent system performs at the best, whereas it exploits a-priori information. As it can be seen, the MIMO approach results in some uncertainty on the position of the target, because of the wide beams of the antenna patterns. On the contrary the DRN approach manages to locate the target with higher accuracy, although it has to be pointed out that this approach requires a thresholding on the output of each pair tx-rx. In particular, the approach to thresholding for this set of results is a standard CA-CFAR, with one guard cell and two secondary cells per side, around the cell under test. The single-pair FAR has been set in this case to $10^{-}1$, which is a fairly high value, but still allows to compare the systems limiting the advantage that the DRN can take from the double-thresholding.

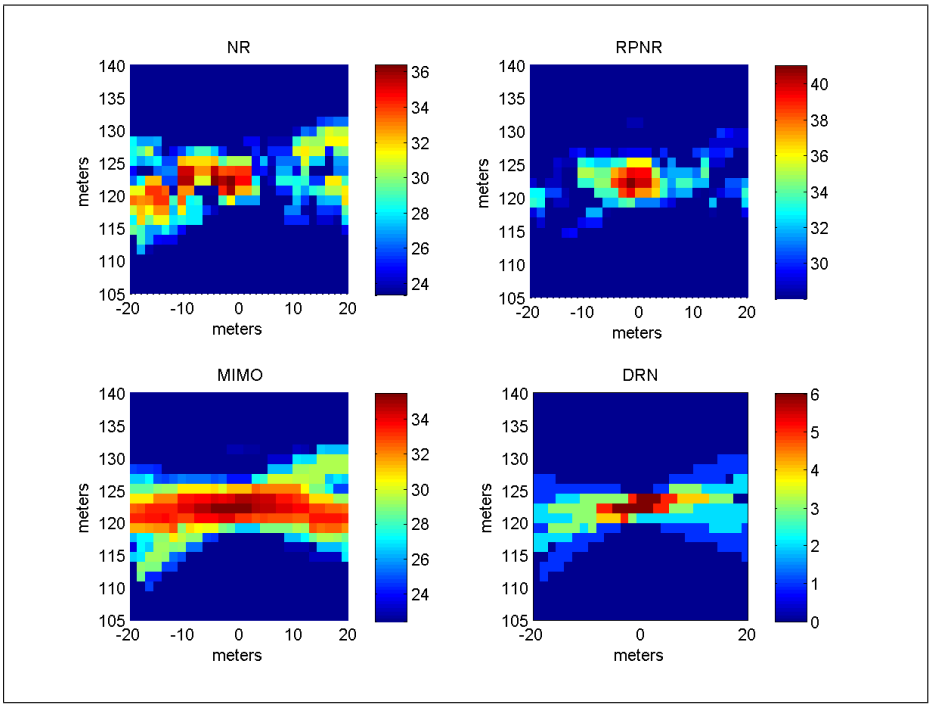

Figure 12.3: Graphical approach to localization, end of acquisition

12.2 Numerical localization and Doppler reconstruction

In this Section a numerical approach to the problem of localization is reported. In addition, Section 12.2.2 and Section 12.2.3 describe some issues related to the range-Doppler measurements of the analyzed data and their solution. Finally Section 12.2.5 shows a convenient way of extracting further information on the movement of the target.

12.2.1 Algorithm

Numerically, the position of one or more targets can be computed by solving the following system

$$\begin{cases} \|v_T - v_{tx,1}\| + \|v_T - v_{rx,1}\| = d_{1,1} \\ \vdots \qquad\qquad\quad \vdots \qquad\quad \vdots \\ \|v_T - v_{tx,i}\| + \|v_T - v_{rx,k}\| = d_{i,k} \\ \vdots \qquad\qquad\quad \vdots \qquad\quad \vdots \\ \|v_T - v_{tx,M}\| + \|v_T - v_{rx,N}\| = d_{M,N} \end{cases} \tag{12.2}$$

with respect to vector of the coordinates of the target v_T, where $v_{tx,i}$ is the vector of the coordinates of the i^{th} transmitter, $v_{rx,k}$ is the vector of the coordinates of the k^{th} receiver and $r_{i,k}$ is the two-way estimated distance. Alternatively, it is possible to minimize a function such as

$$\epsilon(v_T, \mathbf{v}_{tx}, \mathbf{v}_{rx}, \mathbf{r}) = \sum_{i=1}^{M} \sum_{k=1}^{N} \left(\|v_T - v_{tx,i}\| + \|v_T - v_{rx,k}\| - r_{i,k}\right)^2, \tag{12.3}$$

so that

$$\hat{v}_T = \arg\left\{\min_{v_T} \{\epsilon(v_T, \mathbf{v}_{tx}, \mathbf{v}_{rx}, \mathbf{r})\}\right\}, \tag{12.4}$$

since it is more robust when the set of distances $\mathbf{r}$ is not exact but affected by errors (thermal noise, residual clutter and range-estimation errors), as occurs generally in radar systems. However such minimization can be complicated and the complexity grows with the number of all the possible paths between the transmitters, the target and the receivers.

Alternatively, this problem can be slightly simplified by determining at a first stage an evaluation of the distance $\hat{d}_h = \|v_t - v_h\|$ between the target and the h^{th} device (either tx or rx) and in a second stage finding the minimum of a function such as:

$$\epsilon(v_T, \mathbf{v}, \mathbf{d}) = \sum_{h} \left(\|v_T - v_h\| - \hat{d}_h\right)^2 \tag{12.5}$$

and therefore

$$\hat{v}_T = \arg\left\{\min_{v_T} \{\epsilon(v_T, \mathbf{v}, \mathbf{d})\}\right\}, \tag{12.6}$$

In other words, the minimum least square (MLS) optimization of equation (12.3) is divided in two sub-MLS-optimizations. In the first, starting from all the range estimations (as will be seen in Section 12.2.3), the distances between the devices (either tx or rx or both) and the target are computed and then the minimum of the function in equation (12.5) is searched.

In particular, the distances $\hat{d}_h$, can be found as the MLS solution of the following system:

$$\begin{pmatrix} 2 & 0 & 0 \\ 1 & 1 & 0 \\ 1 & 0 & 1 \\ 1 & 0 & 1 \\ 0 & 1 & 1 \\ 0 & 0 & 2 \end{pmatrix} \begin{pmatrix} d_1 \\ d_2 \\ d_3 \end{pmatrix} = \begin{pmatrix} r_{11} \\ r_{12} \\ r_{13} \\ r_{31} \\ r_{32} \\ r_{33} \end{pmatrix}, \tag{12.7}$$

that can be expressed compactly as

$$\mathbf{Ad} = \mathbf{r} \tag{12.8}$$

and therefore admits MLS solution $\hat{d}_{MLS}$ as

$$\hat{\mathbf{d}}_{MLS} = \left(\mathbf{A}^T\mathbf{A}\right)^{-1}\mathbf{A}^T\mathbf{r}. \tag{12.9}$$

It is particularly worth noting that (*i*) the MLS optimization in equation (12.9) is basically costless, whereas the matrix $\left(\mathbf{A}^T\mathbf{A}\right)^{-1}\mathbf{A}^T$ can be pre-computed and does not need to be updated, and (*ii*) the optimization of the function in equation (12.5) presents a much lower level of complexity than the one in equation 12.3.

For completeness, in the analysis of the localization, two further functions have been examined. These take into account the noise of the channel and are as follows:

$$\epsilon(v_T, \mathbf{v}_{tx}, \mathbf{v}_{rx}, \mathbf{r}) = \sum_{i=1}^{M}\sum_{k=1}^{N} \frac{1}{\sigma_{i,k}^2} \left(\|v_T - v_{tx,i}\| + \|v_T - v_{rx,k}\| - r_{i,k}\right)^2, \tag{12.10}$$

and

$$\epsilon(v_T, \mathbf{v}, \mathbf{d}) = \sum_h \frac{1}{\hat{\sigma}_h^2} \left(\|v_T - v_h\| - \hat{d}_h \right)^2, \tag{12.11}$$

where

$$\begin{pmatrix} \hat{\sigma_1^2} \\ \hat{\sigma_2^2} \\ \hat{\sigma_3^2} \end{pmatrix} = \begin{pmatrix} \frac{1}{5} & 0 & 0 \\ 0 & \frac{1}{2} & 0 \\ 0 & 0 & \frac{1}{5} \end{pmatrix} \begin{pmatrix} 2 & 1 & 1 & 1 & 0 & 0 \\ 0 & 1 & 0 & 0 & 1 & 0 \\ 0 & 0 & 1 & 1 & 1 & 2 \end{pmatrix} \begin{pmatrix} \sigma_{1,1}^2 \\ \sigma_{1,2}^2 \\ \sigma_{1,3}^2 \\ \sigma_{3,1}^2 \\ \sigma_{3,2}^2 \\ \sigma_{3,3}^2 \end{pmatrix}, \tag{12.12}$$

i.e. σ_h^2 is an average of the noise of the channels, when the h^{th} device is active as a transmitter and/or as a receiver.

12.2.2 Range-Doppler analysis

In this Section the range-Doppler diagrams for the acquired signals are reported. The aims are (*i*) to validate that the clutter cancellation does not affect the Doppler-shift of the signal, (*ii*) to provide a starting point for an algorithm for improving the range and Doppler estimations and therefore (*iii*) to allow, in a second stage of processing (Section 12.2.5), better localization of the target and reconstruction of the Doppler vector of the target.

Although the acquisition time is 1 second, in a real-time scenario the precessing unit is capable of performing a range-Doppler analysis within a much shorter time interval. As a consequence, the time on target it is assumed to be 50 msec only for producing the range-Doppler plots. Under this assumption and after the clutter removal, the range-Doppler plots for each pair tx-rx become as in Figure 12.4. As seen here, not only the clutter cancellation of the low frequencies result to be lessened, due to the coarse frequency resolution, but also the target's Doppler frequencies fall into the same bin, regardless from the pairs tx-rx. At the same time, because of the geometrical and iso-range configuration of the experiment, also the range bin of the target is the same for any pair of devices.

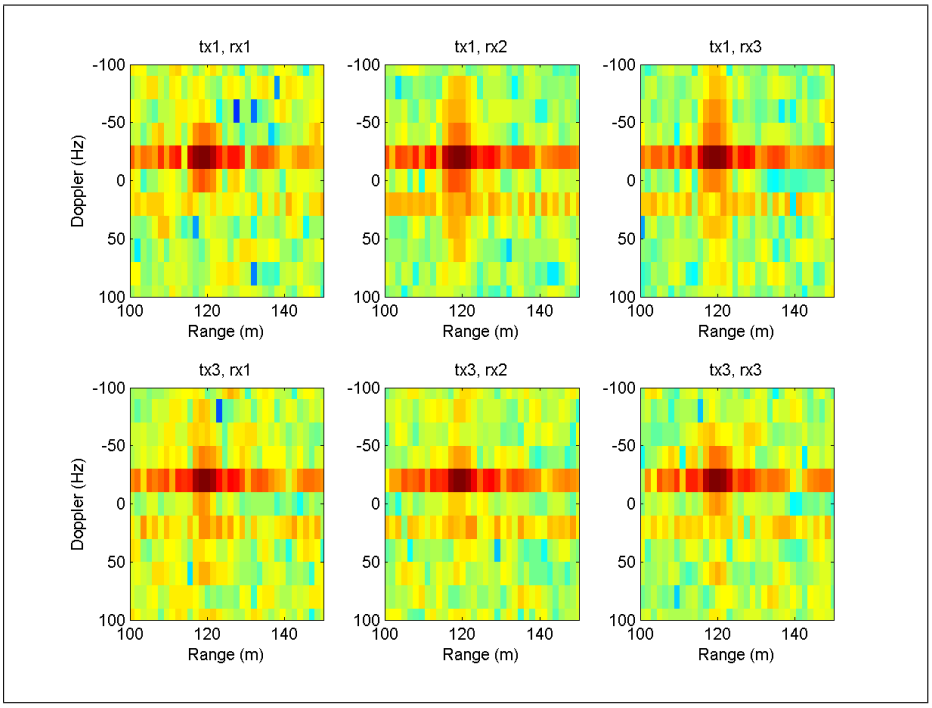

Figure 12.4: Range-Doppler plots over 50 ms

12.2.3 Range-Doppler estimation

To solve the ambiguity in Range and Doppler described in the previous Section, Doppler frequency and range estimation in a single pair tx-rx has been improved through an interpolation method based on fitting a parabolic curve to the logarithm of the absolute value of the peak of the range-Doppler function [25]. Here the method is applied to range estimation only, for brevity, since it is the same as for frequency.

Assuming that the maximum power P_0 (dB) occurs in at the range R_0, we consider the parabolic curve passing through the points $(R_{-1} - R_0, P_{-1})$, $(0, P_0)$ and $(R_1 - R_0, P_1)$, where R_{-1} and R_1 are respectively the range bins respectively before and after R_0 and P_{-1} and P_1 the corresponding power measured (in dB) and a translation from R_0 to the origin has been applied to the range domain. Therefore the power as function of the range is interpolated as

$$P(r) = ar^2 + br + c, \tag{12.13}$$

where a, b and c are unknown coefficients that can be recovered from the information

$$\begin{cases} P_{-1} = P(-\Delta R) = a(\Delta R)^2 - b\Delta R + c \\ P_0 = P(0) = c \\ P_1 = P(\Delta R) = a(\Delta R)^2 + b\Delta R + c \end{cases} \tag{12.14}$$

where

$$\Delta R = R_0 - R_{-1} = R_1 - R_0. \tag{12.15}$$

Under these assumptions, after solving the system, the range r_{max} of maximum power is

$$r_{max} = \frac{1}{2}\frac{P_{-1} - P_1}{P_{-1} - 2P_0 + P_1}\Delta R, \tag{12.16}$$

which gives, translating the origin back to R_0:

$$r_{max} = R_0 + \frac{1}{2}\frac{P_{-1} - P_1}{P_{-1} - 2P_0 + P_1}\Delta R, \tag{12.17}$$

Exactly the same procedure applies to the Doppler frequency and therefore it is not reported for brevity. It is important to highlight that, after these processing, the new measurements in range-Doppler will also allow an improved cancellation of the target [25] and therefore a recursive application of the detection algorithm so to detect multiple targets (if present) with RCS smaller in the area.

12.2.4 Localization results

The optimizations of the functions in equations (12.3), (12.5), (12.10) and (12.11) have been computed with Nelder-Mead simplex method, that is known to be quite robust even if relatively slow. The starting point provides to the algorithm at the q^{th} iteration was the $(q-1)^{th}$ output. For the first iteration the starting point was deliberately set to $(0, 100)$, so to verify the convergence in just a few steps.

Figure 12.5 shows the series of thew localization after the optimization processes when pulses are processed at bursts of 25, i.e. over 2.5 msec. Figures 12.5(a) and 12.5(b) show the Y-axis and X-axis positions after the 1-stage mini-

mization respectively without and with noise as in equations (12.3) (above) and (12.10) (below). Figures 12.5(c) and 12.5(d) show the Y-axis and X-axis positions after the 2-stage minimization respectively without and with noise as in equations (12.5) (above) and (12.11) (below). The average time for achieving the results in the following pictures varied between 2 seconds (2-step MLS algorithm) and 2.75 seconds (original 1-step version). Although the time of processing is greater than the time of acquisition, it has to be pointed out that it has been achieved using a 2 GHz processor and standard commercial minimization macros over an unoptimized hardware.

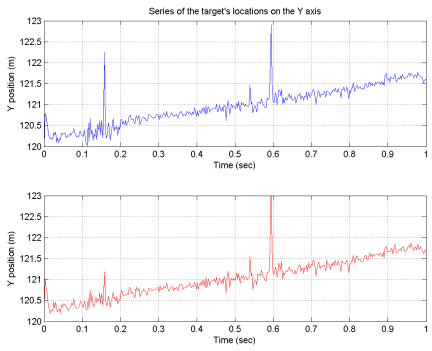

(a) 1-stage algorithm, Y axis, unweighed (up), weighed (down)

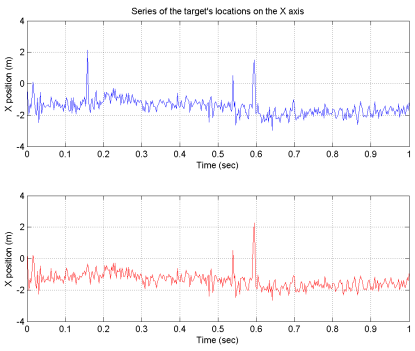

(b) 1-stage algorithm, X axis, unweighed (up), weighed (down)

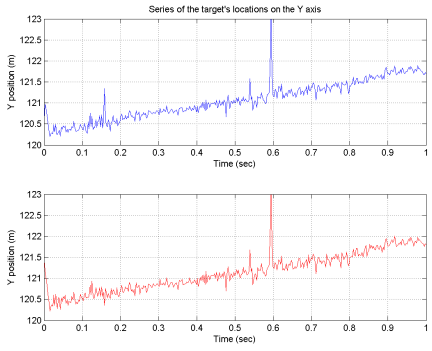

(c) 2-stage algorithm, Y axis, unweighed (up), weighed (down)

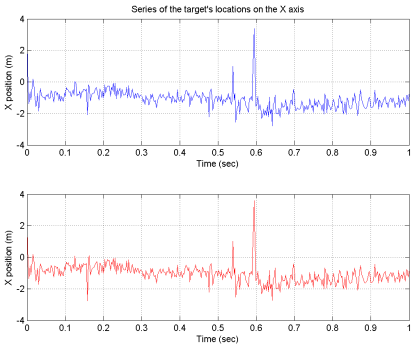

(d) 2-stage algorithm, X axis, unweighed (up), weighed (down)

Figure 12.5: Localization results on buffers of 2.5 msec

In particular, it is observed that:

i The series of localizations, in all cases, is a good representation of the actual path of the target, with a resolution that seems to be improved compared to the nominal one (3.75 m),

ii The 2-stage process performs better than the single-stage one for low SNR. This can be seen from the absence of a couple of noise-affected localizations at approximately 0.16 sec.

iii The standard deviation of the errors in these Figures are between 15 and 17 cm on the Y axis and between 35 and 45 cm on the X axis.

iv For low SNR the weighted versions perform better than the non-weighted, as might be expected. However a higher standard deviation overall (approximately 5% more) has been observed in the latter cases.

Figure 12.6 shows the plots of the localization on the Y and X axis when buffers of 50 msec are processed. In this Figure the results of the minimization according to equation (12.3) only is reported. This is because the differences between the four minimization functions described previously are negligible. In addition, as it can be expected using a longer integration period, here the measurements are averaged, if compared to those in Figure 12.5, and therefore the overall movement of the target appears smoother. The increased length of the data-buffer had also the effect of reducing the measurements in input to any minimization function, leading to a dramatic reduction in the processing time: in this case, for each function taken into account, the time required to provide the output was approximately 0.1 sec, i.e. in the order of $\frac{1}{10}$ of the acquisition time, using unoptimized macros and hardware.

12.2.5 Doppler vector reconstruction

Finally, in this Section the reconstruction of the full velocity vector $\mathbf{W}$ is performed, starting from the measurements of the single radars. The following system of equations describes the relationship between the real Doppler vector $\mathbf{W}$ and the Doppler measurements $\mathbf{F}_D$. The Doppler measurements are as after the process described in Section 12.2.3.

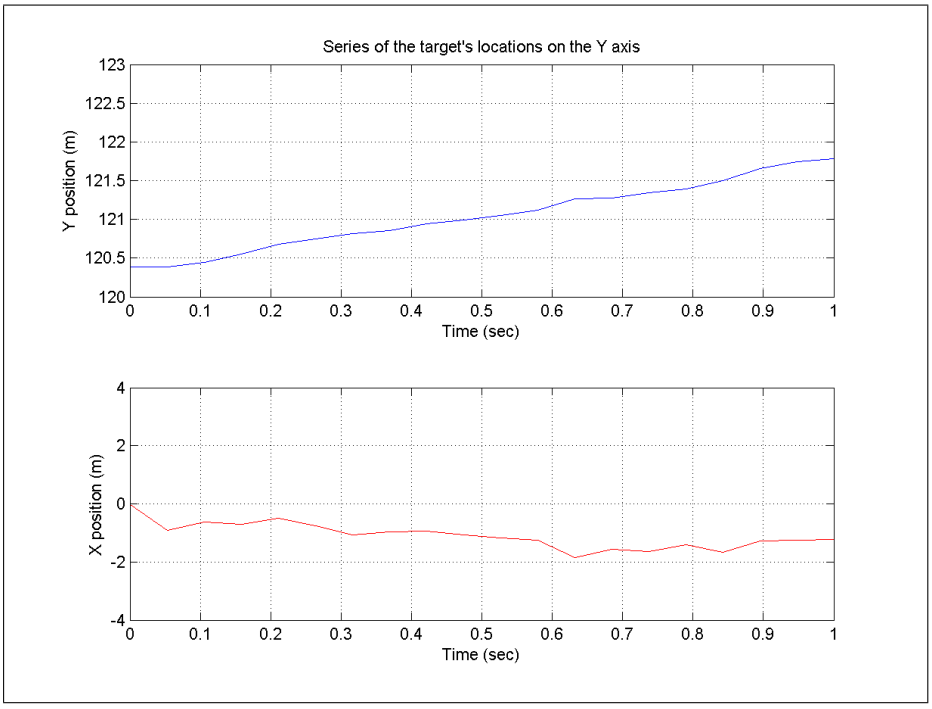

Figure 12.6: Localization results on buffers of 50 msec

$$\begin{pmatrix} b_{x,11} & b_{y,11} \\ b_{x,12} & b_{y,12} \\ b_{x,13} & b_{y,13} \\ b_{x,31} & b_{y,31} \\ b_{x,32} & b_{y,32} \\ b_{x,33} & b_{y,33} \end{pmatrix} \begin{pmatrix} w_x \\ w_y \end{pmatrix} = \begin{pmatrix} f_{D,11} \\ f_{D,12} \\ f_{D,13} \\ f_{D,31} \\ f_{D,32} \\ f_{D,33} \end{pmatrix}, \tag{12.18}$$

where

$$b_{x,ik} = \frac{\cos\theta_{x,TX_i} + \cos\theta_{x,RX_k}}{\lambda}, \tag{12.19}$$

$$b_{y,ik} = \frac{\cos\phi_{y,TX_i} + \cos\phi_{y,RX_k}}{\lambda} \tag{12.20}$$

and $\theta_{x,TX_i/RX_k}$ and $\phi_{y,TX_i/RX_k}$ are, respectively, the angle between the x and y unit vectors in the grid and the vectors connecting the target to either the i^{th} tx or the k^{th} rx. This can be expressed compactly as

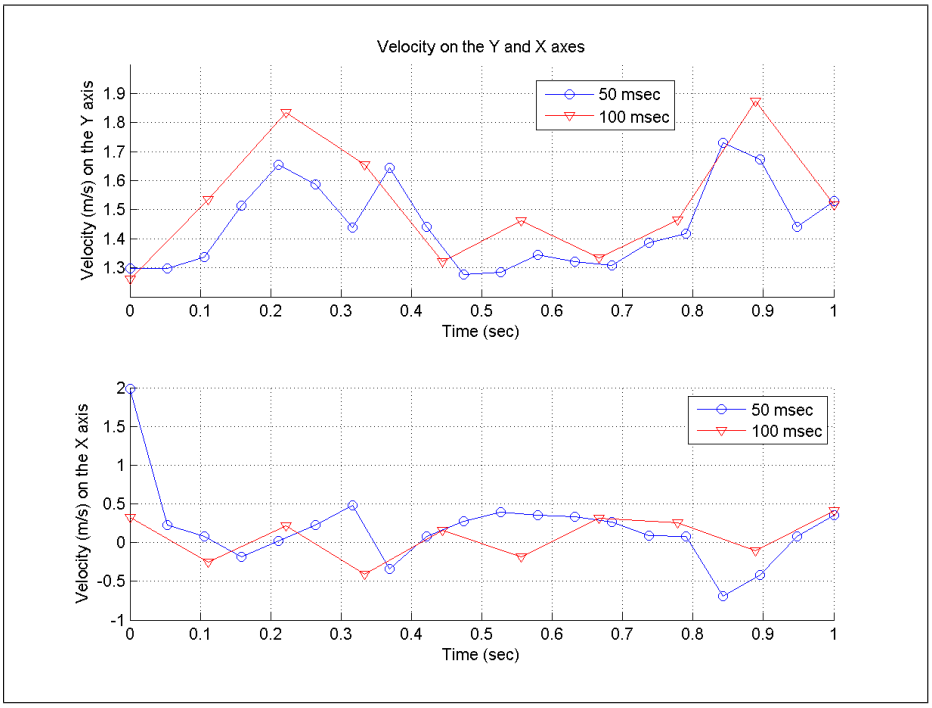

Figure 12.7: Velocity estimation on 50 amd 100 msec buffers

$$\mathbf{BW} = \mathbf{F}_D \tag{12.21}$$

and therefore leads to the MLS solution $\hat{\mathbf{W}}_{MLS}$ as

$$\hat{\mathbf{W}}_{MLS} = \left(\mathbf{B}^T\mathbf{B}\right)^{-1}\mathbf{B}^T\mathbf{F}_D \tag{12.22}$$

Figure 12.7 shows the estimated instantaneous velocity on both Y and X axes for buffers of 50 and 100 msec. From the experiment setup and the previous plots, it is possible to conclude that the target moves approximately with an average speed of 1.5 m/sec on the Y axis and 0 m/sec on the X axis. These values are confirmed by the results shown here.

Chapter 13

Conclusions

It has been shown that, given the limitations of the cases considered here, the MIMO systems have superior detection performance to (not-re-phased) NR. That is due to the fact that, since the phases of the incoming signals are totally uncorrelated, the coherent sum is statistically a disruptive event. The extra complexity required for re-aligning the phases and then to gain a factor L (where L is the number of summed signals) on the SNR is difficult to implement, especially when the systems are working over broad frequency bandwidths and have high carrier frequencies.

It has also been shown that the MIMO concepts achieve a performance in between the two netted cases with a quite simple structure for the detector. Furthermore, generally, a loss of only few dB in terms of SNR has been observed, compared to the re-phased NR. Advantages have been also demonstrated in exploiting the extra-variance of the signal when multipath effect is present. However, real targets are known to exhibit very complex behaviours with unknown three-dimensional scattering functions. This becomes even more complicated at high resolution where different parts of the target show differing statistical behaviours.

However, it has also been reported that a decentralized approach to processing is a valid alternative. It has been shown that DRN systems not only have a simpler structure of detector, but also the losses in SNR are overall moderate. Nonetheless, they allow an increased tolerance to jamming.

The behaviour of a radar networks for localizing and estimating the DOA and

the velocity of the target have been investigated, and it has been shown that as diversity in space can dramatically improve even coarse resolutions, achieving an accuracy below a tenth of the nominal. performance. A clear benefit of multi-angle observations can be immediately seen in the extra information provided on the Doppler frequency. With spatially-different measurements of the Doppler it has been possible to reconstruct the full vector of the velocity of a target, whilst it is well known that with a monostatic case the only possible measurement is on the radial velocity.

In the longer term, the MIMO concept can be applied to classification. Actually it has been recently shown that multiple perceptions can improve significantly the recognition of the target. As the spatial MIMO system provides different looks from different aspect angles, it fits very well the requirements of this technique, so the expected results can be promising. In a second stage the frequency diversity can introduce an ulterior degree of freedom for this purpose, due to the increased information that can be gathered using two or more different bands in transmission.

List of Figures

Bibliography

[1] M.I. Skolnik, *Introduction to radar systems*, McGraw Hill, 1981.

[2] N. Levanon and E. Mozeson, *Radar Signals*, John Wiley & Sons, 2004.

[3] G. Picardi, *Elaborazione del segnale radar*, Franco Angeli, 2000.

[4] N. J. Willis, *Bistatic radar*, SciTech Publishing, 2005.

[5] M. Cherniakov, *Bistatic Radars: Emerging Technology*, John Wiley & Sons, 2008.

[6] D.J. MacKay, *Information Theory, Inference and Learning Algorithms*, Cambridge University Press, 2003.

[7] S.M. Kay, *Fundamentals of Statistical Signal Processing: Estimation Theory*, Prentice Hall, 1993.

[8] S.M. Kay, *Fundamentals of Statistical Signal Processing: Detection Theory*, Prentice Hall, 1998.

[9] R.J.A. Tough, C.J. Baker, and J.M. Pink, "Radar performance in a maritime environment: single hit detection in the presence of multipath fading and non-Rayleigh sea clutter", *Radar and Signal Processing, IEE Proceedings*, vol. 137, no. 1, pp. 33–40, Feb 1990.

[10] A. Farina, F. Gini, M.V. Greco, and P. Lombardo, "Coherent radar detection of targets against a combination of K-distributed and gaussian clutter",

Radar Conference, 1995., Record of the IEEE 1995 International, pp. 83–88, 8-11 May 1995.

[11] T. Bucciarelli, P. Lombardo, and S. Tamburrini, "Optimum CFAR detection against correlated K-distributed clutter", *Signals, Systems, and Electronics, 1995. ISSSE '95, Proceedings., 1995 URSI International Symposium on*, pp. 191–194, 25-27 Oct 1995.

[12] A. Farina and P. Lombardo, "Modelling of a mixture of K-distributed and gaussian clutter for coherent radar detection", *Electronics Letters*, vol. 30, no. 6, pp. 520–521, 17 Mar 1994.

[13] F. Gini, A. Farina, and M.V. Greco, "Detection of multidimensional Gaussian random signals in compound-Gaussian clutter plus thermal noise", *Signal Processing Proceedings, 1998. ICSP '98. 1998 Fourth International Conference on*, vol. 2, pp. 1650–1653 vol.2, 1998.

[14] P. Lombardo, D. Pastina, and T. Bucciarelli, "CFAR coherent radar detection against K-distributed clutter plus thermal noise", *Radar Conference, 1998. RADARCON 98. Proceedings of the 1998 IEEE*, pp. 129–134, 11-14 May 1998.

[15] S.D. Himonas and M. Barkat, "Adaptive CFAR detection in partially correlated clutter", *Radar and Signal Processing, IEE Proceedings*, vol. 137, no. 5, pp. 387–394, Oct 1990.

[16] C.J. Baker, "K-distributed coherent sea clutter", *Radar and Signal Processing, IEE Proceedings*, vol. 138, no. 2, pp. 89–92, Apr 1991.

[17] K.D. Ward, C.J. Baker, and S. Watts, "Maritime surveillance radar. I. radar scattering from the ocean surface", *Radar and Signal Processing, IEE Proceedings*, vol. 137, no. 2, pp. 51–62, Apr 1990.

[18] S. Watts, C.J. Baker, and K.D. Ward, "Maritime surveillance radar. II. detection performance prediction in sea clutter", *Radar and Signal Processing, IEE Proceedings F*, vol. 137, no. 2, pp. 63–72, Apr 1990.

[19] T. Hair, T. Lee, and C.J. Baker, "Statistical properties of multifrequency high-range-resolution sea reflections", *Radar and Signal Processing, IEE Proceedings F*, vol. 138, no. 2, pp. 75–79, Apr 1991.

[20] E.J. Kelly, "Performance of an adaptive detection algorithm; rejection of unwanted signals", *Aerospace and Electronic Systems, IEEE Transactions on*, vol. 25, no. 2, pp. 122–133, Mar 1989.

[21] E.J. Kelly, "An adaptive detection algorithm", *Aerospace and Electronic Systems, IEEE Transactions on*, vol. AES-22, no. 2, pp. 115–127, March 1986.

[22] F.C. Robey, D.R. Fuhrmann, E.J. Kelly, and R. Nitzberg, "A CFAR adaptive matched filter detector", *Aerospace and Electronic Systems, IEEE Transactions on*, vol. 28, no. 1, pp. 208–216, Jan 1992.

[23] P. Monticciolo, E.J. Kelly, and J.G. Porakis, "A noncoherent adaptive detection technique", *Aerospace and Electronic Systems, IEEE Transactions on*, vol. 28, no. 1, pp. 115–124, Jan 1992.

[24] V.G. Hansen, "Constant false-alarm rate processing in search radars", *IEE 1973 International Radar Conference. Proceedings of*, pp. 325–332, 23-25 October 1973.

[25] K.S. Kulpa and Z. Czekala, "Masking effect and its removal in PCL radar", *IEE Proceedings on Radar, Sonar and Navigation*, vol. 152, no. 3, pp. 174–178, 3 June 2005.

[26] M. Schwartz, "A coincidence procedure for signal detection", *Information Theory, IEEE Transactions on*, vol. 2, no. 4, pp. 135–139, Dec 1956.

[27] V.S. Chernyak, "Effective simplified decentralized target detection in multisensor systems", *Information Fusion. Proceedings of the Third International Conference on*, vol. 2, 10-13 July 2000.

[28] H.A. Khan, Y. Zhang, C. Ji, C.J. Stevens, D.J. Edwards, and D. O'Brien, "Optimizing polyphase sequences for orthogonal netted radar", *IEEE Signal Processing Letters*, vol. 13, no. 10, pp. 589–592, October 2006.

[29] H. Deng, "Polyphase code design for orthogonal netted radar systems", *Signal Processing, IEEE Transactions on*, vol. 52, no. 11, pp. 3126Ű3135, 2004.

[30] T. Johnsen, K. E. Olsen, S. Johnsrud, and R. Skjerpeng, "Simultaneous use of multiple pseudo random noise codes in multistatic cw radar", *the IEEE Radar Conference, Proceedings of*, 2004.

[31] E. Hanle, "Distance considerations for multistatic radar", *International Radar Conference*, pp. 100–105, Arlington, VA, April 28-30 1980.

[32] F. Verrazzani L. Gini, F. Lombardini, "Robust monoparametric multiradar CFAR detection againstnon-gaussian spiky clutter", in *Radar, Sonar and Navigation, IEE Proceedings*, Jun 1997, vol. 144.

[33] A. Farina and E. Hanle, "Position accuracy in netted monostatic and bistatic radar", *Aerospace and Electronic Systems, IEEE Transactions on*, vol. AES-19, no. 4, pp. 513–520, July 1983.

[34] C.J. Baker and A.L. Hume, "Netted radar sensing", *Aerospace and Electronic Systems Magazine, IEEE*, vol. 18, no. 2, pp. 3–6, Feb 2003.

[35] S. Miranda, C. Baker, K. Woodbridge, and H. Griffiths, "Knowledge-based resource management for multifunction radar: a look at scheduling and task prioritization", *Signal Processing Magazine, IEEE*, vol. 23, no. 1, pp. 66–76, Jan. 2006.

[36] S.L.C. Miranda, C.J. Baker, K. Woodbridge, and H.D. Griffiths, "Fuzzy logic approach for prioritisation of radar tasks and sectors of surveillance in multifunction radar", *Radar, Sonar & Navigation, IET*, vol. 1, no. 2, pp. 131–141, April 2007.

[37] T.E. Derham, S. Doughty, K. Woodbridge, and C.J. Baker, "Design and evaluation of a low-cost multistatic netted radar system", *Radar, Sonar & Navigation, IET*, vol. 1, no. 5, pp. 362–368, October 2007.

[38] Y. Teng, H.D. Griffiths, C.J. Baker, and K. Woodbridge, "Netted radar sensitivity and ambiguity", *Radar, Sonar & Navigation, IET*, vol. 1, no. 6, pp. 479–486, Dec. 2007.

[39] N.D. Sidiropoulos A.B. Gershman, *Space-Time Processing for MIMO Communications*, John Wiley & Sons, 2005.

[40] W.G. Scanlon and K. Ziricastro, "Modelling of MIMO channels for the populated indoor environment", *MIMO: Communications Systems from Concept to Implementations, IEE Seminar on*, 12 Dec. 2001.

[41] K.I. Ziricastro, W.G. Scanlon, and N.E. Evans, "Prediction of variation in MIMO channel capacity for the populated indoor environment using a radar cross-section-based pedestrian model", *Wireless Communications, IEEE Transactions on*, vol. 4, no. 3, pp. 1186–1194, May 2005.

[42] Jeng-Shiann Jiang and M.A. Ingram, "Distributed source model for short-range MIMO", *Vehicular Technology Conference, 2003. VTC 2003-Fall. 2003 IEEE 58th*, vol. 1, pp. 357–362 Vol.1, 6-9 Oct. 2003.

[43] R. Venkataramani and Y. Bresler, "Multiple-input multiple-output sampling: necessary density conditions", *Information Theory, IEEE Transactions on*, vol. 50, no. 8, pp. 1754–1768, Aug. 2004.

[44] Hao Xu, D. Chizhik, H. Huang, and R. Valenzuela, "A generalized space-time multiple-input multiple-output (MIMO) channel model", *Wireless Communications, IEEE Transactions on*, vol. 3, no. 3, pp. 966–975, May 2004.

[45] G. Latsoudas and N.D. Sidiropoulos, "A hybrid probabilistic data association-sphere decoding detector for multiple-input-multiple-output systems", *Signal Processing Letters, IEEE*, vol. 12, no. 4, pp. 309–312, April 2005.

[46] A. Zanella, M. Chiani, and M.Z. Win, "MMSE reception and successive interference cancellation for MIMO systems with high spectral efficiency",

Wireless Communications, IEEE Transactions on, vol. 4, no. 3, pp. 1244–1253, May 2005.

[47] P. Uthansakul and M.E. Bialkowski, "Multipath signal effect on the capacity of MIMO, MIMO-OFDM and spread MIMO-OFDM", *Microwaves, Radar and Wireless Communications, 2004. MIKON-2004. 15th International Conference on*, vol. 3, pp. 989–992 Vol.3, 17-19 May 2004.

[48] S. Kozlowski, Y. Yashchyshyn, and J. Modelski, "Phased array antennas in MIMO receiver", *Microwaves, Radar & Wireless Communications, 2006. MIKON 2006. International Conference on*, pp. 473–476, 22-24 May 2006.

[49] E. Fishler, A. Haimovich, R. Blum, D. Chizhik, L. Cimini, and R. Valenzuela, "MIMO radar: an idea whose time has come", *Radar Conference, 2004. Proceedings of the IEEE*, pp. 71–78, 26-29 April 2004.

[50] E. Fishler, A. Haimovich, R. Blum, R. Cimini, D. Chizhik, and R. Valenzuela, "Performance of MIMO radar systems: advantages of angular diversity", *Signals, Systems and Computers, 2004. Conference Record of the Thirty-Eighth Asilomar Conference on*, vol. 1, pp. 305–309 Vol.1, 7-10 Nov. 2004.

[51] E. Fishler, A. Haimovich, R.S. Blum, Jr. Cimini, L.J., D. Chizhik, and R.A. Valenzuela, "Spatial diversity in radars-models and detection performance", *Signal Processing, IEEE Transactions on [see also Acoustics, Speech, and Signal Processing, IEEE Transactions on]*, vol. 54, no. 3, pp. 823–838, March 2006.

[52] K.W. Forsythe, D.W. Bliss, and G.S. Fawcett, "Multiple-input multiple-output (MIMO) radar: performance issues", *Signals, Systems and Computers, 2004. Conference Record of the Thirty-Eighth Asilomar Conference on*, vol. 1, pp. 310–315 Vol.1, 7-10 Nov. 2004.

[53] A.M. Haimovich, R.S. Blum, and L.J. Cimini, "MIMO radar with widely separated antennas", *Signal Processing Magazine, IEEE*, vol. 25, no. 1, pp. 116–129, 2008.

[54] Nikolaus H. Lehmann, Alexander M. Haimovich, Rick S. Blum, and Len Cimini, "High resolution capabilities of MIMO radar", *Signals, Systems and Computers, 2006. ACSSC '06. Fortieth Asilomar Conference on*, pp. 25–30, Oct.-Nov. 2006.

[55] H.A. Khan, W.Q. Malik, D.J. Edwards, and C.J. Stevens, "Ultra wideband multiple-input multiple-output radar", *Radar Conference, 2005 IEEE International*, pp. 900–904, 9-12 May 2005.

[56] H.A. Khan and D.J. Edwards, "Doppler problems in orthogonal MIMO radars", *Radar, 2006 IEEE Conference on*, pp. 4 pp.–, 24-27 April 2006.

[57] J. Li and P. Stoica, *MIMO radar signal processing*, John Wiley & Sons, 2008.

[58] D.W. Bliss and K.W. Forsythe, "Multiple-input multiple-output (MIMO) radar and imaging: degrees of freedom and resolution", *Signals, Systems and Computers, 2003. Conference Record of the Thirty-Seventh Asilomar Conference on*, vol. 1, pp. 54–59 Vol.1, 9-12 Nov. 2003.

[59] P. Bidigare, "MIMO capacity of radar as a communication channel", *Adaptive Sensor and Array Processing Workshop*, 11-13 March 2003.

[60] A. De Maio and M. Lops, "Design principles of MIMO radar detectors", *Aerospace and Electronic Systems, IEEE Transactions on*, vol. 43, no. 3, pp. 886–898, July 2007.

[61] D.J. Rabideau and P. Parker, "Ubiquitous MIMO multifunction digital array radar", *Signals, Systems and Computers, 2003. Conference Record of the Thirty-Seventh Asilomar Conference on*, vol. 1, pp. 1057–1064 Vol.1, 9-12 Nov. 2003.

[62] G. San Antonio and D.R. Fuhrmann, "Beampattern synthesis for wideband MIMO radar systems", *Computational Advances in Multi-Sensor Adaptive Processing, 2005 1st IEEE International Workshop on*, pp. 105–108, 13-15 Dec. 2005.

[63] F.C. Robey, S. Coutts, D. Weikle, J.C. McHarg, and K. Cuomo, "MIMO radar theory and experimental results", *Signals, Systems and Computers, 2004. Conference Record of the Thirty-Eighth Asilomar Conference on*, vol. 1, pp. 300–304 Vol.1, 7-10 Nov. 2004.

[64] D.R. Fuhrmann and G.S. Antonio, "Transmit beamforming for MIMO radar systems using partial signal correlation", *Signals, Systems and Computers, 2004. Conference Record of the Thirty-Eighth Asilomar Conference on*, vol. 1, pp. 295–299 Vol.1, 7-10 Nov. 2004.

[65] J. Li and P. Stoica, "Mimo radar with colocated antennas: Review of some recent work", *Signal Processing Magazine, IEEE*, vol. 24, no. 5, pp. 106–114, Sept. 2007.

[66] J. R. Guerci, M. C. Wicks, J. S. Bergin, P. M. Techau, and S. U. Pillai, "Theory and application of optimum and adaptive mimo radar", *Radarcon 2008. Conference Record of*, 26-30 May 2008.

[67] A. Farina, *Antenna-based signal processing techniques for radar systems*, Artech House, 1992.